Understanding the manganese refining path in the converter steelmaking process

A study based on IMPHOS data

by

W.(Wesley) van Maanen

to obtain the degree of Master of Science
at the Delft University of Technology,
to be defended publicly on 27 November, 2020 at 04:00 PM.

Student number:	4217691	
Project duration:	March 2, 2020 – November 27, 2020	
Thesis committee:	Dr. M.W.N. Buxton,	TU Delft, Chair
	Dr. Y. Yang,	TU Delft
	Dr. B.K. Rout,	Tata Steel
	Ir. F.N.H. Schrama,	Tata Steel
	Dr. R. Serna,	Aalto University
	Prof. Dr. B.G. Lottermoser,	RWTH Aachen

Abstract

The main goal of this research is to get a better understanding of the manganese refining path in the steelmaking converter process. This study focuses primarly on manganese refining due to manganese mass transfer, between metal containing droplets and oxidized slag in the metal-slag emulsion zone, in the top part of the steelmaking converter. Manganese and iron content in the slag heavily influences the slag formation path. Controlling the slag viscosity is essential for controlling the efficiency of the steelmaking process and to preserve the quality of the final steel product. Manganese refining in the steelmaking process occurs in three phases, the primary oxidation phase, the reversion phase and the secondary oxidation phase. This manganese reversion phase is hard to predict and influences the final amount of manganese in the end steel product. In order to raise understanding of the reversion behaviour of manganese in the converter, unique data gathered from in situ measurements done in the EU funded IMPHOS project is utilised. The following research questions were formulated and answered in this study:

- Are thermodynamic models for manganese distribution calculation applicable for the prediction of the three different behavioral phases of manganese in IMPHOS?
- What is the influence of the slag-metal emulsion droplets size on the manganese refining behaviour?
- What is the influence of metal-slag data input obtained from 2 different heights in IMPHOS, on the final resulting manganese behaviour in the kinetic model made in python?
- Were there any chemical deviations in different zones of the hot metal bath during IMPHOS project sampling?

IMPHOS heat S1836, S1841, S1844, S1845 were selected and analyzed on their theoretical thermodynamic equilibrium behaviour for manganese. This analysis was done with Suito No. 3 and Morales and Fruehan equilibrium partition model. Furthermore, the heats slag composition data, hot metal data and converter process variables were used as input in a kinetic model. The model is simulating the micro and macro kinetic behaviour of manganese in the converter emulsion zone with a fixed time step of 1s. The mass transfer in the model is based on Fick's first law of diffusion and uses penetration theory by Higbie, to describe mass transfer along metal droplet boundaries. Parameters such as the manganese mass transfer and the predicted manganese content in the hot metal bath were evaluated to validate the model with the measured concentration reported in the IMPHOS study. Bulk chemical analysis is done on physical samples from heat S1836 cup height 2. This is done to check the inhomogeneity in the hot metal bath and the possibility of different reaction zones in the converter process.

The thermodynamic evaluation performed on IMPHOS data showed the difficulty of thermodynamic models derived from laboratory tests, to describe the manganese equilibrium behaviour within the converter. Suito no 3 model gave a better prediction of the manganese distribution than the Morales and Fruehan model. The results from the kinetic model showed a slower primary oxidation and reversion behaviour of manganese compared to the original data. This is mainly due to the manganese equilibrium behaviour of the thermodynamic model and the negligence of the manganese refining in the jet impact zone and metal-slag interface. The model gave a better prediction when a small size droplet range was considered, which implies that the smaller size droplets less than 100 micron are significantly contributing to the manganese transfer from metal to slag and vice versa. The present study reveals that droplet size play an important role and thus need further investigation to accurately describe the size fraction for the accuracy of the kinetic model. The difference between metal-slag data input from the different IMPHOS cup height 4 and 5 on the outcome of the thermodynamic evaluation and kinetic model results, proved to be small enough to be considered negligible. The results from the sample analysis showed deviations for carbon and phosphorus in the new examined cup height 2. These measurements were taken at a high position in the hot metal bath and were different from the measured concentration in the bottom of the hot metal bath. This can indicate deviations in chemical content in the hot metal bath during the original IMPHOS research. More heat data of height 2 , close to the bath surface, is required to confirm this finding.

Acknowledgements

I would like to thank Tata Steel Ijmuiden for giving me the opportunity to work on this project and to learn a lot about the converter steelmaking process. Working on this project was a very learnful experience. Special thanks to Bapin Rout and Frank Schrama from Tata steel, thanks for all your guidance during this project. Thanks for all your support and patience with me. I've learned a lot about steelmaking from your experience of working in the field of research. Thanks for meeting up frequently to answer all my questions. Thanks for providing me all this valuable knowledge. Working together on this project was an amazing experience, which I will never forget. Also special thanks to James Small from Tata steel, who shared his knowledge about working on IMPHOS sample analysis in the past. Thanks for all the guidance and advice during the current IMPHOS sample analysis done in this research. Thanks to everybody else at Tata Steel Ijmuiden who provided me with their advice, support and time during the completion of this project. I would also like to thank Mike Buxton and Yongxiang Yang from the TU Delft for their guidance and feedback. Finally I want to thank all my family and friends for their emotional support during my work on this project.

Wesley van Maanen

Contents

List of Figures

List of Tables

List of Abbreviations and Symbols

Abbreviation or Symbol	Meaning	Unit
BOF	Basic Oxygen Furnace	
BOS	Basic Oxygen Steelmaking	
BF	Blast Furnace	
EAF	Electric Arc Furnace	
LD	Lina-Donawitz Steelmaking	
Blow	Single batch process of turning hot metal into steel	
Heat	Single batch process of turning hot metal into steel	
Pig Iron	Intermediate heated iron product containing (4-5%carbon)	
Hot metal	Intermediate heated iron product containing (4-5%carbon)	
Scrap	Used or Re-used steel	
Slag	Oxidisid material in emulsion above the hot metal bath	
SEM-EDS	Scanning Electron Microscope-Energy Dispersive X-ray Spectroscopy	
OES	Optical Emmission Spectrometry	
ICP	Inductively Coupled Plasma	
IMPHOS	Improved Phosphorus refining project	
Cup height	Measurement level of IMPHOS sample within converter	
Dip Number	Measurement time of IMPHOS sample taken every 2 min	
B2	Basicity	
Fe	Iron	
Mn	Manganese	
P	Phosphorus	
C	Carbon	
S	Sulphur	
Si	Silicon	
wt%	Weight percentage	%
Tuyere	Nozzle through which oxygen gas is blown into converter	
Lance height or h	Position of the oxygen lance within converter	m
PCR	Post Combustion Ratio	
$\Delta G(T)$	Reaction potential	J
L_{Mn}	Partition ratio	
k_{Mn}	Manganese equilibrium	
k'_{Mn}	Apparent manganese equilibrium	
C_{Mn}	Manganese capacity	
K	Mass transfer parameter	m/s
d	Droplet diameter	m
A	Surface area	m^2
V	Volume	m^3
r	Radius	m
N_B	Dimensionless blowing number	
σ_1	Surface tension of steel	N/m
ρ_g	Density of oxygen gas	Kg/m^3
ρ_1	Density of steel	Kg/m^3
g	Gravitational acceleration	m/s^2

Abbreviation or Symbol	Meaning	Unit
u_g	Tangential velocity	m/s
u_j	Jet impact velocity	m/s
u_o	Nozzle exit velocity	m/s
u_{drop}	Droplet ejection velocity	m/s
R	Gas constant	J/mol*K
P_e	Nozzle exit pressure	Pa
P_o	Atmoshperic pressure	Pa
a	velocity constant for hot metal data	
d_{throat}	Nozzle throat diameter	m
R_B	Droplet generation rate	Kg/s
F_G	Gas flow rate	m^3/s
R_S	RRS distribution function	%wt
n	parameter describing homogeneity of size distribution	
d'	Variable parameter describing droplet fineness	
D	Diffusivity	m^2/s
t_c	Droplet contact time	s
μ	Viscosity	Pa*s
T	Temperature	K
E_{Kd}	Kinetic energy adsorbed by droplets	J
E_{Kg}	Kinetic energy exerted by gas	J
W_{bath}	Total mass of hot metal bath	Kg
WMn_{bath}	Total mass of manganese in the hot metal bath	Kg
WFe	Mass of iron leaving the hot metal bath	Kg
WC	Weight of carbon leaving the hot metal bath	Kg

Part I

Introduction

1

Introduction

The role of Manganese in steelmaking is complex. On one hand it increases mechanical properties in the final steel product on the other hand it heavily influences the slag formation path during a heat (sometimes also referred to as blow). A heat is the batch process in steelmaking were hot processed iron ore (also called pig iron which still contains around 4-5% carbon) is fed together with lime and scrap metal into a steelmaking converter to reduce remaining impurities from the hot metal, which are for instance carbon, phosphorus, manganese and sulphur. This removal of impurities is done by blowing oxygen gas into the hot metal bath, which reacts with the iron and impurities to form an oxidised slag-metal emulsion on top of the hot metal bath. This process takes place with temperature conditions ranging from 1600K at the beginning of a heat until 2000K at the end of a heat. The slag composition is important, because it can either become very liquid(less viscous slag) or dry(very viscous slag) depending on varying manganese and iron oxide content in the slag. A very liquid slag can lead to inefficiency losses because of slopping. A very dry slag can be hard to remove from the refined hot metal, this also leads to efficiency losses. Controlling slag viscosity is essential for improving the efficiency during a steelmaking blow. The chemical behaviour of manganese in steelmaking is complex because the element is readily oxidized in conditions found in steelmaking (Rout et al. 2018).

The 2007 IMPHOS: improved phosphorus refining project, provides in-situ measurements at multiple heights within the steelmaking converter for the first time. This is an unique experiment conducted by the EU research fund for coal and steel in cooperation with Corus UK, Tata Steel and MEFOS. Every 2 min during the 16 min blow, 8 samples were taken from 7 different heights within the 6t MEFOS pilot scale converter. These valuable samples were obtained with an experimental automated sampling lance for in total 20 different heats. Analysis of these samples resulted in information about the hot metal bath and metal-slag emulsion composition and temperature over time at various locations. This research was originally done to investigate how phosphorus refines within the converter and how it influenced slag formation and slag development. It was found that when the slag is highly oxidised, the metal droplets in the metal-slag emulsion are readily oxidised in the slag. Furthermore it was found that carbon and manganese reactions were primarly driven by metal-slag reactions and not bulk bath-slag reactions. More details about IMPHOS methodology and findings are explained in chapter 3 of this report.

Manganese shows multiple oxidation and reversion stages throughout the blow due to the dependence on temperature and slag composition of the reaction direction. Especially the reversion phase is interesting for this research. This "manganese reversion" is a phenomena where MnO in slag dissociate into Mn and transfer of Mn takes place from slag to bulk metal. This phase is very hard to predict with modelling and will be of key interest for this research. Manganese masstransfer between the hot metal bath and slag takes place in 3 different zones: the jet Impact zone at the top of the hot metal bath, were the oxygen reacts first with the hot metal bath. The slag metal-bath reaction zone, a thin interface between the hot metal bath and the slag emulsion. Finally the 3rd reaction zone is the slag-metal emulsion zone where droplets containing CO gas and metal react with the oxidised slag. Rout et al. (2018) showed that this zone contributes the most to the masstransfer of manganese during the reversion phase. The scope of this research will be focused on the manganese transfer in the slag-metal emulsion zone. The contribution of manganese mass transfer in the jet

impact zone and slag-hot metal bath interface to the overall manganese mass transfer and refining behaviour will be out of scope for this research. More explanation about the steelmaking process and the role of manganese in steelmaking can be found in chapter 2.

The main goal of this research is to get a better understanding of the manganese refining path, due to manganese mass transfer in the slag-metal emulsion zone, by using the data collected from the IMPHOS project published in Millman et al. (2011).

The following research questions were formulated in order to reach the goal of this study:

- Are thermodynamic models for manganese distribution calculation from literature, applicable for the prediction of the 3 different behavioral phases of manganese in IMPHOS?
- What is the influence of the slag-metal emulsion droplets size on the manganese refining behaviour?
- What is the influence of metal-slag data input obtained from 2 different heights in IMPHOS, on the final resulting manganese behaviour in the kinetic model made in python?
- Were there any chemical deviations in different zones of the hot metal bath during IMPHOS project sampling?

To answer these research questions the following work is done during this research:

- Thorough data analysis is performed on the IMPHOS data to identify heats showing reversion and to identify the heats without reversion. Multiple thermodynamic models were tested on this data, to identify the most accurate manganese equilibrium calculations based on thermodynamic relations from literature. These equilibrium calculations are used in developing a kinetic model that will be based on the IMPHOS sample data. Chapter 4 of this report contains the methodology used for the thermodynamic analysis of the IMPHOS heats selected for this research. This heat selection is also described in this chapter. The results of the thermodynamic data analysis can be found in chapter 7 of this report.
- A kinetic model is made in python, were the kinetics involving the manganese mass transfer in the slag-metal emulsion zone as predicted by this model, will be influenced by different process parameters. These parameters are converter conditions as temperature, slag composition, amount and velocity of oxygen flow and lance height position of the oxygen blowing lance, the amount of droplets in the slag emulsion, their size , velocity and residence time within the slag emulsion. How these parameters are implemented in the kinetic model written in python is explained in chapter 5 of this report. The results and most important findings by the modelling done are described in chapter 7 of this report.
- Original IMPHOS samples taken from one height in the top part of the hot metal bath were analysed for one IMPHOS heat. This analysis is done to investigate wether the hot metal bath in the 6t MEFOS pilot scale converter, contained structural deviations in chemical content. These original IMPHOS cup samples are processed and analyzed with different measurement techniques further explained in chapter 6. This chapter contains the methodology used in analysing the physical IMPHOS samples. These samples were never analyzed before due to a lack of resources. The outcome of this analysis will be published in this report. The original IMPHOS hot metal bath chemical composition was derived from the lowest measurement height within the hot metal bath. By comparing the results from this sample analysis at the top part, with the values obtained at the bottom part, these possible deviations within the IMPHOS hot metal bath can be obtained. The results of this physical sample analysis can be found in chapter 9.

The project results are discussed in chapter 10 of this report. From this discussion the most important conclusions of this research are presented in chapter 11. In this chapter all research questions will be answered. Finally in chapter 12 the most important recommendations are discussed for future research about manganese refining in converter steelmaking.

Part II

Theory

2

Background Information

This chapter discusses the overall steelmaking converter process together with the importance and details of manganese refining in steel making. Furthermore different manganese thermodynamic equilibrium models will be discussed. Also more information will be given about past manganese kinetic modelling studies.

2.1. The converter process

2.1.1. Steelmaking overview

The integrated route steelmaking process from iron ore to steel consists of multiple steps. In modern steel making there are two possible routes to produce steel. These routes can be seen in figure 2.1. The first and the most popular one is the blast furnace (BF) route in the bottom part of the figure. At the start of this route prepared iron ore is fed together with coke of different mixed carbon contents to obtain liquid(pig) iron. This pig iron is then fed together with scrap and lime into the oxygen steel making converter known as the BOS (Basic Oxygen Steelmaking), BOF(Basic Oxygen Furnace Steelmaking) or LD process (Lina-Donawitz steelmaking), where impurities are reduced to obtain steel (Williams 2016). Paragraph 2.1.2 will discuss the oxygen steelmaking converter more into detail.

The other steelmaking route in the top part of figure 2.1 first processes iron ore with the so called direct reduction method into a low carbon containing solid (sponge) iron. This sponge iron is then fed together with scrap and lime to the electric arc furnace (EAF). The electric arc furnace can also be fed with 100% scrap to produce steel. After the refining in the BOF and EAF, the steel is casted in a continuous casting plant (Williams 2016). The final processing step includes the casted steel being sent to the rolling mills. There are several different types of mills available where the casted steel can be processed into a varying thickness of 0.1mm to 5mm. depending on the purpose/use of the steel end product.

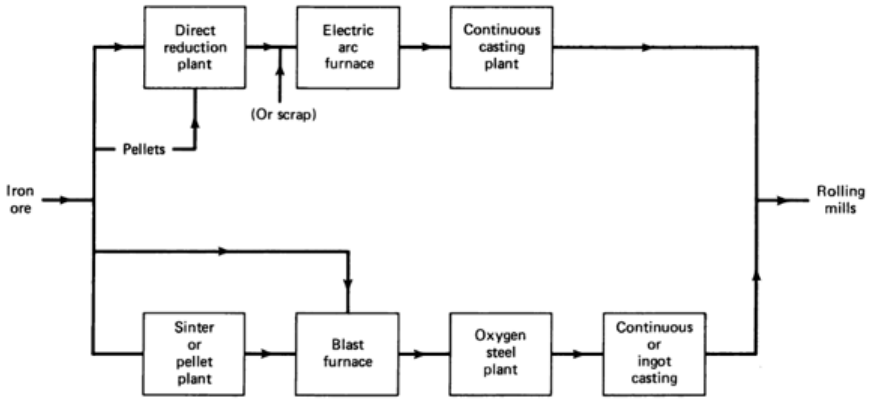

Figure 2.1: Overview of the steelmaking process routes (Williams 2016).

2.1.2. The oxygen steelmaking process

The main feature in the oxygen steelmaking process is the blowing of pure oxygen into a bath consisting out of a mix of pig iron and scrap. The goal of this process is to lower the carbon to a value under 1 % (usually less than 0.1%) in combination with reducing the value of other impurities like phosphorus and sulphur. Figure 2.2 shows the different steps during a blow (Miller et al. 1998). A converter vessel can be divided in 3 different parts a spherical bottom, a cylindrical shell and an upper cone. Capacity varies from 50 - 400 t but most of the converter vessels have a capacity over 200 t. The converter is filled inside with refractory lining consisting out of mixtures of magnesia and lime. This mixture reduces the wear of the lining against corrosive materials in the slag (Jalkanen & Holappa 2013).

The first step of the process is charging the barrel shaped converter with scrap metal. According to Turkdogan (1996) scrap composition should always be considered and calculated before the start of the heat. Scrap can contain unwanted residual elements that cannot be oxidised in the converter for instance tin or nickel. Scrap density is also important in steelmaking heavy scrap and light scrap is often mixed 1:1. The light scrap is loaded in first to reduce wear on the present refractory lining within the converter. The main purpose of adding scrap together with the hot metal is cooling the total temperature of the heat. The heat released in oxidation of carbon and other components is consumed in melting of the charged scrap, in heating the iron melt well over the melting temperature of low-carbon steel, typically to 1923–1973 K (1650-1700°C), and in heat losses (Jalkanen & Holappa 2013).

The 2nd step in the process is the loading of the converter with the initial desulphurized hot metal. Table 2.1 from Turkdogan (1996) gives the general composition of the pig iron. The actual hot metal composition is calculated at the beginning of the blow. The hot metal feed also influences the starting basicity of the slag. This basicity is given in equation 2.1 and is often referred to as B2.

$$B2 = \frac{\%CaO}{\%SiO_2} \tag{2.1}$$

Before the start of the blow the hot metal is pre-treated. This hot metal desulphurization is done by injecting lime and magnesium to the hot metal, leading to a significantly typical reduction from 0.0025% to 0.002% of sulphur (Miller et al. 1998).

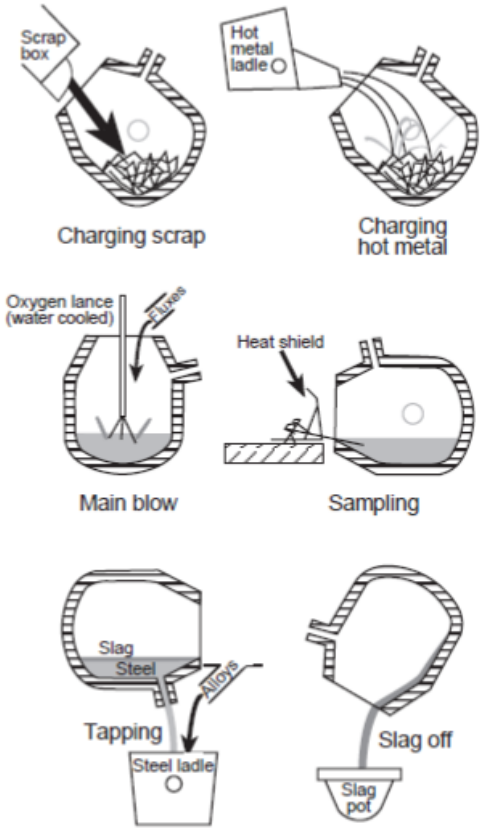

Figure 2.2: Schematic of operational steps in BOF process (Miller et al. 1998).

Table 2.1: General composition of elements found in the hot metal input in steelmaking (Turkdogan 1996).

Element	wt %
C	5
Mn	0.4-0.7
Si	0.4-1.0
P	0.05-0.10
S	0.002-0.005

The 3rd step is the main oxygen blow through the converter. There are 3 different variations used in industry for the Main blow process.

- Top blowing process
- Bottom blowing process
- Combined blowing process

The top blowing process uses a water cooled lance from the top that sprays oxygen gas at supersonic velocities, through 3 to 5 nozzles located at the end of the lance. The lance will then be lowered hanging from the top of the converter into the furnace. Lime is added from above as additional slag forming flux. Changing the lance height, heavily influences the rate of forming of the slag and oxidation of manganese and iron leading, to a lower viscosity of the slag for a higher lance position and higher viscosity of the slag for a lower lance position. Normal oxygen blowing rate is 6-10 $m^3 min^{-1} ton^{-1}$ Jalkanen & Holappa (2013).

In the bottom blowing process oxygen comes from tuyeres installed in the bottom of the converter vessel. A tuyere is a nozzle through which oxygen gas is blown into the converter. These tuyeres are cooled with methane by thermal decomposition of the gas. Because the oxygen comes from beneath the vessel, it creates stirring in both the bath and the slag emulsion.

The combined blowing process uses both features of the top blowing process and the bottom blowing process. Companies normally chose for a combined blowing process, to reduce operating costs. This is done because there is more slag forming and reduced FeO in the slag by the additional bottom stirring (Miller et al. 1998). Figure 2.3 shows the possible blowing layouts of the steel converter. At Tata steel Ijmuiden the BOF top blown process is used.

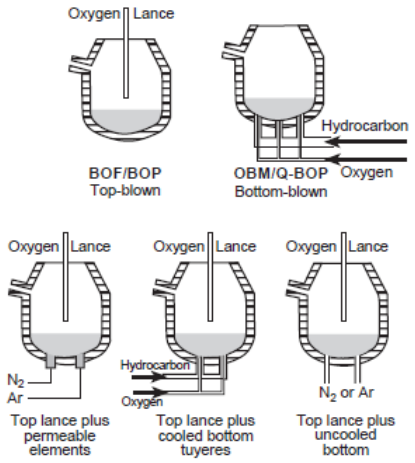

Figure 2.3: Overview of the steelmaking process routes (Miller et al. 1998).

For the normal top blow process lance height position determines the stirring of the slag. If the lance is lowered too much the carbon removal is high, but the removal of phosphorus and iron oxide is lower because of less slag formation. If the lance position is too high the carbon removal rate is lower and the possibility of slopping occurs. Determining correct lance height is often done on a trial and error basis.

The 4th Step in the converter process is the sampling. Sampling is done with a sampling sub-lance to check the mechanical condition of the converter and the chemical analysis of the heat. This can lead to maintenance of the converter or to the decision that an additional change to the heat should be made. The tap is most often done with a sub-lance in while the furnace is in a tilted position.

The final step is the tapping of the final steel product and the removal of the impurities containing slag. The success of a tap depends on the efficiency of the slag removal from the steel. The main reason for this is that

some slag can enter the tapping ladle near the end of the tap. On the other hand the loss of the steel in the slag pot is also possible when steel is prevented to enter the tap openings.

2.1.3. Waste slag recycling

The final steel product is moved to the casting plant, while the slag is rapidly cooled using water. The average final slag composition range according to Huiting & Forssberg (2003) is found in table 2.2.

Table 2.2: General end composition of converter slag (Huiting & Forssberg 2003).

Oxides	wt%
Fe_tO	14-30
CaO	25-55
MgO	2.5-15.0
SiO_2	9-19
MnO	1.5-10.0
Al_2O_3	0.9-7.0
P_2O_5	≤0.9
S	≤0.07

To reduce the waste from slag as much as possible, the slag can used for many different purposes. Reusing slag is very important for improving the contribution of steelmaking to the circular economy. Table 2.3 shows the usage of converter slag according to its different characteristics. The information used is retrieved from Huang et al. (2012).

Table 2.3: Different re-usage purposes of slag according to slag characteristics Huang et al. (2012).

Characteristics	Applications
Hard, wear-resistant, adhesive, rough	Aggregates for road and hydraulic construction
Porous, alkaline	Waste water treatment
FeOx, Fe components	Iron reclamation
CaO, MgO, FeO, MgO, MnO components	Fluxing agent
Cementitious components (C3S, C2S and C4AF)	Cement and concrete production
CaO, MgO components	CO_2 capture and flue gas desulphurization
FeO, CaO, SiO_2 components	Raw material for cement clinker
Fertilizer components(CaO, SiO_2, MgO, FeO)	Fertilizer and soil improvement

2.1.4. Thermodynamics in converter steelmaking

The rate of removal of impurities in oxygen steelmaking is driven by the thermodynamic equilibrium from each element with its oxide. This thermodynamic equilibrium gives an indication, wether an element oxidises or refines in the converter during a certain period within the blow. In the converter there are different oxidation phases occurring , There is primary oxidation of carbon, iron and other impurities by oxygen blowing in the jet impact area. There is secondary oxidation occurring in the metal emulsion where iron droplets are reacting with slag in the emulsion. There is also tertiary oxidation along the metal bath-slag interface. These phenomena occur during the heat under an increasing temperature leading to different rates of chemical reactions occurring over time. Next to this the oxide containing slag is always changing due to the addition of flux to the converter (Jalkanen & Holappa 2013).

The following standard reactions take place within the converter according to Turkdogan (1996):

$$[C] + \frac{1}{2}O_2 \rightarrow CO(g) \tag{2.2}$$

$$[Si] + O_2 \rightarrow SiO_2 \tag{2.3}$$

$$[P] + \frac{5}{4}O_2 \rightarrow \frac{1}{2}P_2O_5 \tag{2.4}$$

$$[Mn] + \frac{1}{2}O_2 \rightarrow MnO \tag{2.5}$$

$$[Fe] + \frac{1}{2}O_2 \rightarrow FeO \tag{2.6}$$

The thermodynamic equilibrium controls whether the element in the converter oxidises(reaction moves to right)into the slag layer or reverts(reaction moves to the left) to metal bath. Figure 2.4 shows the typical oxidation profiles for different elements within the converter.

In the figure the profiles from Mn and P and Si show rapid oxidation during the first part of the blow. Because of this rapid oxidation, the oxidation of carbon is sligthly slower in the beginning of the blow, due to less availability of oxygen to react with. In figure 2.4 it can also be seen that manganese and phosphorus are experiencing a reversion phase after the primary oxidation phase after which the both elements are oxidising again. The oxidation rate of carbon is important within the converter process. Postcombustion of formed carbon monoxide into carbon-dioxide can increase the temperature within the converter until a certain threshold value is reached, a higher postcombustion ratio can result in a more efficient process. Equations 2.7 and 2.8 gives the formula for postcombustion and the calculation of the postcombustion ratio (Jalkanen & Holappa 2013).

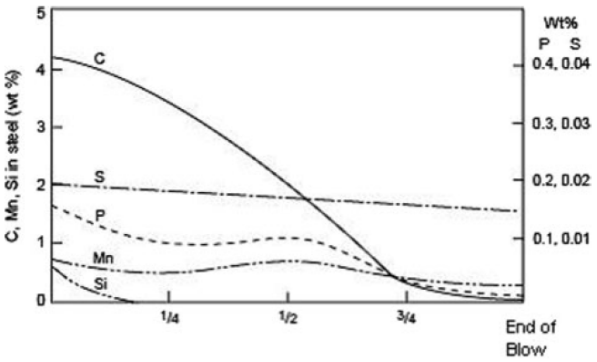

Figure 2.4: Typical metal composition change during blow (Hewage et al. 2016).

$$CO(g) + \frac{1}{2}O_2(g) \rightarrow CO_2(g) \tag{2.7}$$

$$PCR = \frac{\%CO_2}{\%CO + \%CO_2} \tag{2.8}$$

The main driving force in the removal profiles of impurities is the standard affinity of oxidation of the different elements or reaction potential. It defines the amount of oxygen a certain element can consume in the iron melt. Equations 2.9 and 2.10 gives the standard oxidation reaction with its reaction potential (Jalkanen & Holappa 2013).

$$\frac{2\alpha}{\beta}[E]_{Fe} + O_2(g) = \frac{2*(E_\alpha O_\beta)_{slag}}{\beta} \tag{2.9}$$

$$\Delta G(T) = \Delta_r G^*(T) + RTln[\frac{x^{\frac{2}{\beta}}(E_\alpha O_\beta)_{slag}}{(\frac{p_{O_2}}{p^*})*x_{[E]}^{\frac{2\alpha}{\beta}}}] + RTln[\frac{\gamma^{\frac{2}{\beta}}(E_\alpha O_\beta)_{slag}}{(\frac{p_{O_2}}{p^*})*\gamma_{[E]}^{\frac{2\alpha}{\beta}}}] \tag{2.10}$$

In this equation E stands for a general element(Mn,P,Si,Fe etc).α and β stands for molar fraction of the element in the reaction with oxygen. G is the Gibbs energy which gives the reaction potential of a chemical reaction. T is the temperature in K. R is the molar gas constant in $J*K^{-1}*mol^{-1}$. x_i is the concentration and y_i is the activity coefficient of the element in the reaction. P_{O_2} gives the oxygen pressure and P^* is the standard pressure.

If the reaction potential moves to zero the reaction rate moves to zero to and a state of equilibrium is reached. If the potential becomes more negative the reaction rate increases, the reaction is moving away from equilibrium. More information about the thermodynamic equilibrium of manganese will be presented in paragraph 2.2.2.

2.1.5. Monitoring the converter process and importance of IMPHOS data

In today's steelmaking practices static models are widely used. According to Williams (2016) "A static model is one which based on the known input parameters to the furnace, such as hot metal quality, hot metal weights and the required end point expressed in terms of carbon sulphur and other analyses" (Williams 2016). The model itself then predicts the other input parameters required like flux and oxygen content. The following figure 2.5 gives an overview of all the different parameters involved in these static models. The figure shows that first an initial weight composition and strength for the final steel is described as preferred result. According to steel needs the estimated loss of heat of slag and waste gas is used as input to predict the decarbonization(reduction of carbon) rate and iron loss to the slag. Based on the final result and the predicted reaction rates, the hot metal input is calculated in combination with the desired oxygen flow. Furthermore the amount of scrap and lime which should be added to hot metal is calculated. After the heat starts it is very difficult to change process variables in situ to alter the outcome of the final steel product.

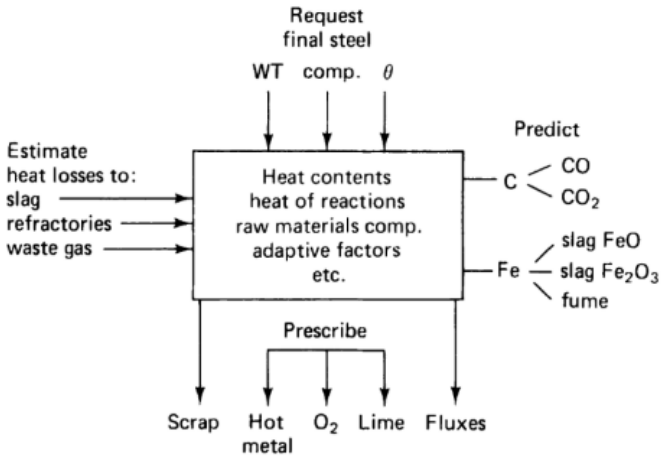

Figure 2.5: Static model input parameters (Williams 2016).

In modern steelmaking there is a growing need for more dynamic models, to make the steelmaking process more efficient. Dynamic models use in-situ measurement of metal and slag composition, to change process variables as position of the oxygen blowing lance during the blow. The height of the oxygen lance influences

the oxygen feed into the converter. 'The problem so far is that these in-situ measurements are very hard to obtain, because of the extreme conditions within the converter. IMPHOS improved phosphorus refining project was the first project in the world, where in the MEFOS 6t converter unique in-situ measurements were performed over 16 min of the blow at different heights. These physical hot metal and metal-slag emulsion samples taken from the pilot scale converter, are the base for future improvement of understanding in-situ reaction kinetics and for the development of more time-varying converter models. More about the IMPHOS sample measurements can be found in chapter 3.

2.2. Manganese in steelmaking

2.2.1. Manganese properties in steel

Manganese has multiple important functions in the steelmaking process. It serves as an important alloying element in commercial grades of steel. A high percentage of manganese in the steel end product can improve the mechanical properties of the steel, such as hardenability, toughness and strength (Morales & Fruehan 1997). However normally adding manganese to create a high strength steel comes with a decrease in plasticity (Kaar et al. 2019). In contrast to this strength increase, low Mn is required for ULC (ultra-low carbon) steels that require deep drawing applications. These are very flexible steels. (Rout et al. 2018).

High manganese yield and precise control of manganese are becoming important. Manganese yields are affected by several factors, e.g., oxygen potential, slag composition, slag volume, temperature and so on. These factors must be examined and improved in order to get high manganese yield (Takaoka et al. 1993). To raise the amount of manganese in the end steel product, most steelmaking companies favor the economic benefits of adding extra manganese ore to the converter process, instead of adding ferromanganese in secondary steelmaking. Lytvynyuk et al. (2013) showed that adding 10kg of additional manganese containing lean iron ore, can lead to an increase between (0.03%-0.04%) of manganese in the end steel product. Manganese highly influences the slag viscosity. Low slag viscosity due to high manganese contents can lead to slopping, refractory lining consumption and yield losses (Rout et al. 2018). In contrary low MnO and FeO content slag can lead in combination with high silicon, to a very dry slag because silicon also influences the activity of MnO as stated in both Vargas-Ramirez et al. (2002) and Jamieson & Coley (2017). Steelmaking in practice is always finding a balance between optimizing the decarbonization rate, without a drastic change in slag viscosity that can lead to very viscous or dry slag. Dry slag will lead to a lower efficiency in removal of the slag from the metal bath in the final converter step, when the steel is tapped from the vessel.

Figure 2.6 shows the lance position during a blow. Lowering the lance height will cause a faster decarbonization rate and more variation in the removal of impurities, but can lead to a very dry slag due to the reduction of FeO and MnO. If the lance position is too high the slag starts becoming less viscous and then the slopping problems occur. Each converter process is unique, so understanding the slag forming path of manganese is crucial in optimizing the converter process. As discussed in paragraph 2.1.4 static models are currently used in industry, developing a kinetic model which can predict the refining of Mn during the blow, which is necessary to accomplish this understanding.

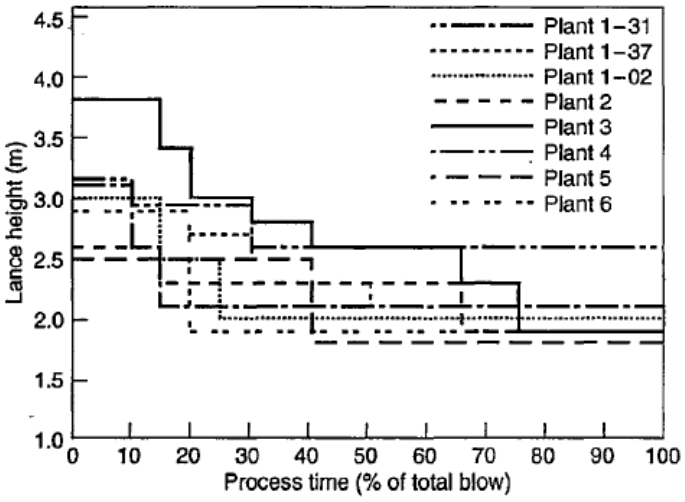

Figure 2.6: Overview of typical lance position during blow (Turkdogan 1996).

2.2.2. Thermodynamic equilibrium models for manganese

A lot of previous research is done to predict the thermodynamic equilibrium of manganese under varying temperature, basicity and slag composition. The results obtained from these studies are used to develop correlations for the partition ratio. The partition ratio describes the relation of the element as metal to its oxide in the slag. The partition ratio for manganese is described in equation 2.11 retrieved from Morales & Fruehan (1997).

$$L_{Mn} = \frac{(\%MnO)}{[\%Mn]} \tag{2.11}$$

The apparent equilibrium and equilibrium are often found as relation of the manganese oxide content to iron oxide content and manganese in the metal bath. For this type of research the equilibrium and apparent equilibrium quotient is often found as described in Morales & Fruehan (1997):

$$k_{Mn} = C * \frac{\gamma_{MnO}(\%MnO)}{f_{Mn}[\%Mn] * \gamma_{FeO}(\%Fe_O)} \tag{2.12}$$

$$k'_{Mn} = \frac{(\%MnO)}{[\%Mn] * (\%Fe_tO)} \tag{2.13}$$

Were γ_{MnO},γ_{FeO} and f_{Mn} are the activity coefficients of the manganese oxide in the slag, the iron oxide in the slag, and the manganese in the hot metal. $(\%MnO)$, $(\%FeO)$ and $(\%Mn)$ are the mass percentages of manganese oxide in the slag, iron oxide in the slag and Manganese in the hot metal respectively. sometimes a relation is derived for the manganese capacity. For instance in equation 2.14 retrieved from Suito & Inoue (1984*b*).

$$C_{Mn} = \frac{(\%Mn)}{[a_{Mn}] * [a_O]} \tag{2.14}$$

All these relations are not directly obtained from scientific formulas but are semi-empirical. Most of the research is performed under experimental conditions within a lab and do not include the kinetics of manganese under converter condition. The goal of using these relations is to find an equilibrium value of manganese content at slag-metal reaction interface.

The most important findings from previous research are presented as follows:

- Duan et al. (2017) stated that the oxidation rate of manganese through use of fine iron ores is higher than using pure oxygen. Also the activity of MnO in the slag decreased with basicity and increasing Fe_tO content. This relation is also found in Shin et al. (2019) were the behaviour for phosphorus was found to be opposite to manganese for a decreasing basicity.

- Morales & Fruehan (1997) Also discovered that the value of the manganese partition ratio was decreasing with decreasing basiscity B2 and increasing with Fe_tO content. Thus the manganese content in the slag is increasing with decreasing basicity.

- Extensive thermodynamic research of Hideaki Suito and Ryo Inoue resulted in the development of 3 different manganese distribution models. Suito & Inoue (1984*a*) researched the manganese distribution between 1550 and 1650 °C with added MgO crucibles and found that the manganese distribution ratio was increasing with an increase in SiO2 content and decreasing with temperature. This conclusion was supported by Suito & Inoue (1984*b*). The 3rd model derived in Suito & Inoue (1995) analyses a $CaO - SiO_2 - Fe_tO - P_2O_5$ slag at 1600 °C . It was found that the manganese distribution ratios were also more dependent on iron content and increased with increasing basicity.

- Meraikib (1993) researched the manganese distribution between sponge iron and scrap between 1550-1670°C. Temperature was found to be of bigger influence on the activity coefficient of manganese oxide than basicity. The same was concluded for the manganese capacity.

- An increase of iron oxide activity and manganese oxide activity was found for an increase in slag basicity in Kim et al. (2013) and for a higher FeO content at constant slag basicity. Finally in Jung (2003) an increased manganese partition was also found for a higher Fe_tO content.

Table 2.4 and 2.5 shows the different conditions as slag composition and temperature range for the different thermodynamic studies. A summary of the thermodynamic correlations used to derive the manganese distribution in different studies, can also be found in Duan et al. (2016).

Table 2.4: Summary of slag composition and temperature range for the different thermodynamic equilibrium studies on manganese distribution.

Model	Slag composition	Temperature range in K
Suito No.1	MgO-saturated CaO-Fe_tO-SiO_2-MnO	1823-1923
Suito No.2	Fe_tO-MnO-MO_x (MO_x = P_2O_5-SiO_2-$AlO_{1.5}$-MgO-CaO)	1823-1923
Suito No.3	CaO-SiO_2-Fe_tO-P_2O_5 <0.9 - MnO(8-16%)	1623-1923
Merakaib	FeO-MnO-CaO-MgO-SiO_2-P_2O_5	1823-1943
Kim	FeO-MnO-MgO-P_2O_5-SiO_2($-CaO$)	1673
Jung	CaO-SiO_2-FeO-MgO-MnO with saturated $CaO*SiO_2$ and MgO	1823-1923
Morales and Fruehan	CaO-SiO_2-MnO-Fe_tO-P_2O_5-MgO	1873

Table 2.5: Summary of apparent equilibrium for the different thermodynamic equilibrium studies on manganese distribution.

Model	K'_{Mn}
Suito No.1	$\frac{\%MnO}{([\%Mn]*(\%FeO))}$
Suito No.2	$\frac{N_{MnO}}{(N_{FeO}*[\%Mn])}$
Suito No.3	$\frac{\%MnO}{([\%Mn]*(\%FeO))}$
Merakaib	$\frac{(\%MnO)}{([\%Mn]*[\%O])}$
Kim	-
Jung	-
Morales and Fruehan	$\frac{\%MnO}{([\%Mn]*(\%FeO))}$

It can be seen that multiple thermodynamic studies resemble the same conclusions for different experimental set-ups. For the modelling of manganese kinetics in this research different equilibrium models will be evaluated beforehand. It is important that the equilibrium model used for modelling should resemble the same temperature range and slag composition as used in the IMPHOS data where this research is based on. More information about manganese thermodynamic equilibrium selection can be found in chapter 4.

2.2.3. Manganese refining and kinetic modelling

To understand the manganese refining, knowledge of the reaction kinetics is essential in predicting the intermediate compositions of the metal and slag phases over time, during the process achieving instantaneous equilibrium (Deo & Boom 1993). However as explained in 2.1.4 currently only static models are often used in the steelmaking industry. These static models only captures the slag-metal equilibrium at the final stage and gives no information about the equilibrium condition during the intermediate stage of refining.

For developing dynamic BOF models, a understanding of the manganese refining profile and the reactions taking place in different parts of the converter are necessary. Figure 2.7(a) from Rout et al. (2018) shows the typical Manganese refining path in a top blowing oxygen steelmaking process.

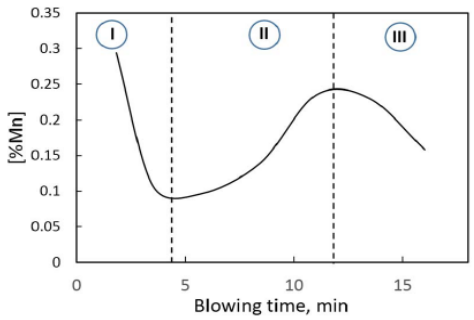

(a) Typical manganese refining path in top blow converter (Rout et al. 2018).

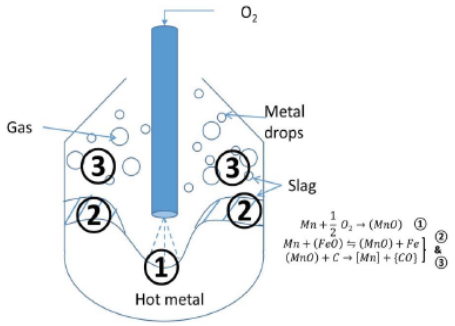

(b) Schematic view of 3 regions within converter where oxidation and reduction takes place (Rout et al. 2018).

Figure 2.7: Manganese typical refining profile(a) and reaction zones(b) in the converter

In the first part of the blow(region I) the manganese rapidly oxidises until 1/3rd of the blow and then the manganese starts to revert from the slag into the metal bath in region II. This reversion is slower than the primary oxidation as proven by Kawai et al. (1982). Region III gives the second oxidation stage resulting in a manganese end value in the final steel. According to Rout et al. (2018) and Takaoka et al. (1993) oxidation and reduction takes part in 3 different regions within the converter. Figure 2.7(b) from Rout et al. (2018) shows these 3 different regions within the converter. The first region is the jet impact zone, the main region where the oxygen blown through the top jet reacts with the hot metal as shown in equation 2.15.

$$[Mn] + \frac{1}{2}O_2(g) = (MnO) \tag{2.15}$$

The 2nd region is the slag/metal-bath interface. Thermodynamic research as presented in paragraph 2.2.2 concluded that this reaction was driven by the Fe/Fe_tO potential. So the manganese in the bulk metal reacts with the FeO in the slag. The 3rd reaction zone is the slag-metal emulsion zone above the hot metal bath where metal and carbon containing droplets are reacting with manganese oxide forming manganese and carbonoxide gas. Equation 2.16 and 2.17 illustrates these reactions.

$$(FeO) + [Mn] = (MnO) + [Fe] \tag{2.16}$$

$$[C] + (MnO) = [Mn] + CO(g) \tag{2.17}$$

The reactions in 2.16 and 2.17 around the droplet-slag interface are schematically displayed in figure 2.8

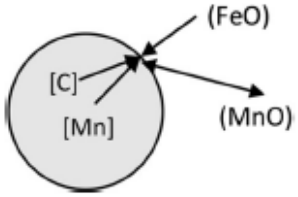

Figure 2.8: Mass transfer reaction between droplet and slag (Rout et al. 2018).

Modelling manganese kinetics is not simple, Hewage et al. (2016) designed a model with first order kinetics based on the IMPHOS data. This model evaluated the refining path of silicon, carbon, manganese, and phosphorus, with the use of simple reaction kinetics. The basics of reaction kinetics in steelmaking is often given by Fick's first law of diffusion. The law states that the diffusion of the species is proportional to the concentration gradient of the species (Dogan 2011). Equation 2.18 gives Fick's first law of diffusion.

$$\frac{dC}{dt} = k * A * \frac{\rho_m}{W_M}(C_b - C_e q) \tag{2.18}$$

It was found that using first order kinetics and static equilibrium worked for predicting silicon and carbon accurately. However the prediction of manganese only worked for a certain amount of heats. The heats with a more severe manganese reversion shows less resemblance to the calculated refining path, than heats with less reversion. First order kinetic models are not always accurate in predicting reversion, because of a missing detailed description of parameters as droplet interfacial area, droplet volume change and mass transfer coefficient.

In Rout et al. (2018) The mass transfer in the emulsion zone was found to have the biggest influence on the manganese reactions. Experimental data was used from a 200t and 55t converter. Figure 2.9 shows the total Mn exchange between 3 zones. It is clearly shown that oxidation takes place in the jet impact zone and that reversion is mainly happening in the emulsion zone.

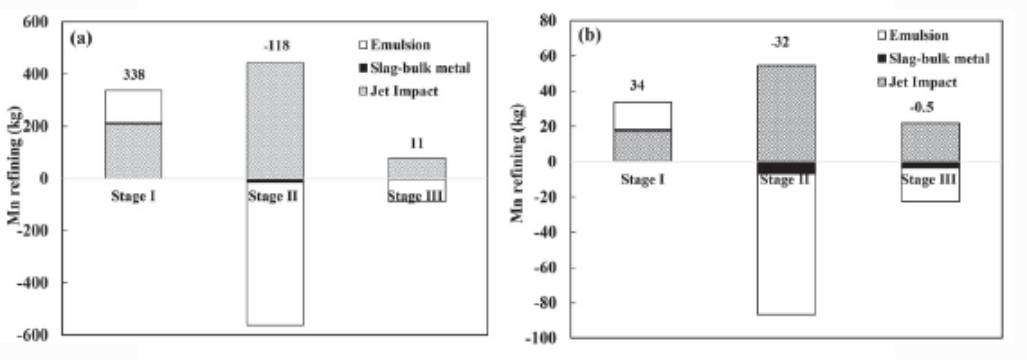

Figure 2.9: Total Mn exchange between metal and slag during stages of blow for a 200t converter(left) and 55t converter(right) (Rout et al. 2018).

One of the first attempts of kinetic modelling of manganese was done by Daines & Pehlke (1971). This research was based on reduction of manganese oxide by using the carbon reaction in equation 2.17. The authors concluded that the reduction of MnO by C is slow and stirring had no apparent effect on the reaction rate. Kato & Okuda (2003) found that for the bottom blow process gas-metal reactions have more influence on manganese distribution than slag metal reactions compared to the top blow process.

Another complete different approach to estimate the manganese content in the BOF process was done by Wang et al. (2012). Semi-heuristic genetic algorithms were used to calculate the Mn content in combination with the back propagation neural network, these results were compared with a multi-linear regression model. The GA-BP network showed better results with 90% of predictions were within 0.03% Mn content.

Finally Kadrolkar & Dogan (2019) researched how the impact of the oxygen blow on the metal bath, causing stirring plumes within the bath, influences refining kinetics with surface renewal theory. It was found that the top blown jets causes a negligible renewal of the surface at the jet impact zone. The stirring plumes causes more metal circulation but were not changing the refining rates at impact and slag metal zone. The most important conclusion was that the contribution of jet impact and slag metal zone to refining is also minor in comparison with the emulsion zone. This supports the findings from Rout et al. (2018)) in figure 2.9.

The next chapter will explain more about the background of the IMPHOS research performed in 2007. Data from this research is used in the current study in this report

3

The IMPHOS Research

This chapter contains a summary of the EU funded RFCS research project undertaken in 2007. The full research report was published in a 200 page report in Millman et al. (2011). Sample data collected from this research is used in the current study on the behaviour of manganese refining. Understanding the project setup and input data and results is a crucial basis for this report.

3.1. IMPHOS project objectives

The IMPHOS project was initially set up to improve monitoring and control of phosphorus refining. Understanding parameters as droplet size and distributions, the stability of foaming in the emulsion and chemical activity at interfaces between different liquid phases and solid phases in the slag , will lead to a better understanding of dynamics that play a role in phosphorus refining. The research is performed in a 6t MEFOS BOS converter where more than 500 samples were taken over twenty-three heats (Millman et al. 2011). For this research the same focus parameters as the IMPHOS research are used, but these parameters as for instance droplet size and distribution are used with a focus on the refining of manganese instead of phosphorus. The measurements were done with a complex sampling device described in paragraph 3.2.2. This initial design enables a sample to be taken from 7 different heights at the same time. This device was used in the converter to take sample measurements at 8 different times during the 16 min blow. Thus a sample was collected from all these heights every 2 minutes. Figure 3.1(a) shows the schematic of the converter where the sampling lance is installed. Figure 3.1(b) shows sampling test measurement. More details about the scale of the sample pot can be found in figure 3.3(c).

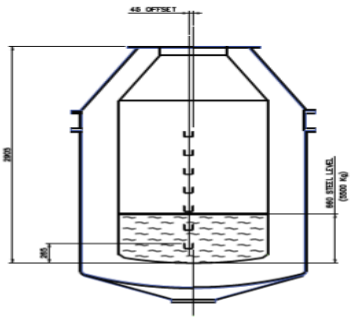

(a) Schematic of the converter showing the 7 different heights of the sampling lance (Millman et al. 2011).

(b) Picture of a sampling test (Millman et al. 2011).

Figure 3.1: Schematic of the sampling lance(a) and picture of a sampling test(b)

3.2. IMPHOS experimental sampling technique

3.2.1. Initial project sampling

To carry out the sample measurements a complex sample system had to be made. First an experimental set up was designed to test the initial sample system design. A schematic sideview of this test sample system can be seen in 3.2. 3.3(b) shows the single testing pot connected to three steel rods. These rods are then connected to another set of steel rods. The purpose of this 2nd set of rods is to make it possible to open and close the lid of the sampling pots. Testing was initially done to check, wether the dimensions of the proposed design were able to withstand extreme conditions within the converter. Chemical segregation and sticking within the sample was reduced as much as possible, by making the sample pot massive. To protect the sampleholder from reacting with high thermal testing environment(1480-1570°C, it was treated with an extra zirconia wash coat on the outside.

The measurement itself was done with a counterbalance mechanism seen in the side view of 3.2. Testing of the sampling design resulted in the choice for the thickest steel rods that were tested, because of some mechanical alteration of the thinner rods due to the extreme conditions within the converter.The high zirconia refractory was proven to be working against skulling melting and distortion (Millman et al. 2011).

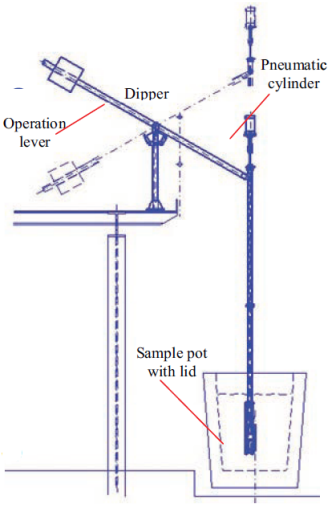

Figure 3.2: Initial side view of the test sampling process (Millman et al. 2011).

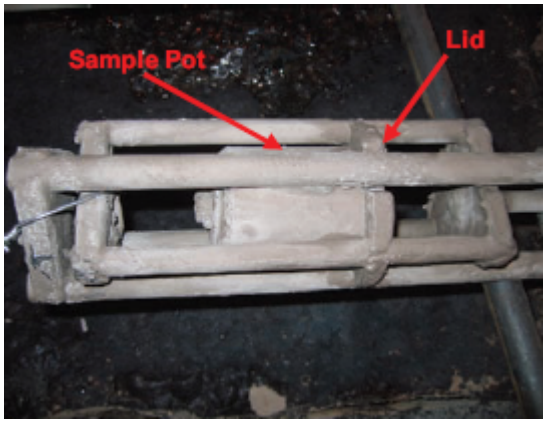

Figure 3.3: Test sample coated with high zirconia refractory (Millman et al. 2011).

3.2.2. Final sampling design

The final sampling design consisted out of the double sets of rod with 7 sampling pots welded inbetween at different heights along the rods. The sampling was done by 5m long automated sampling lances connected to a circular cassette seen in figure 3.4(a). This automated system could perform measurements every 2 min during the 16 min blow. Figure 3.4(b)shows a schematic side view of 1 sampling lance. The schematic of one sampling pot, as already seen in figure 3.3(a) can be seen in 3.4(c). The final sampling design was used to take the samples within the converter during the IMPHOS heats.

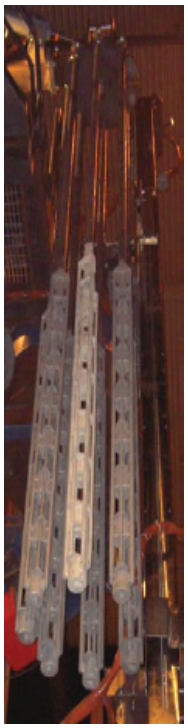

(a) Automated sampling lances connected to the cassette (Millman et al. 2011).

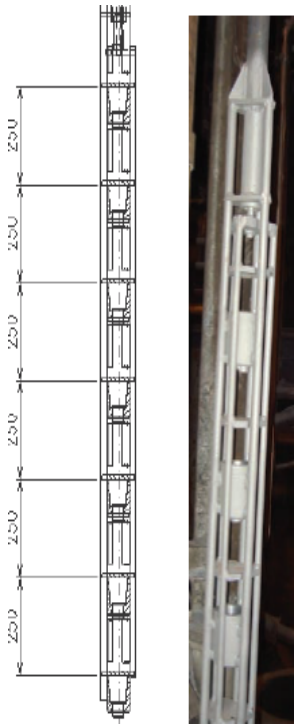

(b) Sample lance schematic (Millman et al. 2011).

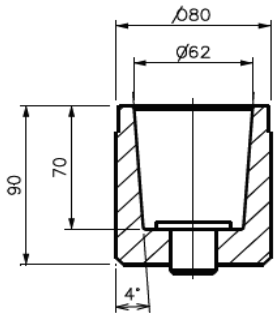

(c) Sample pot schematic (Millman et al. 2011).

Figure 3.4: Sampling casette with connected sampling lances(a) and a schematic view of the sampling lance(b)

3.3. MEFOS BOS pilot converter operation

A schematic of the converter is shown in 3.5(a). The nominal liquid steel height in the converter is 660 mm from the vessel bottom. The converter is lined with Mag-C bricks and is fitted with a single bath agitation tuyere that blows nitrogen at a nominal rate of 0.5 Nm^3/min (Millman et al. 2011). The automated sampling was done with the use of a robotic arm, which took the sampling lances from the cassette above. The sampling lance was placed at 170 mm from the converter bottom. In 3.5(b) the position of the lance can be seen inside the converter. The sample pots were then filled up with steel or slag/metal emulsion between 3-5 seconds. Temperature was also measured with the sublance when the slag samples were taken.
To keep the measurements reliable for comparison and analysis, a standard hot metal composition feed to the converter was necessary. This hot metal was produced in a MEFOS 6t EAF. Table3.1 gives this composition note that heat 1-5 were test heats to optimise the converter operation. In IMPHOS the important heats are numbered from S1828 to S1847. In table 3.1 and 3.2 heat S1828 is heat 6 and S1847 is heat 25.

Table 3.1: Aim of content of base elements present in the hot metal composition feed to the converter (Millman et al. 2011).

Heat	C in wt%	Si in wt%	Mn in wt%	P in wt%	S in wt %	Temp °C
6-11	4.75	0.45	0.45	0.085	0.03	1375
12-17	4.75	0.6	0.45	0.085	0.03	1375
18-25	4.75	0.6	0.45	0.085	0.03	1375

The ratio between the hot metal composition and scrap was calculated beforehand, Also the lime additions to reach the desirable basicity were estimated. Table 3.2 shows these additions in kg. The last column shows the B2.

Table 3.2: Calculated additions to hot metal in kg (Millman et al. 2011).

Heat number	Lance	Lime 80% Yield	Lime in Kg	Scrap in Kg	CaO wt%/SiO2 wt%
6-11	Single Port	210	170	500	3.5
12-17	Single Port	240	194	615	3
18-25	Single Port	280	225	600	3.5

After the samples were, taken the samples were stored in double wrapped plastic. These bags were signed with Heat number / Dip Number(Time of measurement)/ Cup number(Height in converter)). These sample containing bags were then stored in sample containers. The next paragraph discusses the types of analysis done on the sample. Due to financial difficulties because of a declining steel price a decade ago, not all planned analysis could be done at the time. Analysis was done at multiple locations and for a while, the samples were stored at an external location. Tata steel recently regained possession of these sample containers. It is still not very clear which parts of the original samples and analyzed samples are present in these containers. Extensive documentation of the current volume within the boxed containers still needs to be done.

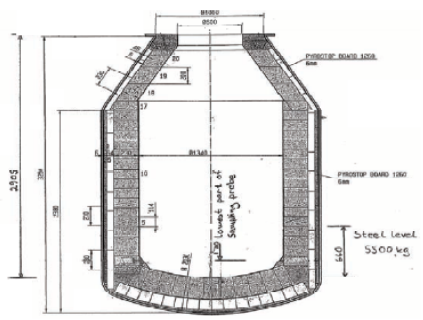

(a) Schematic view of the top blown converter (Millman et al. 2011).

(b) Vertical crossection of metal sample in the sampling pot (Millman et al. 2011).

Figure 3.5: Schematic view of the top blown converter(a) and vertical cross section of metal sample in the sampling pot(b)

3.4. IMPHOS sample analysis

After analyzing the initial collected data eventually 20 heats produced enough data to produce results. These heats are numbered from S1828 until heat S1847. The steel bath samples (sample height number 1) of these heats were analysed on the following as a function of time, sample position and operating practice according to Millman et al. (2011):

- Metal/slag ratio profiles
- Size distribution of steel droplets and bubbles in the slag/metal emulsion
- Steel composition as function of droplet size(C,Si,Mn,P,S)
- Steel bath composition changes(C,Si,Mn,P,S)
- Slag composition($P_2O_5, CaO, SiO_2, MnO, MgO, FeO$)
- Phosphorus distribution at slag steel droplet interfaces
- Phosphorus distribution in the slag component phases
- Lime dissolution characteristics
- Morphology of the slag/metal emulsion samples

Before these calculations were carried out, the metal/emulsion samples were removed from the sample pots and processed with different analytical measurement techniques.

3.4.1. Sample processing and texture analysis

The first step of sample processing was separating the sample from the cup holder. This was done in 2 different ways. The full metal cups at height 1 were horizontally cut 1 cm from the bottom, then a 5 mm thick metal sample could be retrieved from this cut bottom. The slag emulsion samples were treated with resin first and chiseled out because some material was found to be attached to the sample wall. Valuable material was collected with magnetic separation.

The metal samples were first analyzed on bulk chemical composition with Spark OES measurements. Because very porous samples were encountered from 10-12 minutes into the blow these samples were also analyzed with XRF mainly to confirm the Spark OES measurements. The following elements were evaluated: Si, Mn, P, Ca and V. Additional Leico analysis was done to evaluate C and S.

The slag emulsion samples form heat S1845 were analysed with SEM-EDS (Scanning Electron Microscope-Energy Dispersive X-ray Spectroscopy). Because the slag emulsion contained a lot of loose flakes these had to be restored with creating a sort of photoshop mozaik. With these measurements metal droplet compositions could be analysed against droplet size. High calcium concentrations can indicate secondary fluorescence of surrounding slag and creating slight overestimates of manganese and phosphorus (Millman et al. 2011). Figure 3.6 gives the droplet composition of phosphorus and manganese versus size. From this analysis it was concluded that smaller droplets are more refined in comparison to bigger droplets within the metal-slag emulsion.

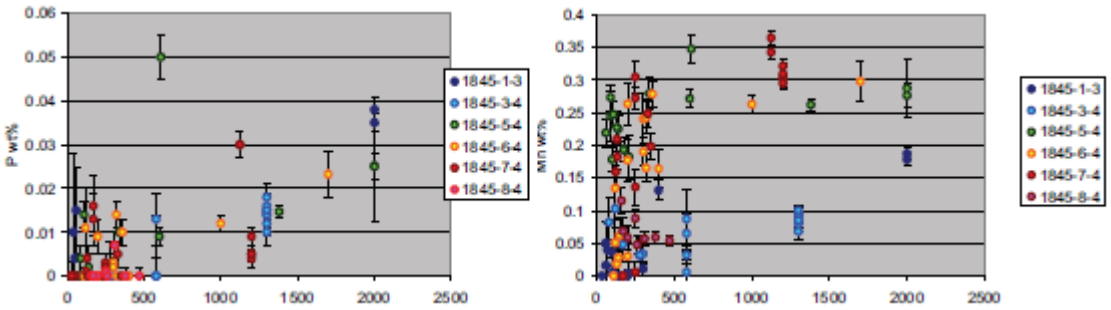

Figure 3.6: Droplet composition of phosphorus(left) and manganese(right) against droplet size (Millman et al. 2011).

3.4.2. Refining profiles

Figure 3.7 gives an example of manganese content over the whole duration of a heat in both the bulk bath as the slag emulsion. For all heats the typical primary oxidation phase can be seen the first 6 minutes. After 6 minutes the reversion starts and the Mn content starts increasing in the bath for heat S1835 and S1836. Until its peak after 14 min and then another short oxidation phase occurs until the end of the blow is reached after 16 minutes. Note that comparing S1835 and S1836 with heat S1843 perfectly illustrates the variance and the difficulty of estimating the manganese reversion behaviour. The IMPHOS report contains many of these kind of data for all relevant elements over the 20 heats.

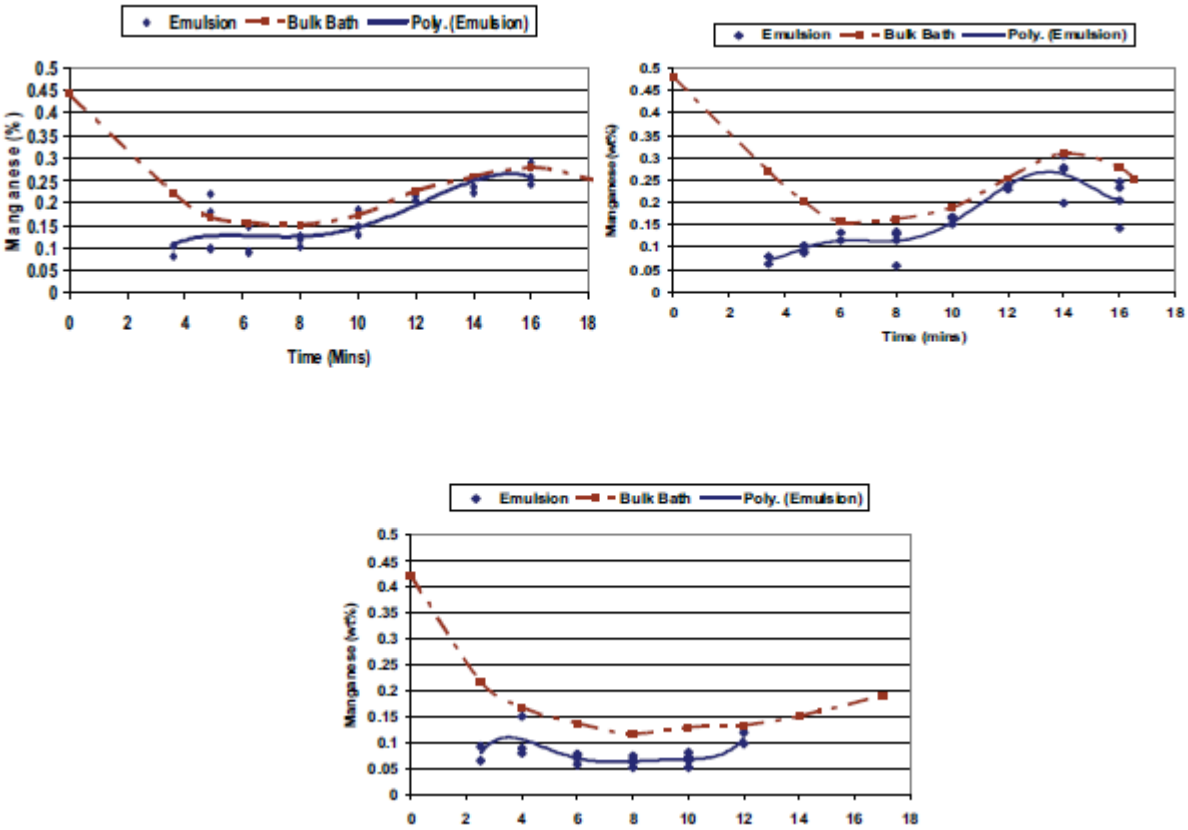

Figure 3.7: Manganese profiles in bulk bath and emulsion for heat S1835(Top left), S1836(Top right and S1843 (bottom) (Millman et al. 2011).

3.5. IMPHOS conclusion

The IMPHOS report contained some very important discoveries for metal refining research. It was found that when the slag is highly oxidised the metal droplets are readily oxidised in the slag. Consistent slag foaming only begins at 2/3 of the way into the blow. Very little oxygen dissolves into the bulk bath until 6 min into the blow. Carbon and manganese oxidation is driven by metal-slag reactions and not bulk bath-slag reactions (Millman et al. 2011).

As discussed in paragraph 2.1.4 , the in-situ measurements done in IMPHOS are still very rare in the steel-making industry. The IMPHOS research was done to analyze the behaviour of phosphorus, but the measurements and calculations for all the other steel bath(C,Si,Mn,S) and slag(S,Ca,Si,Mn,Mg,O) elements were also performed in IMPHOS. Therefore the IMPHOS sample measurements are suitable as base data for the modelling of refining of these elements. More information about how this IMPHOS data is used in the current research can be found in chapters 4,5 and 6 where the outline of the methodology is discussed.

Part III

Methodology

4

Method: IMPHOS Data Analysis

This chapter describes the different features involved in analysing the existing original IMPHOS data. First, a detailed description is given about the classification of interesting IMPHOS heats, and why they were selected for this research. Secondly, the existing format of the data is discussed. Finally, the different thermodynamic models for manganese distribution discussed in paragraph 2.2.2 were chosen to evaluate the selected heats. The data from different heats and the thermodynamic model described in this chapter, will be used as input in the kinetic model that is further described in chapter 5. The results of the thermodynamic evaluation of the manganese distribution can be found in chapter 7.

4.1. Method outline

The flowchart in figure 4.1 describes the different steps performed during the data analysis phase of this research. Each step will be described in the following paragraphs of this chapter.

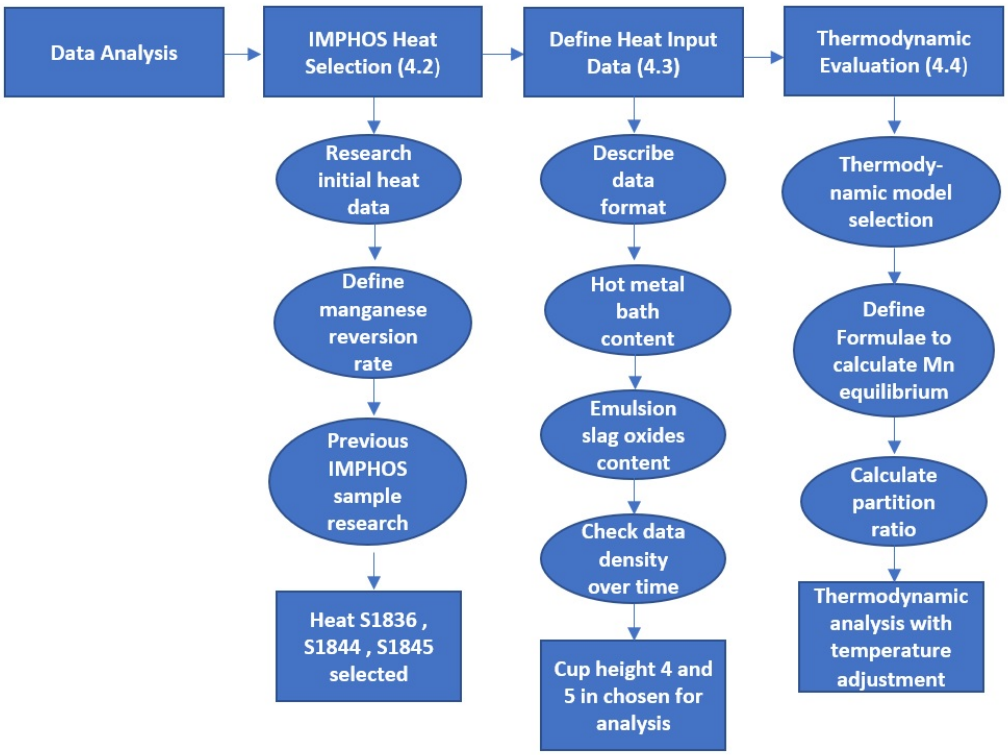

Figure 4.1: Flowchart of data analysis performed on IMPHOS data.

4.2. Heat selection

The total IMPHOS data collection exist out of 20 different heats. These heats were numbered from S1828-S1847. To select the most interesting heats from these 20 heats a distinction was made between differences in important properties of these heats. The properties researched were:

- Initial heat data
- Rate of manganese reversion
- Previous IMPHOS research done

The final heats selected based on these 3 criteria are used for thermodynamic evaluation of the manganese distribution. These heats will also be used in the kinetic modelling part of this study.

4.2.1. Initial heat input data

The initial IMPHOS heat hot metal composition was selected together with hot metal/scrap ratio, and addition of lime was calculated to maintain a certain basicity as explained in paragraph 3.3. The actual hot metal composition always varies from the initial calculated composition. This actual composition was measured every heat by sampling with a sub lance at the start of the heat.

Table 4.1 shows the actual essential data of 20 different IMPHOS heats. Because the majority of decarbonization and refining of hot metal is influenced by lance height and iron refining potential as explained in 2.2.1. It is displayed in this table. The basicity was mainly influenced by changing the SiO_2 concentration in the slag by adding extra sillicon to the hot metal. The final partition ratio for manganese given the final oxidation potential was calculated according to 2.11. The data was collected from Millman et al. (2011).

Table 4.1: Si content, lance height, partition ratio and basicity(B2) at the start of IMPHOS heats.

Heat	HM Si wt%	Lime(Kg)	Basicity(B2)	Start Lance Height(mm)	(wt%Mno)/[wt%Mn]	Slag FeO wt%
S1828	0.54	300	3.92	178.0	31.7	19
S1829	0.51	300	3.47	180.3	25.0	17
S1830	0.47	300	3.98	179.4	29.1	19
S1831	0.46	300	3.72	180.5	25.3	15
S1832	0.58	300	3.38	179.5	19.5	12.9
S1833	0.46	350	4.44	170.5	27.7	20
S1834	0.66	350	3.42	171.3	27.5	19.5
S1835	0.60	350	3.15	171.1	13.6	8.5
S1836	0.64	350	3.55	179.9	12.8	8.3
S1837	0.59	350	3.95	179.8	28.3	18.9
S1838	0.67	300	3.19	180.3	38.0	21
S1839	0.67	300	3.22	169.8	47.5	26.1
S1840	0.58	300	4.00	180.3	52.0	30.4
S1841	0.61	250	2.98	181.5	66.0	30.5
S1842	0.88	250	2.27	169.4	21.6	11.6
S1843	0.56	250	2.87	171.8	20.0	11.3
S1844	0.62	250	2.8	169.9	20.6	13.8
S1845	0.53	250	3.23	170.8	27.3	19.4
S1846	0.55	250	3.67	170.0	26.0	18.6
S1847	0.43	250	4.67	170.7	32.7	22.7

What makes the data difficult to analyze is the lack of slag emulsion composition at start of the heat. The first calculated emulsion measurements are done on the first samples around 2-3 min into the heats for most of the heats. In the original IMPHOS reports the heats were grouped by dephosphorization rate leading to evaluation of different heat numbers in non-chronological order to describe the heats with similar phosphorus refining behaviour. It already indicates the difficulty in prediction of the phosphorus refining path, because a similar heat input can lead to a different refining rate. Manganese shows a similar difficulty in the prediction

of this reversion. The next paragraph shows the differences in manganese reversion for the heats. A distinctive difference should exist between the initial input and results of the heats, to make the heats agreeable for comparison with the thermodynamic manganese equilibrium calculations and the final use as input data in the kinetic model in chapter 5.

4.2.2. Rate of manganese reversion

After bulk chemical analysis different manganese refining profiles were constructed during IMPHOS. Figure 4.2 from Millman et al. (2011) show all the Manganese profiles for heats S1828-S1847.

In figure 4.2 Most of the heats show the classical oxidation and reversion behaviour for manganese. The primary oxidation phase happens until approximately 6 min into the blow. Then the reversion starts to happen gradually until 14 min of the blow after which the 2nd oxidation phase occurs. This oxidation rate is slower than the primary oxidation phase. However not all heats show this classical behaviour. For some heats the reversion rate stays low after the primary oxidation phase. The manganese content in the steel gradually moves to a constant end value in the steel.

For this research a division is made based on their manganese reversion behaviour, into 3 different categories to classify each heat. The following categories are used.

- No/Slow manganese reversion for 0-0.05 Mn% increase in Mn content during the reversion phase
- Average manganese reversion for 0.05 - 0.10 Mn% increase in Mn content during the reversion phase
- Fast manganese reversion for > 0.10% increase in Mn content during the reversion phase

The heats containing the most manganese reversion are the ones most interesting for evaluation in this study. A faster change of manganese content means a faster change in slag viscosity and more difficulty to control the efficiency of the blow. Hewage et al. (2016) also showed that the heats with less manganese reversion are easier to predict with a first order kinetic model than the heats with a higher reversion rate. Therefore for the modelling part, it will be more interesting to evaluate the heats which can't be explained with first-order kinetics. Table 4.2 shows the different heats and their apparent rate of manganese reversion. This table can be compared with the manganese refining profiles in figure 4.2 to see the difference in manganese reversion rates.

Table 4.2: Division of visible rate of manganese reversion for the different IMPHOS heats.

Heat	No/Slow manganese reversion rate	Average manganese reversion rate	Fast manganese reversion rate
S1828			X
S1829		X	
S1830		X	
S1831		X	
S1832			X
S1833		X	
S1834		X	
S1835			X
S1836			X
S1837		X	
S1838	X		
S1839	X		
S1840	X		
S1841	X		
S1842			X
S1843	X		
S1844			X
S1845			X
S1846		X	
S1847	X		

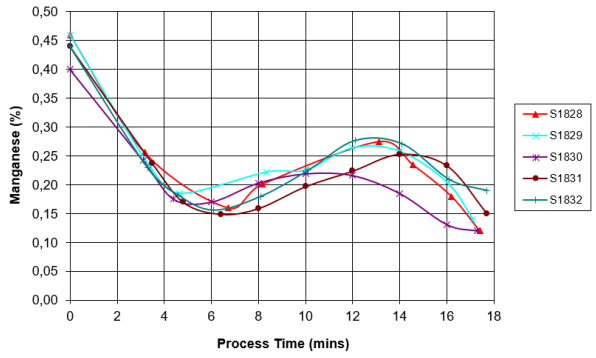

(a) Manganese content in metal bath for heat S1828-S1832.

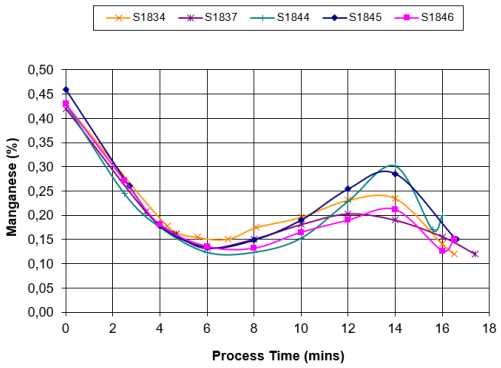

(b) Manganese content in metal bath for heat S1834, S1837, S1844-S1846.

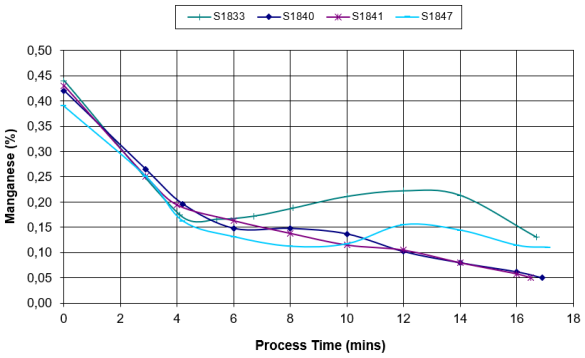

(c) Manganese content in metal bath for heat S1833, S1840-S1841, S1847.

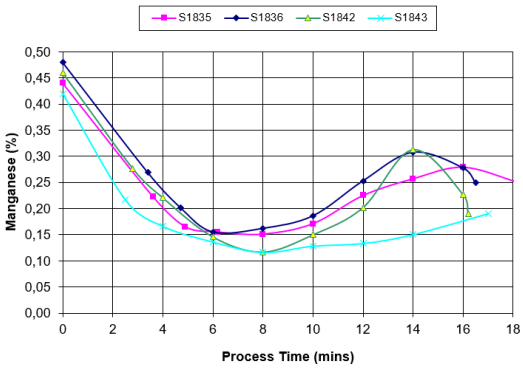

(d) Manganese content in metal bath for heat S1835-S1836, S1842-S1843.

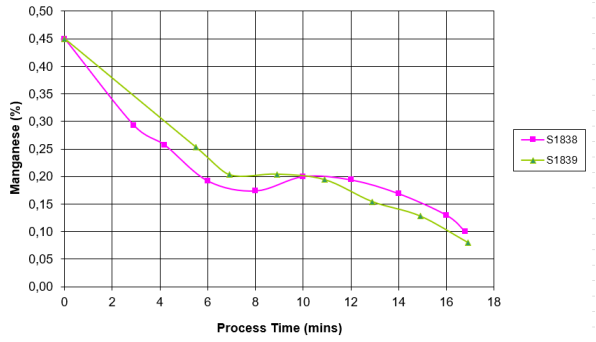

(e) Manganese content in metal bath for heat S1838-S1839

Figure 4.2: Manganese content in metal bath for the 20 different IMPHOS heats. All measurements were taken from cup height 1, the lowest part in the hot metal bath.

4.2.3. Previous analysed IMPHOS heats

Chapter 3 described the different sample analysis methods applied to measure slag and bath concentration during the IMPHOS research. Spark OES and XRF analysis was done on every sample from the different heats to measure the bulk chemical compositions of Mn,P,Si,C and S, which lead to the different refining profiles in the previous paragraph and to measure the slag composition. Spark-OES is a method were a light spark is used to excite electrons on a surface. When these electrons are excited they reach a new energy level. Each element has its own unique energy spectrum which can be used to identify these elements within the material. More explanation about these bulk chemical analysis methods can be found in paragraph 6.4. Extensive texture analysis and SEM-EDS(Scanning Electron Microscope - Energy-dispersive X-ray spectoscropy) analysis was only done of the slag-metal emulsion samples for four different heats. Heat S1841 and S1845 were analyzed and discussed before in unpublished IMPHOS work by J.Small. Heat S1837 and S1840 were previously analysed for the PhD research of Obasohan (2015). The work done previously can be compared with input and results in the current study therefore it's essential to identify the previously analysed heats.

4.2.4. Final heat selection

For the final sample selection, the seven different heats with fast reversion from table 4.2 were evaluated on the behaviour of their Mn refining profiles shown in figure 4.2 and important heat input data from table 4.1. From these seven heats , three heats will be researched in the modelling part of this study due to a limited amount of time.

Comparing the table containing the essential data with the rate of reversion of the different heats, its immediatly apparent that in general, the heats with no/slow manganese reversion have higher iron oxide values in the final slag composition. The opposite can also be said, the heat with higher manganese reversion rates have in general, less iron oxide content in the final slag composition. This supports the conclusions of most thermodynamic research from paragraph 2.2.2. , that the iron oxide to iron content ratio heavily influences the oxidation potential controlling the manganese distribution and equilibrium value (Morales & Fruehan 1997). With a higher FeO content in the slag, the manganese partition ratio is generally higher, Thus the ratio between manganese oxide in the slag and manganese in the hot metal bath is bigger.

Some IMPHOS heats with the same data input ended up with different refining profiles for manganese during the steelmaking heat. It perfectly illustrates the complexity of predicting the manganese content in the steel bath during the heat. Between heat S1842 and S1843, both iron oxide final contents are almost the same. Starting Lance height practices are similar aswell as end manganese partition ratio(S1843 is the only heat with slow manganese reversion and a low iron oxide content.) Both heats show the same odd behaviour where the primary oxidation phase lasts 8 min instead of the usual 6. However, Heat S1842 shows a very fast manganese reversion whereas heat S1843 shows a very fast primary oxidation phase until the same low Mn content as in heat S1842 is reached after this first phase. This value is also below the normal 0.15% Mn observed in the other IMPHOS heats. The reversion in heat S1843 is very slow in contrast to S1842 and never ends until the end of the blow. The only clear difference between the heats is the basicity level, Heat S1842 has a Si content in the starting hot metal of 0.88%, the highest of all IMPHOS heats. It leads to a low end basicity in the slag of 2.27, The lowest value for all IMPHOS heats. Possible explanation of the difference in slopping during the two heats. According to Millman et al. (2011) heat S1843 Slops heavily after 8 min this can lead to a loss of metal material in the slag emulsion. This can lead to less manganese dilution from the slag into the metal bath.

Looking at the seven different heats containing fast reversion, it appears that some heats have a more gradual change of manganese content, while heat S1828 and S1842 show a less gradual change of manganese content. This is less favorable for predicting the manganese content with kinetic modelling. Therefore it was decided not to select these heats. For the remaining five heats it is important that there is enough difference in the important heat values in table 4.1. Heat S1832 and S1836 have the same starting lance Height position around 180 mm, while S1835,S1844 and S1845 have a starting lance height position around 170 mm. Final iron oxide content can be divided in 8% for heat S1835 and S1836 and 13% for heat S1832 and S1844. Heat S1845 has the highest final iron oxide content with 19.4%. Final basicity is different for all five heats, only heat S1835 and S1845 have a resembling basicity. To make the comparison of results easier heat S1845 was selected because of the more elaborate texture analysis and emulsion droplet composition. Heat S1836 was selected because a complete original metal sample set was found for height 2 of heat S1836. This sample set can be very valuable for analysis, a further explanation can be found in chapter 6. Heat S1844 was selected because of the very low

end basicity value compared to the other four heats. Heat S1836, S1844, S1845 together have the most deviated input data from the 5 heats and are therefore the most interesting for this study. To validate the accuracy of the kinetic model explained in chapter 5 for a heat without reversion, heat S1841 was also selected to be evaluated in kinetic modelling.

4.3. Input data

This paragraph describes the different data obtained from previous IMPHOS research which can be used for the thermodynamic analysis described in paragraph 4.4 and chapter 7. Some of the data is also used as input for the kinetic model as explained in chapter 5.

4.3.1. Data format

All original IMPHOS calculations were stored in excel files. The data from the three selected heats :S1836, S1844 and S1845 are also stored in these files. The excel files can be divided in three different categories:

- Metal data
- Slag data
- Raw heat data

The metal data contains the calculated metal content of manganese , phosphorus, silicon, carbon, sulphur, chromium, nickel, copper and vanadium. The data contains both the metal content in the hot metal bath and the content measured in the emulsion. The measurements were coded in the following way: Heat number-Dip number(time)-Cup number(Height). There are normally seven different cup numbers and eight different dip numbers. The time of measurement can be found by multipying the Dip number with 2 min. The temperature measured in the metal bath at a certain dip time is also stored in this file. The three different heats have the following range of concentrations, as presented in table 4.3 and 4.4.

Table 4.3: Range of weight percent of elements and base metals found in the hot metal bath

Heat	C	Si	Mn	P	S	Cr	Cu	Ni	V
S1836	0,18-4,06	0,000-0,64	0,155-0,480	0,026-0,086	0,012-0,0513	0,030-0,036	0,0062-0,01	No data	0,016-0,169
S1844	0,025-4,02	0,0023-0,62	0,124-0,43	0,023-0,098	0,02-0,052	0,028-0,032	0,0035-0,0067	No data	No data
S1845	0,02-4,07	0,000-0,53	0,134-0,46	0,019-0,095	0,017-0,045	0,028-0,034	0,0038-0,0058	No data	0,028-0,165

Table 4.4: Range of weight percent of elements and base metals found in the metal-slag emulsion.

Heat	C	Si	Mn	P	S	Cr	Cu	Ni	V
S1836	0,111-3,19	0,015-0,159	0,058-0,303	0,004-0,057	0,017-0,048	0,014-0,038	0,031-0,035	0,031-0,035	0,009-0,16
S1844	0,029-3,48	0,006-0,23	0,064-0,28	0,009-0,006	0,028-0,053	0,015-0,036	0,002-0,004	0,027-0,035	0,006-0,13
S1845	0,03-3,39	0,016-0,11	0,068-0,231	0,008-0,068	0,018-0,038	0,015-0,033	0,003-0,004	0,032-0,036	0,003-0,11

The slag data contains the original metal oxide contents from the metals described above at different heights within the slag emulsion. The weight percentages of the different oxides are used in some thermodynamic semi-empirical relations, used to calculate the manganese equilibrium as for instance in Suito & Inoue (1995). The range for the weight percentage metal oxides in the slag can be seen in table 4.5. In the slag data used the correction for free lime within the slag has already be done. The correction for the presence of solid lime is applied to determine the actual oxide concentration in the liquid slag.

Table 4.5: Range of weight percent of oxides found in the metal-slag emulsion.

Heat	Fe_tO	CaO	SiO_2	MgO	Al_2O_3	P_2O_5	MnO
S1836	6,350-19,16	31,91-53,05	17,31-26,03	1,237-7,349	0,820-4,132	1,113-2,043	2,526-11,48
S1844	7,796-25,04	28,24-51,26	17,18-25,45	1,289-6,484	0,966-4,503	1,264-2,563	2,964-8,268
S1845	10,10-26,72	28,57-51,62	15,15-25,05	1,897-7,618	1,187-3,057	1,268-3,070	3,236-9,025

The 3rd type of data is the raw heat data from the 3 heats. It's basically a log where some important process variables as oxygen flow rate, decarbonization rate, lance height position and temperature are measured every second during the blow. The raw data related to process variables also contains the amount of CO and CO_2 in the exhaust gas during the blow. Most data from this log can be used as input data in the kinetic modelling part described in chapter 5.

4.3.2. Data points

The three different heats evaluated have a different amount of datapoints collected during the heat. Due to the boundary of the evaluation method, not all cup heights are evaluated. For instance, for metal bath calculations, only cup height 1 samples are evaluated. Cup height 2 samples were never evaluated before on their the metal bath content. This research also partly focuses on analyzing the metal content in cup height 2. The emulsion zone located at cup height 3-7, contains different data measurement points. Table 4.6 show the amount of emulsion slag content datapoints at the different cup heights. The data from the different cup heights is distributed on dip time instead of cup height, so data filtering was done to analyze the measurements at different cup heights.

Table 4.6: Amount of datapoints at 7 different heights for heat S1836, S1844 and S1845.

Cup Height	S1836	S1844	S1845
1	0	0	0
2	0	0	0
3	2	7	2
4	7	7	7
5	7	7	6
6	3	4	4
7	0	2	2

After collecting the datapoints at the different cup heights, it was decided to only evaluate cup height 4 and 5 for the modelling part in the current study. This is done to achieve the most reliable amount of data density, which is used as input in the model. As explained in chapter 2, the slag composition heavily influences the manganese equilibrium calculation. Reliable slag input data is necessary to improve the reliablity of the model.

4.4. Thermodynamic evaluation

This paragraph describes the thermodynamic models used to check their accuracy predicting oxidation and reversion of the manganese during the blow. It also describes the way the analysis was done.

4.4.1. Model selection

For the thermodynamic evaluation of the interesting cup heights, two different thermodynamic models described in paragraph 2.2.2 are selected. The selection of the models is based on the temperature and slag composition range that is similar to the IMPHOS conditions. The used slag composition is a CaO, MgO, Fe_tO, SiO_2, P_2O_5 slag in a temperature range from 1600-2000 K. Both models selected are the fastest to evaluate based on the semi-empirical relation between the apparent equilibrium and the manganese content in the bath, the iron oxide content in the slag and the manganese oxide content in the slag.

The 2 models selected are:

- Suito and Inoue number 3 model (Suito & Inoue 1995).
- Morales and Fruehan model (Morales & Fruehan 1997).

For Suito & Inoue (1995) the equation for apparent equilibrium in Suito number 3 model is presented in 4.1.

$$log k'_{Mn} = -0.0180 * [(\%CaO) + 0.23(\%MgO) + 0.28(\%Fe_tO) - 0.98(\%SiO_2) - 0.08(\%P_2O_5)] + \frac{7300}{T} - 2.697 \quad (4.1)$$

Where k'_{Mn} is the apparent equilibrium for manganese. The rest of the input parameters are weight percentages of different oxides in the slag and Temperature T in Kelvin. Note that the Al_2O_3 which is present in the IMPHOS slag, is not taken into account in Suito's model. Equation 2.13 from chapter 2 also describes the apparent equilibrium used by Suito number 3.

$$k'_{Mn} = \frac{(\%MnO)}{[\%Mn] * (\%Fe_tO)} \quad (2.13)$$

By solving both equations the %Mn can be found as manganese equilibrium value. When these calculations are done for all data points manganese equilibrium curves are constructed. These curves are compared with the manganese value in the hot metal bath and emulsion at the different IMPHOS dip measurement times.

For the Morales and Fruehan model the apparent equilibrium value was found in Morales & Fruehan (1997) as a temperature function presented in equation 4.2 based on research by Turkdogan & Pearson (1953).

$$log k'_{Mn} = \frac{7406}{T} - 3.436 \quad (4.2)$$

This equation can be solved again together with 2.13 to find the equilibrium manganese content for the Morales model. For this model equilibrium curves are also constructed and compared with the measured IMPHOS data.

For both models the manganese partition ratio according to 2.11 are also calculated and compared with the original partition ratio curves constructed with IMPHOS data. The equation for partition ratio is:

$$L_{Mn} = \frac{(\%MnO)}{[\%Mn]} \quad (2.11)$$

Where L_{Mn} is the partition ratio of manganese to its oxide, $\%MnO$ is the manganese oxide weight percentage in the slag, $\%Mn$ is the weight percentage of manganese in the hot metal bath.

4.4.2. Temperature adjustment test

The equilibrium values and partition ratio are also calculated with a temperature adjustment of 50K, In the previous calculation hot metal bath temperatures are used, while most input data is collected from slag data. The temperature of the slag is known to be slightly higher than the hot metal bath (Deo & Boom 1993). Therefore these temperature adjustment tests are necessary for a more accurate prediction of the equilibrium. All results from the thermodynamic analysis of the IMPHOS data can be found in chapter 7.

5

Method: Kinetic Model for Manganese in the Converter

This chapter describes the development of the kinetic model for the prediction of the manganese refining path. The model is written in the python programming language. The basic model concept will be discussed and its most important assumptions, furthermore the details of micro and macro kinetics influencing the mass transfer of manganese in the converter will be evaluated. Finally this chapter also contains the overal model input data and the most important limitations, which are affecting the outcome of the kinetic model. The results from the kinetic model can be found in chapter 8.

5.1. Method outline

This paragraph presents an overview of the different steps involved in developing the kinetic model. Each step is described in the following paragraphs. The kinetic model is written in python will be evaluated with data retrieved from IMPHOS cup height 4 and 5 , for all 4 heats chosen in the IMPHOS heat selection in paragraph 4.2. Figure 5.1 shows the overview of the method explained in this chapter.

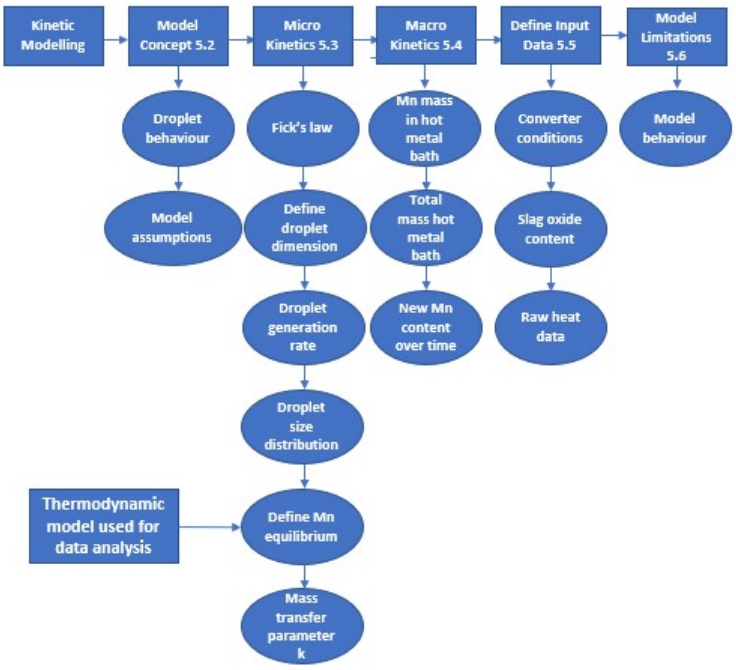

Figure 5.1: Flowchart describing kinetic modelling method of IMPHOS heats.

5.2. Model concept

In paragraph 2.2.3 a lot of basic information about the mass transfer of manganese in the converter is already presented. The mass transfer takes place in 3 different zones: The jet impact zone, the slag-bath interface zone and the slag emulsion zone within the converter. Rout et al. (2018) showed that the most significant contribution of manganese metal refining takes place in the emulsion zone. This model will be solely based on the micro kinetics (particle mass transfer of droplets and slag) happening in this emulsion zone and how it influence the macro kinetics (overall mass transfer by droplets from hot metal bath) within the converter.

According to Rout (2018) the refining within the emulsion zone happens in a few different steps: First hot metal droplets are ejected from the metal bath into the emulsion, due to the impact of oxygen flow into the hot metal bath. The ejected droplets are carrying multiple metal elements Mn,P,S,Fe,Si etc. After a certain time the droplet loses density, because of the formation of CO gas from within. The loss of density causes the droplet to rise within the emulsion. After a certain time the gas escapes and the droplet gets more dense again, causing the droplet to fall within the emulsion. Eventually droplets fall back to the hot metal bath, causing the hot metal bath to dilute with the remaining metal impurities within the droplet. Figure 5.2 from Rout (2018) describes this droplet behaviour schematically.

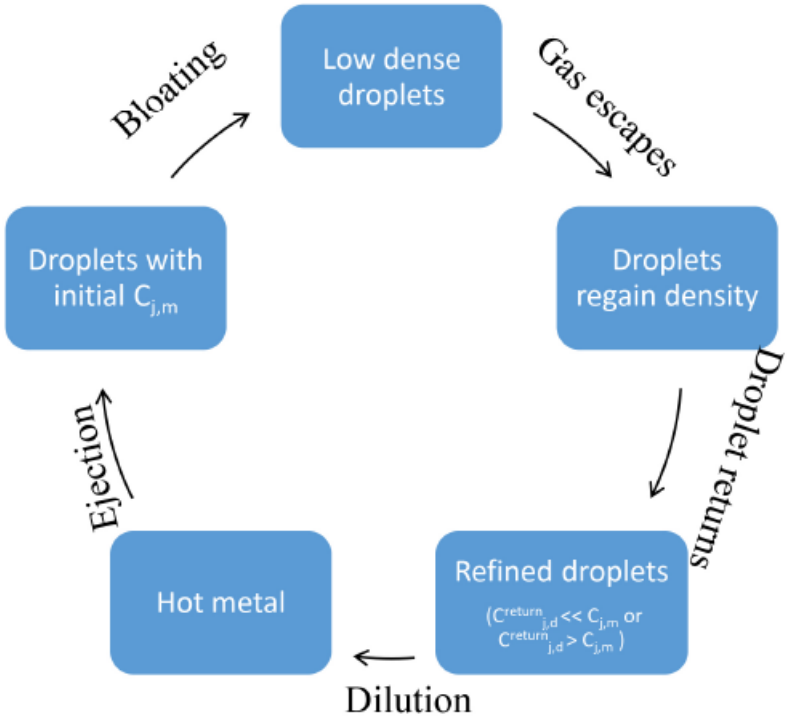

Figure 5.2: Schematic of droplet refining in the emulsion zone (Rout 2018).

The time the droplet travels through the emulsion, is called the droplet "residence time" This residence time is influenced by the bloating of CO gas. This can influence the amount of refining a droplet experiences within the emulsion, because at the local droplet boundaries the droplet also tends to move towards equilibrium over time. From Millman et al. (2011) it appeared that at certain cup heights the smaller droplets are more refined than the bigger droplets. Goal of this kinetic model is to understand the refining behaviour of manganese for different droplet sizes within the emulsion. Apart from manganese other metal contents in the droplets are ignored for this research, however different metal oxides in the slag are used in the manganese equilibrium calculations in paragraph 5.3.4.

The model approach for this research contains a few important assumptions:

- Total computational period is to be the same as the refining time of 16 min.
- Standard fixed time step is taken to be as Δt = 1s, at each time step the input data like lance height, flow rate and slag composition are fed to the model.
- The slag content data at time t=0 is the same as the first slag data point measured in IMPHOS around 2-3 min.
- Manganese content of the droplet at ejection is the same as the manganese content in the hot metal bath.
- Droplet temperature is taken to be the same as the temperature of the hot metal bath.
- Residence time describing the bloating behaviour is evaluated as a fixed parameter of 1s for the droplets.
- Droplet shape is spherical and does not change over the whole heat.
- Mass transfer at droplet boundary takes place based on penetration theory based on Higbie (1935).

5.3. Micro kinetics

The rate of mass transfer of droplets ejected in the emulsion can be described by Fick's first law of diffusion (Hewage et al. 2016).

Ficks first law of diffusion for manganese will become:

$$\frac{dMn\%}{dt} = -(k_t^d * \frac{A^d}{V^d}) * (\%Mn_t^d - \%Mn_t^{d*}) \tag{5.1}$$

Where dMn/dt represent the change of manganese at time t within the emulsion. k_t^d represents the mass transfer parameter which will be explained later in section 5.3.5. A^d and V^d represents the droplet area and volume for a droplet size class d in m^2 and m^3. The droplet dimensions and its size classes will be discussed in paragraph 5.3.1. $\%Mn_t^d$ is the starting weight percentage content of manganese droplets ejected from the metal bath discussed in paragraph 5.3.2.. $\%Mn_t^{d*}$ is the manganese equilibrium weight percentage content between slag and metal , from thermodynamic research discussed in paragraph 5.3.4. All values will be evaluated for subscripts t and d representing the time and droplet size class.

5.3.1. Droplet dimensions

For this research all droplets ejected from the metal bath are spherical in shape and the dimensions of the droplets are not changing within the converter. In reality droplets will lose or gain shape based on all the reactions happening within the droplet. If droplets are spherical the droplet area for a certain size class d can be found in equation 5.2:

$$4\pi * r^2 \tag{5.2}$$

Where r is taken as the average radius of the droplets within size class d_i. The droplet volume for size class d_i can be found in equation 5.3:

$$\frac{4}{3}\pi * r^3 \tag{5.3}$$

The ratio of droplet area to volume describes the theoretical reaction surface, where iron oxide in the slag can react with the manganese and carbon in the droplet. 3 droplet size distributions were made: 20-500 micron, 20-1000 micron and 20-2000 micron. These distributions were divided in 12 size classes. In unpublished work by J. Small the most droplets were found in the size range of 20-500 micron.

5.3.2. Starting manganese weight content and droplet mass generation

The manganese content used in 5.1 is still presented in weight percentage Mn content. For this research it is assumed, that the droplets being ejected into the emulsion carry the initial manganese weight percentage content of the hot metal bath. The initial manganese weight contents are presented as input in table 5.2.

Extreme converter conditions prevent the real time fluid splashing behaviour from being measured. To estimate the actual weight of droplets generated for time t in the emulsion, The physical influence of the supersonic oxygen jet on the hot metal bath should be described. Figure 5.3 from Kadrolkar & Dogan (2019) shows the different gas velocities occurring in the impact zone of the metal bath.

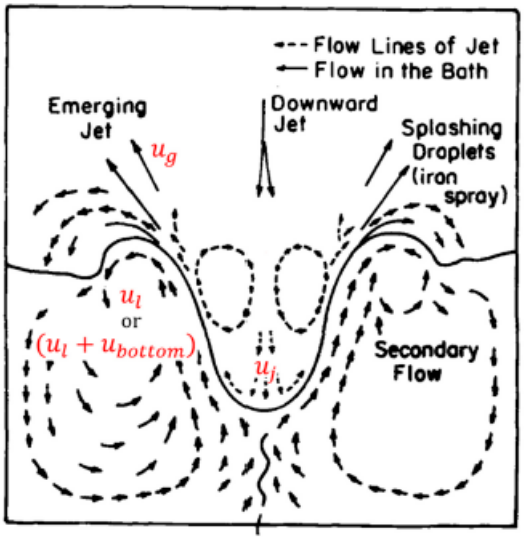

Figure 5.3: Fluid flow behaviour at impact zone by gas jet oxygen (Kadrolkar & Dogan 2019).

The most important velocities described above, are the jetstream velocity into the hot metal bath at the jet impingement point u_j and the tangential gas velocity u_g, emerging from the hot metal bath. To estimate the droplet generation rate as mass, Subagyo et al. (2003) first used the relation in equation 5.4 to calculate the droplet generation as dimensionless blowing number based on the Kelvin-Helmholtz instability.

$$N_{B,t} = \frac{\rho_g * u_{g,t}^2}{2 * \sqrt{\rho_1 * \sigma_1 * g}} \tag{5.4}$$

In this equation N_b is the dimensionless blowing number, $\rho_g$is the gas density in Kg/m^3, u_g^2 the tangential velocity in m/s, ρ_1 the liquid steel density in Kg/m^3, σ_1 is the surface tension of steel in N/m and g the acceleration due to gravity in m/s^2. This formula is used in the kinetic model most input parameters are constants found in table 5.2.

The only parameter which needs to be calculated in detail every second is the tangential velocity emerging from the jet impact zone. This tangential velocity u_g is calculated as presented in equation 5.7 by Subagyo et al. (2003). This tangential velocity is calculated as relation of the jet impact velocity u_j. This jet impact velocity is dependant of the starting jet velocity u_o at the nozzle exit and can be found in 5.6. The calculation for the velocity at nozzle exit can be found in equation 5.5. The exit velocity of a Laval nozzle is calculated based on isoentropic theory as follows:

$$u_o = (\frac{2 * \gamma}{\gamma - 1} * (R * 1000 * \frac{293}{32}) * (1 - \frac{P_e}{P_o})^{\frac{\gamma-1}{\gamma}})^{0.5} \tag{5.5}$$

With u_o the Nozzle exit velocity in m/s, γ the isentropic expansion factor: 1.4 for diatomic gas, R the gas constant in $J/mol * K$ and P_e the nozzle exit pressure and P_o, the atmospheric pressure both in Pa. The jet impact velocity becomes:

$$u_{j,t} = u_o * \frac{0.97}{\frac{2*a*h_t}{d_t hroat} + 0.29} \tag{5.6}$$

With u_j the jet impact velocity in m/s at time t , u_o the nozzle exit velocity in m/s , a velocity constant for hot metal data, h_t the lance height at time t within the blow and d_{throat} the nozzle throat diameter in m. Finally the tangential velocity for splashing to occur due to shearing action of the jet is then found by Subagyo et al. (2003):

$$u_{g,t} = 0.4471 * u_{j,t} \tag{5.7}$$

The following functional relation derived by Subagyo et al. (2003) can be used to calculate the droplet generation rate in kg mass per s. This relation is presented in equation 5.8.

$$R_{B,t} = \frac{N_{B,t}^{3.2}}{[2.6 * 10^6 + 2 * 10^4 * N_{B,t}^{12}]^{0.2}} * F_G \tag{5.8}$$

In this equation $R_{B,t}$ is the droplet generation rate in kg/s, $N_{B,t}$ is the dimensionless blowing number and F_G the gasflowrate of the oxygen into the converter in M^3/s. This droplet generation rate presents the total mass of droplets formed per s. This droplet generation rate is calculated for an oxygen jet flow through a cold atmosphere. More is explained in the model limitations in paragraph 5.6.

5.3.3. Droplet size distribution

The droplets ejected from the emulsion are all different in size. These different sizes can influence the reaction surface and therefore the masstransfer between the droplets and the emulsion. To divide the total mass of droplets formed per second, a droplet size distribution was made. According to Rout (2018) The Rosin-Rammler-Sperling(RRS) distribution can be used to find this distribution. The RRS formula can be found in equation 5.9.

$$R_s = 100 * \exp(-d/d')^n \tag{5.9}$$

In the equation above R_s gives the weight percentage of screen oversize with diameter d. d' is a variable parameter which describes the droplet fineness. n is a variable parameter describing the homogeneity of the size distribution.

3 size ranges are made with 12 different size classes. For this research 3 different distributions were made:

- A distribution with 12 size classes between 20-500 micron
- A distribution with 12 size classes between 20-1000 micron
- A distribution with 12 size classes between 20-2000 micron

By multiplying the weight percentage from the size distribution with the droplet generation rate for each size d, the average contribution of mass from each droplet size class was found per second. This transforms the blowing number $R_{B,t}$ from a time dependant parameter, to a parameter $R_{B,t}^d$ depending on both time and average droplet class size d. The model can be tested with the 3 different droplet size distributions created to analyse the mass transfer kinetics of manganese for these different scenarios. Table 5.1 presents the found values for n and d'.

Table 5.1: Droplet size distributions parameters used for this research

Distribution	Size range in micron	n	d'
1	20-500	2.72	0.48
2	20-1000	1.74	0.57
3	20-2000	1.61	1

The final 3 RRS distributions can be found in appendix A.

5.3.4. Manganese equilibrium content

Returning to Fick's first law of diffusion used in 5.1. The manganese equilibrium input value Mn_t^{d*} can be determined by using the thermodynamic models for manganese distribution described in paragraph 4.4.1. As mentioned before the manganese equilibrium value describes wether the reaction between manganese and oxide moves to the left (more creation of manganese) or to the right (more creation of manganese oxide). Here both Suito number 3 model (Suito & Inoue 1995) and Morales and Fruehan model (Morales & Fruehan 1997) were discussed and used to verify the behaviour of these models, in comparison with the behaviour of the manganese in the IMPHOS metal bath and emulsion.

The heats checked for their thermodynamic behaviour are the same as used in the model: S1836,S1844 and S1845. The results of the data analysis in chapter 7 shows that Suito number 3 model is more accurate in predicting the equilibrium behaviour of manganese over a longer period of the blow than Morales and Fruehan. Therefore the Suito Number 3 model based on slag composition and temperature, was used in the kinetic model in python, to predict this manganese equilibrium value at time t. The equations used and programmed in this model are equations 4.1 and 2.13 from paragraph 4.4.1. The heat S1841 where no manganese reversion occurred was not checked for its thermodynamic equilibrium. This heat is evaluated for the model, to provide extra validation of the models prediction for heats without manganese reversion.

5.3.5. Kinetic mass transfer coefficient

The kinetic mass transfer coefficient gives the quality of the kinetic reaction between the droplet and the emulsion. Higbie (1935) assumed that different metal species within the droplets are experiencing unsteady state diffusion or penetration, when a droplet surface is in contact with the surrounding slag. The Higbie penetration theory assumes that around droplet boundaries the mass transfer behaviour is equivalent to movement behaviour of a Newtonian falling film. Penetration theory also assumes a local equilibrium around the gas-liquid interface. In the x-direction mass transport takes place by diffusion. In the y direction mass transport takes place primarly due to the flow in the liquid layer over the droplet contact surface as described in van Elk et al. (2007). Figure 5.4 shows the basics behind the penetration theory along a droplet boundary, when a droplet is rising within a liquid.

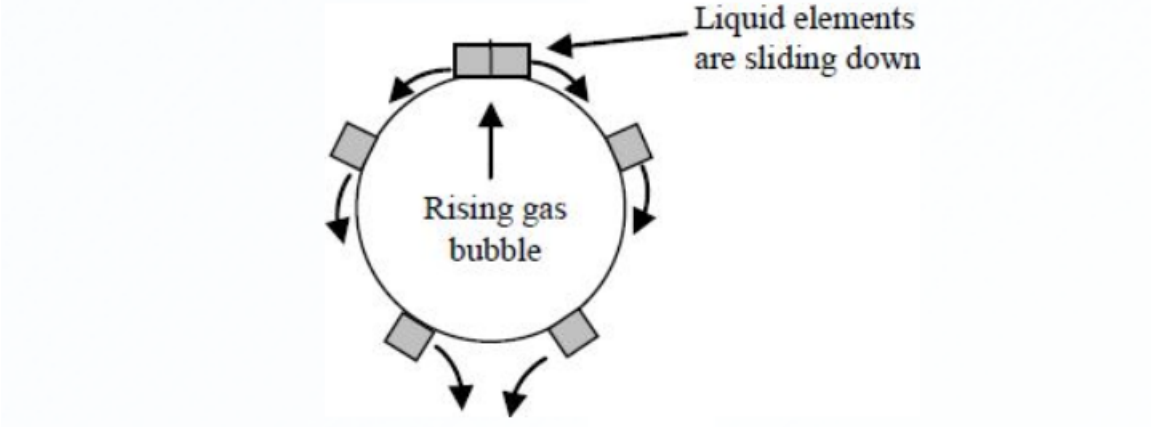

Figure 5.4: Schematic of mass transfer between rising a rising gas droplet in contact with the surrounding liquid (Higbie 1935).

Higbie found that the mass transfer coefficient is proportional to the square root of the diffusion during a certain contact time. Estimation of contact time between the liquid and the gas droplets is currently impossible in converter steelmaking. According to Rout et al. (2018) in the case of spherical bubbles the contact time can be assumed as a ratio between the velocity and diameter of the droplet. The calculation of mass transfer parameter for manganese is described in equation 5.10:

$$k_t^d = 2 * \sqrt{\frac{D_{Mn,t}}{\pi * t_c}} = 2 * \sqrt{\frac{D_{Mn,t} * u_{drop,t}^d}{\pi * d}} \tag{5.10}$$

Where k_t^d is the kinetic mass transfer coefficient for manganese at time t for average droplet size d. $D_{Mn,t}$

gives the droplet diffusivity for manganese at time t. t_c is the droplet contact time, $u_{drop,t}$ is the droplet velocity in m/s at time t and droplet size class d_i. d is the average droplet size in m corresponding to its size class d_i.

In this formula the diffusivity and droplet ejection velocity should be calculated for different times t. In Rout et al. (2018) The Stokes-Einstein equation was used to incorporate the influence of temperature and hot metal viscosity on the mass diffusivity of manganese. The Stokes-Einstein equation applied to this problem can be found in equation 5.11.

$$D_T^{Mn} = D_{1873}^{Mn} * (\frac{T}{1873}) * (\frac{\mu_m, 1873}{\mu_m, T}) \tag{5.11}$$

In this equation D_T^{Mn} represents the diffusivity of manganese in m^2/s for temperature T in kelvin measured at time t, D_{1873}^{Mn} is a measured diffusivity constant at 1873K for manganese. $\mu_{m,1873}$ is the hot metal viscosity measured at 1873K and $\mu_{m,T}$ is the hot metal viscosity for temperature T. The used diffusivity constant of manganese at 1873K is $7 * 10^{-9}$. The viscosity is calculated in the model using the modified Urbain model proposed by Kondratiev & Jak (2001). It is based on the different molar concentrations of metal oxides within the converter.

In equation 5.10 droplet ejection velocity for a certain size class d can be found by several empirical relations derived by Subagyo et al. (2005). These equations are all applicable to top gas blowing process. The droplet ejection velocity is dependant on the droplet generation rate calculated in 5.8 and the kinetic energy absorbed by the droplets. The kinetic energy absorbed by the droplets can be found in equation 5.12.

$$E_{Kd,t} = 0.00143 * N_B^{0.7} * E_{Kg,t} \tag{5.12}$$

Where E_{Kd} is the kinetic energy adsorbed by the droplets at time t, $N_{B,t}$ is the blowing number at time t, $E_{Kg,t}$ the kinetic energy of the top blowing gas at time t. This kinetic energy exerted by the gas is also derived by Subagyo et al. (2005). The equation is presented in equation 5.13.

$$E_{Kg,t} = N_{b,t} * F_g * \sqrt{\sigma * g * \rho_1} \tag{5.13}$$

In this equation $E_{Kg,t}$ is the kinetic energy of the the top blowing gas at time t, $N_{B,t}$ is the dimensionless blowing number at time t, F_g is the average flow rate of oxygen in N/m^3 per s, σ is the surface tension of steel in N/m, g is the gravitational constant in m/s^2 and ρ_1 is the liquid density of steel.

When the kinetic energy absorbed in equation 5.12 by the droplets, is calculated with the kinetic energy of the blowing gas in equation 5.13. The ejection velocity of the metal droplets is found in equation 5.14 by Subagyo et al. (2005).

$$u_{drop,t}^d = \frac{E_{Kd,t}}{\frac{1}{2} * R_{b,t}^d} \tag{5.14}$$

Where $u_{drop,t}^d$ is the droplet ejection velocity in m/s at time t for droplet size class d, $E_K d, t$ is the kinetic energy absorbed by the droplets at time t and $R_{B,t}^d$ is the droplet generation rate at time t corresponding to droplet size class d.

The equations in this paragraph are all incorporated in the kinetic model, to describe the micro kinetics part in manganese refining within the converter. However due to the dynamic nature of this process and the time limitations for this research, the current model evaluated will have some limitations due to assumptions made during this research. The model limitations are described in paragraph 5.6.

5.4. Macro kinetics

The macro kinetics describes the total change of manganese in the oxysteel converter hot metal bath. Equation 5.1 gives the change in weight percentage of manganese at time step t. The first assumption to describe the macro kinetics is that ejected droplets will contain the weight percentage of manganese content in the metal bath. The calculation of manganese content in kg in the metal bath is found in equation 5.15.

$$WMn_{bath,t} = W_{bath,t} * (Mn_t/100) \tag{5.15}$$

Where $WMn_{bath,t}$ is the mass in kg of the manganese in the metal bath at time t, W_{bath} is the total mass of the hot metal bath. Mn_t is the manganese content in weight percentage at time t. The change of manganese content in the metal bath is dependant on the mass transfer of the droplets leaving the metal bath. Equation 5.16 displays the total change of manganese in the metal bath at time t and for droplet size class d. The size class is now involved in this calculation because of the changing weight of mass transfer for different droplet sizes. Therefore the influence of droplet size on the change of manganese mass in the bath will also be different.

$$WMn^d_{bath,t+1} = WMn^d_{bath,t} - (\frac{dMn\%}{dt} * R^d_{B,t}) * \Delta t \tag{5.16}$$

With $WMn^d_{bath,t+1}$ the manganese content in the metal bath in kg at time t+1 for size class d. $WMn^d_{bath,t}$ the manganese content in the metal bath in kg at time t for size class d. $\frac{dMn\%}{dt}$ the mass transfer at time t, and $R^d_{B,t}$ the droplet generation rate at time t for size class d. Δt is the time step used in the model taken as 1 s for this research. The starting mass of the hot metal bath is different for the evaluated IMPHOS heats and can be found in table 5.2.In order to calculate the new total mass of the converter bath, the changing manganese mass in the hot metal bath due to ejection of metal droplets is subtracted from the total mass of the bath. Equation 5.17 displays the total mass change of the hot metal bath.

$$W^d_{bath,t+1} = (W^d_{bath,t} + Scrap^t - WMn^d_{bath,t} - WFe_t - WC_t) + WMn^d_{bath,t+1} \tag{5.17}$$

Where $W^d_{bath,t+1}$ is the new total mass of the hot metal bath at time t+1 for size class d. $W_{bath,t}$ is the total mass of the hot metal bath at time t. $WMn^d_{bath,t}$ Is the mass of the manganese in the metal bath at time t and $WMn^d_{bath,t+1}$ is the new mass of the manganese in the hot metal bath at time t+1 for size class d. $Scrap_t$ is the calculated weight of scrap which melts into the hot metal bath per s calculated by Hewage et al. (2016) as 1.83 Kg/s. WFe_t is the weight in kg of iron which is reacting from the hot metal bath with the slag emulsion. WC_t is the weight of the carbon from the hot metal bath which react with oxygen gas at time t.

Finally the new manganese content is calculated by dividing the new manganese content in the metal bath, with the new total mass of the hot metal bath times 100%. Equation 5.18 presents The new manganese content in the metal bath over time. After completion of the algorithm, this new Mn content will then be inserted again in 5.1.

$$Mn^d_{t+1} = \frac{WMn^d_{bath,t+1}}{W^d_{bath,t}} * 100\% \tag{5.18}$$

In this equation Mn^d_{t+1} is the new manganese weight percentage content at time t and for size class d. $WMn^d_{bath,t+1}$ is the new weight of the manganese in the hot metal bath in at time t+1, and size class d and $W^d_{bath,t}$ is the new weight of the hot metal bath at time t+1 and for size class d.

By integration of Fick's law for diffusion in equation 5.1, The mass transfer of manganese can be found over a certain residence time t_res, the residence time describes the amount of time the droplet is floating in the emulsion before it reverts back into the metal bath. This new mass transfer formula is found in equation 5.19.

$$Mn_{t-1} = \%Mn^d_t + (\%Mn^d_t - \%Mn^{d*}_t) * \exp^{\frac{-k^d_t * A^d}{V^d * tres}} \tag{5.19}$$

Where $\%Mn_{t-1}$ is the integrated manganese weight percentage content, $\%Mn_t$ is the manganese weight percentage content at time t, $\%Mn^{d*}_t$ is the manganese equilibrium content for time t, $-k^d_t$ is the mass transfer coefficient at time t for droplet class size d, A^d and V^d the area and volume for a droplet size class d. Finally

t_{res} is the residence time of the droplets in s. The residence time of this model will be fixed and evaluated for 1s. The manganese content found in the model can be compared with the original datapoints found in IMPHOS.

5.5. Input data

The heat input data for the model mainly consist out of The IMPHOS input described in paragraph 3.3 table 3.1 and 3.2 for heat S1836, S1844 and S1845. Important heat data can also be found in paragraph 4.2 and 4.3. The most important model input data are the slag composition weight percentages, necessary in Suito number 3 model in order to calculate the apparent equilibrium leading to the manganese equilibrium value. As seen in the macro kinetics part, it describes if the mass transfer is positive(ejected from the bath) or is negative(reverts into the bath). This data is collected from cup height 4 and 5 due to the highest amount of datapoints present at this height as explained in paragraph 4.3. These 6-7 slag datapoints are interpolated with linear interpolation to form 960 datapoints over time. These 960 datapoints for the different slag components are then also used for calculation of the slag viscosity with the modified Urbain model. The original slag component datapoints at different heights can be found in appendix B. Besides the slag datapoints the temperature during the heat is very important, the temperature datapoints are also interpolated over time to work as temperature input per s.

For the 3 heats raw data for oxygen flow and lance height are used for calculating the generation of metal droplets within the metal bath. The lance height profiles used over 16 min of the blow can be found in chapter 8. An overview of data used in the model is presented in table 5.2

Table 5.2: Kinetic model input parameters

Parameter	Symbol	S1836	S1841	S1844	S1845	Unit
Time	t	960	960	960	960	s
Hot Metal Bath Weight	W_{bath}	5060	4610	4510	4410	Kg
Scrap Weight	Scrap	700	700	700	700	kg
Starting manganese content in bath	Mn_{con}	0.480	0,430	0.430	0.460	%
Temperature range	T	1577-1990	1587-1943	1583-1987	1555-2005	K
Slag composition		Suito No 3 Morales and Fruehan	Suito no 3 Morales and Fruehan	Suito No 3 Morales and Fruehan	Suito No 3 Morales and Fruehan	
Droplet size range	d	20-500 20-1000 20-2000	20-500 20-1000 20-2000	20-500 20-1000 20-2000	20-500 20-1000 20-2000	μm
Density gas	ρ_g	1.43	1.43	1.43	1.43	Kg/m^3
Density liquid steel	ρ_1	7000	7000	7000	7000	Kg/m^3
Surface tension steel	σ_1	1.4	1.4	1.4	1.4	N/m
Gravitational constant	g	9.81	9.81	9.81	9.81	m/s^2
Isentropic expansion factor	γ	1.4	1.4	1.4	1.4	
Lance atmospheric pressure	P_o	1001325	1001325	1001325	1001325	Pa
Lance exit pressure	P_e	101325	101325	101325	101325	Pa
Diameter Lance Nozzle throat	d_t	0.0155	0.0155	0.0155	0.0155	m
Lance Height	h	Raw data	Raw data	Raw data	Raw data	m
Gas constant	R	8.314	8.314	8.314	8.314	$J/mol*K$
Oxygen flow rate	F_g	0.289	0,288	0,276	0,290	N/m^3*s
Velocity constant	a	0.0393	0.0393	0.0393	0.0393	
Diffusion coefficient of Manganese at 1873K	D_{Mn}^{1873}	$7*10^{-9}$	$7*10^{-9}$	$7*10^{-9}$	$7*10^{-9}$	m^2/s
Slag viscosity	μ	Urbain model	Urbain model	Urbain model	Urbain model	Pa*s
Residence time	t_{res}	1	1	1	1	s

5.6. Model limitations

In this paragraph the most important limitations which influences the kinetic model are discussed. This paragraph is mainly based on previous research and experience regarding metal kinetic refining modelling. Due to the extensive dynamic nature of the oxysteel converter process in combination with a limited amount of time for this research, decisions were made to include or intentionally leave out certain micro kinetic phenomena or parameters influencing these phenomena. In reality these phenomena still contribute to the overall refining behaviour of the metal droplets in the emulsion.

5.6.1. Thermodynamic equilibrium

A limitation in the equilibrium model used by Suito & Inoue (1995) is the lack of Al_2O_3 in the experimental setup. In paragraph 4.3.1 a range of 0.8-4.5% is found which is not taken into account in the equilibrium calculations. Furthermore the oxide slag data used as experimental input is linearly interpolated. The slag

data is transformed from 6 or 7 to 960 datapoints leading to some local inaccuracies, especially at the point with missing data (In IMPHOS, there would be 8 datapoints over 16 min).

5.6.2. Droplet generation rate

The droplet generation rate calculation depends on the tangential velocity, calculated by Subagyo et al. (2005). This tangential velocity is based on the jet velocity at the impingement point of the hot metal bath. The jet velocity is dependant on the ratio of dynamic lance height and Nozzle throat diameter. According to Rout et al. (2016) the jet velocity calculation at impingement point is influenced by a temperature effect, leading to a different density and velocity of the blowing gas. The blowing number $N_{B,t}$ was found to be double in magnitude compared to the value found by Subagyo et al. (2005). This gas temperature effect is not taken into account for this research.

5.6.3. Droplet composition

Ideally the droplet size composition, used in the droplet distribution can be determined with SEM texture analysis. Due to the unavailability of pre-cut emulsion samples for texture analysis. The decision was made to only perform XRF and Spark OES on the physical bulk metal samples. More about this is explained in chapter 6. Instead literature data was used based on unpublished research of J.Small on heat S1845, to determine the range of the droplet size composition.

5.6.4. Control of mass transfer

In this research it is assumed that the micro kinetics mass transfer parameter k is controlled by the metal droplets instead of the slag, thus penetration theory by Higbie (1935) is applied. In Rout et al. (2018) the manganese refining in the emulsion zone was calculated with mixed kinetics. Both the mass transfer parameters of the metal droplets and slag were taken into account, the mass transfer parameter of the slag was calculated by a formula from Oeters (1994). The mass transfer parameter is described there for fluids as dimensionless Sherwood number and is based on a relation between the Reynolds and Schmidt number.

5.6.5. Droplet temperature

In this research the droplets were assumed to have the same temperature as the hot metal bath they were ejected from. According to Rout (2018) it can be expected that the droplet will first gain temperature when ejected from the metal bath and then cools down gradually due to heat dissipation within the emulsion. This can influence the micro kinetic reaction at the droplet-slag interface.

5.6.6. Residence time and droplet dimension

The residence time for this research will be evaluated as a fixed parameter of 1 s. This fixed residence time gives an indication how the residence time influences the droplet refining within the emulsion due to bloating phenomena. Subagyo et al. (2005) used an approach were the droplet area and volume changes based on relation between changing density and decarbonization rate to estimate the total dimension change of the droplet within the emulsion due to bloating.

In practice its difficult to predict the residence time of the droplets within the emulsion. Subagyo et al. (2005) used an approach based on 2D - ballistic motion of an ejected droplet within the emulsion. The droplet gets ejected at an angle of repose into the emulsion and slows down and moves due to difference in droplet and slag density , gravitational force and a certain drag coefficient. This drag coefficient is mainly based on the Reynolds number of the spherical droplet. In this research droplet shape and size are assumed constant over the total time of the blow. Residence time should be assigned randomly to droplets to estimate the actual effect of a droplet reverting back to the metal bath in modelling.

5.6.7. Macro kinetics

The refining of manganese is influenced by 3 different refining zones within the oxysteel converter. The jet impact zone , slag-metal interface zone and the emulsion zone. Rout et al. (2018) researched manganese refining based on kinetic plant data of all 3 zones together. Altough it was concluded that the emulsion zone contributes the most to the refining of manganese, there are still reactions taking place in the other 2 zones contributing to the overall refining. This research focuses on the refining of manganese in the emulsion zone. The contribution of manganese refining from the other 2 zones is out of the scope of this research.

6

Method: IMPHOS Sample Analysis

This chapter describes the work done on the physical IMPHOS samples, currently stored at TATA steel in Ijmuiden. First the goal of the sample analysis is presented in combination with the method outline. The decisive factors for the final sample selection are discussed together with the approach of the sample preparation. Finally the workings of the Spark OES and ICP analysis method are explained. The results from the sample analysis can be found in chapter 9.

6.1. Method outline

This paragraph contains a flowchart of all the steps performed during IMPHOS sample analysis, all steps will be explained in the remainder of this chapter. The flowchart can be seen in figure 6.1

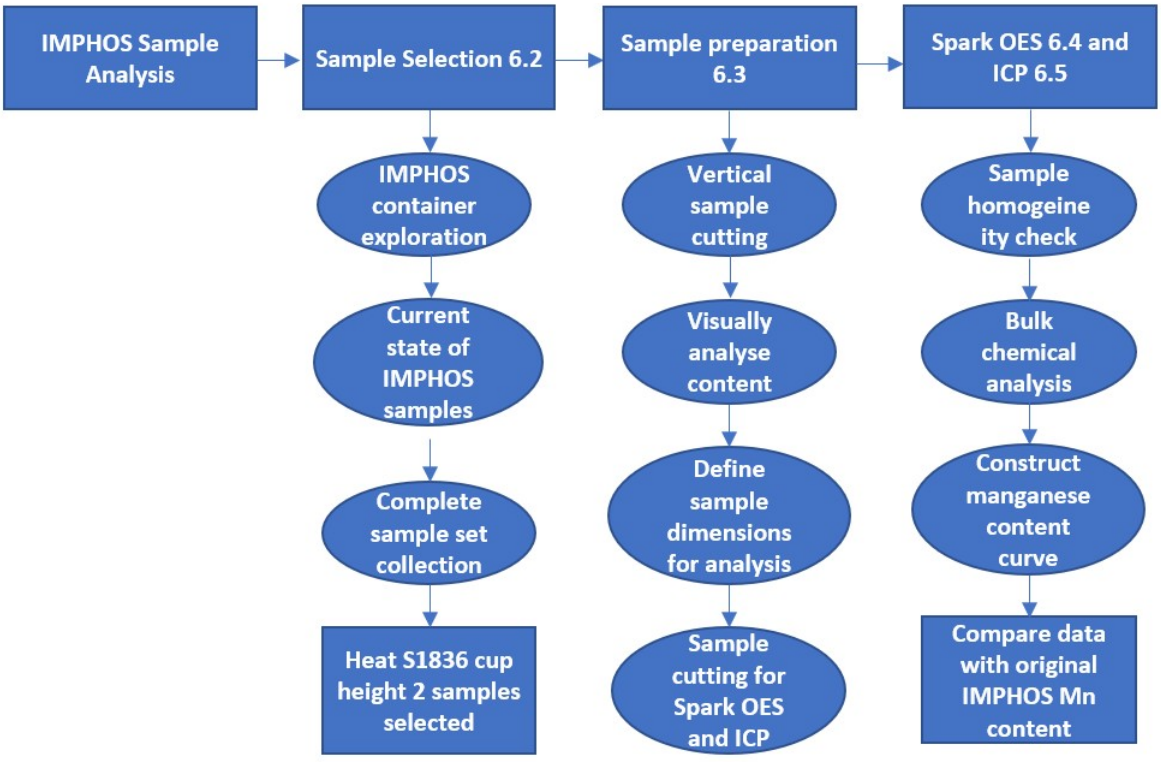

Figure 6.1: Flowchart describing physical sample analysis performed on IMPHOS samples.

6.2. IMPHOS physical sample selection

The IMPHOS samples are stored in air sealed bags in red storage boxes currently stored at TATA steel Ijmuiden. The goal of the sample analysis is to acquire data which can be used to incorporate in the kinetic model to improve the model validation. Initially the sample analysis would be done with SEM-EDS analysis to acquire droplet size ranges and content to implement in the kinetic model explained in the previous chapter. SEM-EDS analysis is a very time consuming process were all pictures of individual images made should be connected together to form final sample results. For this analysis we expected to find already prepared samples for the 3 IMPHOS heat selected in this research S1836, S1844 and S1845. Especially because heat S1845 was already analysed in Millman et al. (2011). However no prepared samples were found. Most samples found in the original boxes were full metal sample pots, which were never touched before. Unfortunately the sample preparation explained in the next paragraph was too time consuming, it was decided to skip the SEM texture analysis and to focus on bulk chemical analysis by Spark OES and ICP analysis explained later in this chapter. This is done in order to verify the hot metal bulk data from IMPHOS, which is used to validate the kinetic model. Figure 6.2 from Millman et al. (2011) shows the sample boxes and sealed conditions of the samples encountered during the sample investigation.

(a) Sample pot storage boxes (Millman et al. 2011).

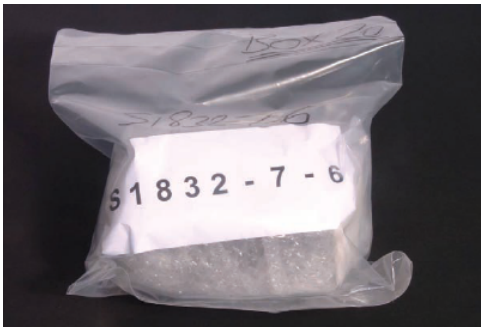

(b) Sealed Sample bags Millman et al. (2011).

Figure 6.2: Sample pot storage boxes(a) and Sealed sample bags(b)

The storage boxes from heat S1836, S1844 and S1845 were explored. Because of a lack of emulsion samples at cup heights 4-8, it was decided to investigate a complete sample set of cup height 2. For Heat S1844 and S1845 only incomplete sample sets were found in the storage boxes. For heat S1836 a complete sample set for dip number (every 2 min of measurement) 1-8 at cup height 2 was found, therefore it was decided to use this sample set for the sample analysis in this research. A complete sample set will give the most complete picture over the 16 min of the blow. There are multiple reasons for analysis of cup height 2, which can potentially contribute to this research. These reasons are:

- Cup height 2 was never analysed during previous IMPHOS research
- IMPHOS hot metal bath metal content data is only dependant on analysis of cup height 1
- Cup height 2 potentially contains the hot metal bath-slag interface

Cup height 2 was never analysed before, so it can lead to new insights in the evolution of hot metal bath content over the full 16 min of a heat. The current hot metal bath content used in IMPHOS is solely derived on cup height 1 content. The analysis described in paragraph 6.4 and 6.5 is done the same as in IMPHOS as possible to make a comparison with old IMPHOS results possible. The comparison can be found in chapter 9. The hot metal bath - slag interface could potentially be interesting because of the droplet behaviour and metal content at boundary interface, however the interface was never found at cup height 2 for heat S1836.

6.3. Sample preparation

Sample preparation was done in multiple phases, first identification of the content within the physical sample pot was needed. Therefore it was decided to vertically cut the IMPHOS samples open, to visually analyze the content within the sample. Figure 6.3 shows the sample pot on the left and the figure on the right shows a sample pot cut open vertically.

(a) Top view of massive sample pot S1836-8-2 without lid.

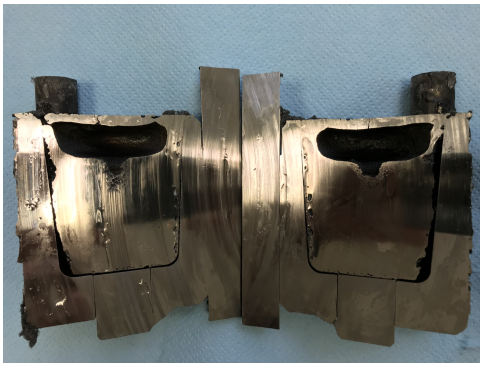

(b) Vertical crossection of sample S1836-3-2.

Figure 6.3: Top view of a S1836 sample pot(a) and vertical crossection of a S1836 sample(b)

The two different pictures above illustrate the sample development over time. The picture on the right is from S1836-3-2 or the measurement after 6 min at height 2. In this sample mainly metal material is encountered. In the picture on the left, a top view of S1836-8-2 or the measurement after 16 min at height 2, shows a lot of softer flake like material in combination with metal. This soft material is most likely emulsion slag. Figure 6.4 show to other metal samples were differences on the surface can be seen.

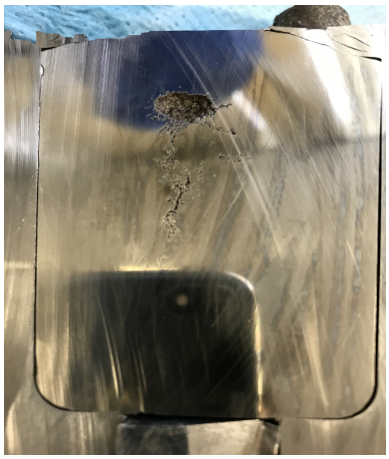

https://www.overleaf.com/project/5f22bafc29cb790001c063bd

(a) Vertical crossection of sample S1836-1-2.

(b) Vertical crossection of sample S1836-7-2.

Figure 6.4: Vertical crossection of heat S1836 height 2 at 2 min into heat(a) and 14 min into heat(b)

The figure on the left shows the metal sample 2 min into the blow. One small void is visible in the middle of the sample, compared to figure 6.2(b) the sample is still more solid. The figure on the right shows the metal sample 14 min into the blow. This measurement is taken 2 min before the cup sample in figure 6.2(a) altough no soft content was encountered in this metal sample, However more small voids are visible in comparison with the samples in the earlier part of the blow.

In order to analyse the metal content within the material, the material should be cut further into more suiting dimensions necessary for the mechanical requirements of the Spark OES and ICP analysis. these methods would be further explained in paragraph 6.4 and 6.5. The metal samples shown in 6.3(b) can be directly reduced in size by cutting the samples. The soft content in samples containing softer material as in 6.3(a) should be first removed before cutting the sample further into the required dimensions. This removal is being done by chiseling out the soft material from the bulk content in the cup.

To make the samples suitable for further cutting the real content of the sample has to be extracted from the exterior sample pots first. Further cutting of the 2 vertical halves of each sample is done in the following 2 different ways:

- 1 cm from the bottom a half moon part is extracted horizontally
- 30 by 20 mm block is extracted vertically

The samples which are cut out vertically are being used for a homogeneity analysis of the metal content within the sample. The homogeneity analysis is done to check for deviations in metal content within the sample.

Deviations in metal content can say something about the trustworthiness of sample measurements, also the measurements done a decade ago. Figure 6.5 displays the vertical cut samples for used for homogeneity analysis. Every extracted sample block is numbered with the dip number(measurement number), so that every sample of heat S1836 cup height 2 remains identified.

Figure 6.5: Vertical cut IMPHOS samples used for homogeneity analysis

The horizontal cut out samples are cut in the same way as done in the original IMPHOS research. This makes the samples suitable for bulk metal content analysis to compare the results with the original data. This is the main goal of the IMPHOS sample analysis. The original IMPHOS cutting method was never published in Millman et al. (2011) but was retrieved from a unpublished intermediate report and by contacting a former IMPHOS researcher who confirmed the method. More is explained about bulk chemical analysis in paragraph 6.4 and 6.5.

6.4. Spark OES analysis

Spark optical emission spectrometry is a relatively old optical analytical method. Currently this method is mainly used for the analysis of metal or alloys in the metallurgy industry (Zhou et al. 2005). The used light source is a spark on the surface of the of the researched sample.

For this research spark OES is performed on IMPHOS heat S1836 cup height 2 samples, with a Bruker Q4 Tasman optical spectrometer. The resulting bulk chemical analysis contains weight percentage content of 32 different elements. The most important elements for this research are the same as highlighted in chapter 3 : manganese, sulphur , phosphorus, carbon, silica. Figure 6.6 shows the optical spectrometer used.

(a) Spark OES optical spectrometer

(b) Spark OES testing with sample

Figure 6.6: Spark OES test

The picture on the left shows the optical spectrometer unused. In the picture on the right the sample is put on the pedestal and the tube is lowered onto the sample to cause the spark necessary at the sample surface. For the homogeneity analysis on the vertical samples no calibration is necessary beforehand, because only a number comparison is used to check for homogeneity. For the bulk chemical analysis performed on the horizontal cut bottom samples detailed values are of importance, then the machine needs to be calibrated first. Figure 6.7 shows the order of measurements performed on IMPHOS sample 1836-7-2 for homogeneity analysis.

(a) Spark OES performed on bottom

(b) Final spark OES measurement performed on whole sample

Figure 6.7: Spark OES performed on vertical sample

For the homogeneity analysis a standard order of measurements on every sample was done. First 5 sample measurements were taken from the bottom. Figure 6.7(a) shows the sample and the spots were the 5 sample measurements were taken. The spark used in the optical emission method leaves a circular white mark on the sample, therefore the measurements are recognisable. After the bottom measurements 3 measurements were taken from the middle of the sample and 3 measurements were taken from the top of the sample. This is done to identify any deviations within the sample, probably caused by the sample solidification due to cooling after an IMPHOS sample was taken from the converter. The results of the sample homogeneity analysis and bulk chemical analysis can be found in chapter 9.

6.5. ICP analysis

The samples cut 1 cm from the bottom of the sample pot can be seen in figure 6.8. They are analysed on their bulk chemical content for manganese, phosphorus, and sillicon with both Spark OES and ICP analysis. The ICP analysis was chosen besides Spark OES, because some horizontal samples contained holes in them. These holes can lead to inaccuracies in the contact between the light spark and the sample during Spark OES analysis.

Figure 6.8: Horizontal IMPHOS samples cut 1 cm from sample bottom used for bulk chemical analysis

The ICP analysis is a wet method where the electrons within the water dissolved sample are reaching an excited state by the thermic energy caused by a hot 6000K-10000K argon plasma. When the electrons return to their original energy level they emit their own characteristic emission spectrum. ICP analysis is in contrary to Spark OES not dependant on the smoothness of the metal surface. Therefore ICP-OES gives more reliable results than Spark OES in this case according to the TATA steel lab worker responsible for this analysis.

Part IV

Results

7

Results: IMPHOS Data Analysis

In this chapter the results from the thermodynamic data analysis on IMPHOS heats S1836, S1844 and S1845, is presented for two different thermodynamic manganese distribution models: Suito number 3 model (Suito & Inoue 1995) and Morales and Fruehan model (Morales & Fruehan 1997) as explained in chapter 4. This thermodynamic evaluation is done using metal content data and slag data at 2 different cup heights 4 and 5, within the 6t MEFOS converter used in the IMPHOS research. Two main parameters are used for this analysis: the calculated manganese equilibrium value and the manganese equilibrium partition ratio. The estimated equilibrium concentration is compared with the measured values from the respective IMPHOS heats. The formulas used for calculating the thermodynamic equilibrium for both models can be found in paragraph 4.4.1. In this chapter the figures contain multiple colored arrows. The green arrows are at the position where the manganese reversion should happen in IMPHOS. The red arrow indicates the prediction of both models for the start of the manganese reversion. The blue arrow indicates the position where the manganese reversion is ending in IMPHOS and the 2nd oxidation phase is starting.

7.1. IMPHOS heat S1836

7.1.1. Cup height 4

The calculated manganese equilibrium for both thermodynamic models can be found in figure 7.1.

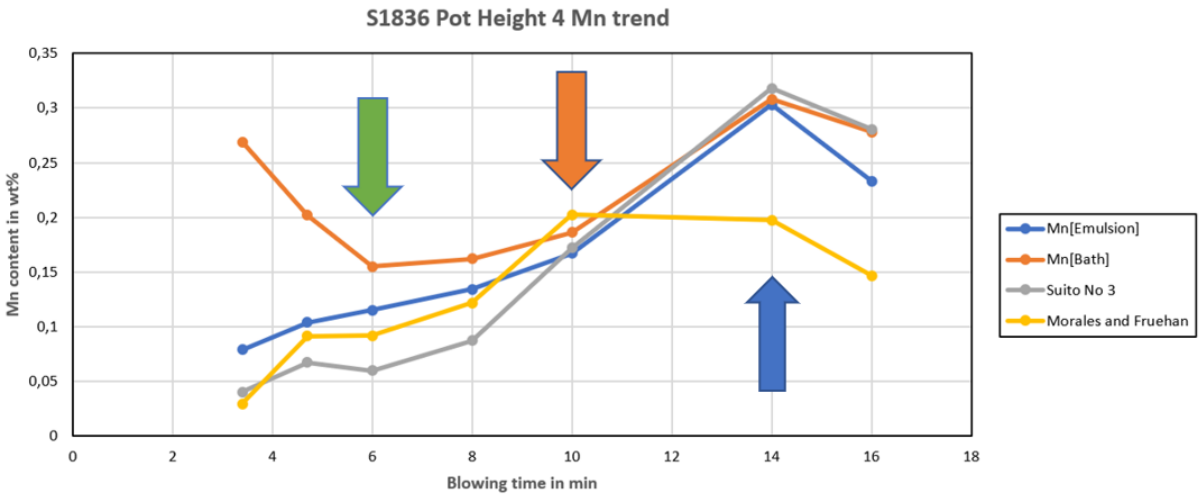

Figure 7.1: Manganese equilibrium values compared with measured IMPHOS manganese values along the time of heat S1836 in minutes.

In the figure above data from cup height 4 is used. The hot metal bath manganese content (red line) is oxidising until 6 min (green arrow), after which the reversion of the hot metal starts until 14 minutes, after which the second oxidation phase starts (blue arrow). The manganese content found in the emulsion(blue line) is

also increasing over time until 14 minutes, after which it decreases. This can indicate manganese mass transport from the hot metal bath into the slag-metal emulsion due to the ejection of metal droplets into the slag. The manganese content in the emulsion never exceeds the manganese content in the hot metal bath.

The calculated manganese equilibrium contents for the Suito no 3 model (grey line) and the Morales and Fruehan model (yellow line) are both very low at the beginning of the heat. They both are increasing over time due to a change in temperature in the hot metal bath and changing slag composition during the heat. Suito's number 3 model has a peak at 14 minutes which is the same time as the maximum manganese content from the real IMPHOS data. The Morales and Fruehan is consistently lower than the bath concentration after 10 min. Both models are not accurately predicting the moment at which manganese reversion begins after 6 min(green arrow). The models are predicting the reversion around 10 min(red arrow).

From theory the manganese equilibrium value should be lower than the actual manganese content when the manganese in the hot metal bath is oxidising. When reversion is happening the equilibrium manganese content should be higher than the actual observed values. Comparing both models it is obvious that when the manganese reversion starts, both models still need to reach an equilibrium value higher than the observed value in the hot metal bath and emulsion. This delay is slightly bigger for the Suito number 3 model in comparison with the Morales and Fruehan model. However, the peak of the Suito number 3 model at 14 min (blue arrow) is higher than the peak manganese content of the hot metal bath and emulsion which means the model predicts the reversion. The actual manganese reversion however should start at 6 min(green arrow). The equilibrium value of the Morales and Fruehan model is lower than the metal bath so manganese oxidation should happen. However the manganese in the bath is still reversing around this time.

Figure 7.2 shows the partition ratio of manganese for heat S1836 cup height 4.

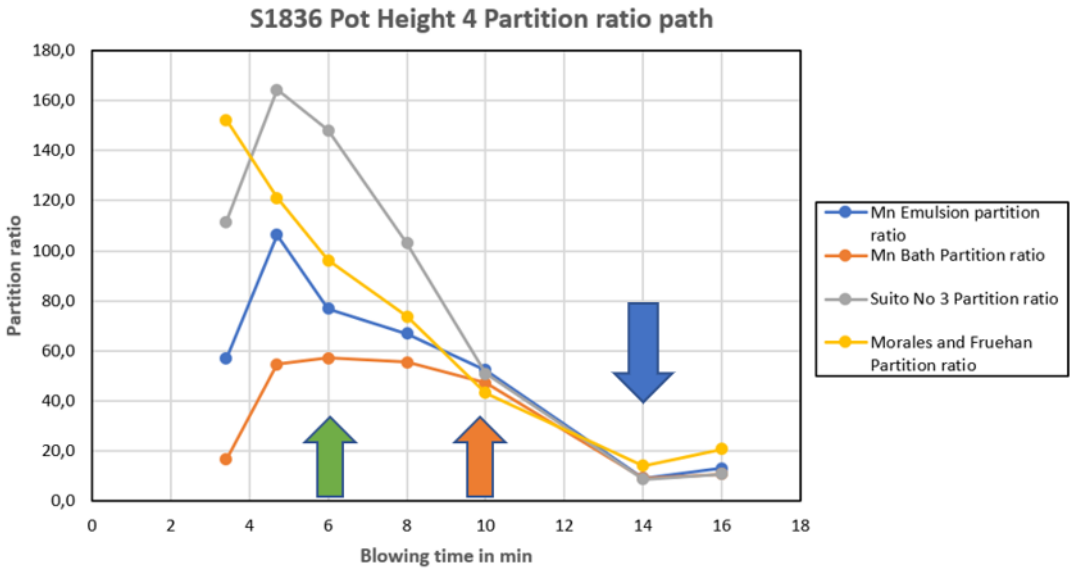

Figure 7.2: Manganese partition ratio values compared with measured IMPHOS manganese partition ratio values along the time of heat S1836 in minutes.

In this figure it can be seen that in the beginning of the heat, the equilibrium partition ratio estimated by both models is way higher than the actual observed partition ratio in IMPHOS. This indicates a higher theoretical oxidation potential. According to the partition ratio manganese reversion should happen after 10 min(red arrow). The models are not able to explain the manganese reversion after 6 min.(green arrow)

As explained in chapter 4, calculations are done for this heat with 7 datapoints. The missing data point for this heat is at 12 minutes. So between 10 and 14 minutes(blue arrow) the accuracy of the partition ratio interpolation is less accurate.

The thermodynamic analysis is also done with a temperature adjustment which is 50 K higher than the observed temperature in the hot metal bath. This is done because in the industrial process the temperature of the slag is in the range of 50-100K higher (Deo & Boom 1993). The calculated manganese equilibrium for these temperatures can be found in figure 7.3. Furthermore the calculated partition ratio for this temperature can be found in figure 7.4.

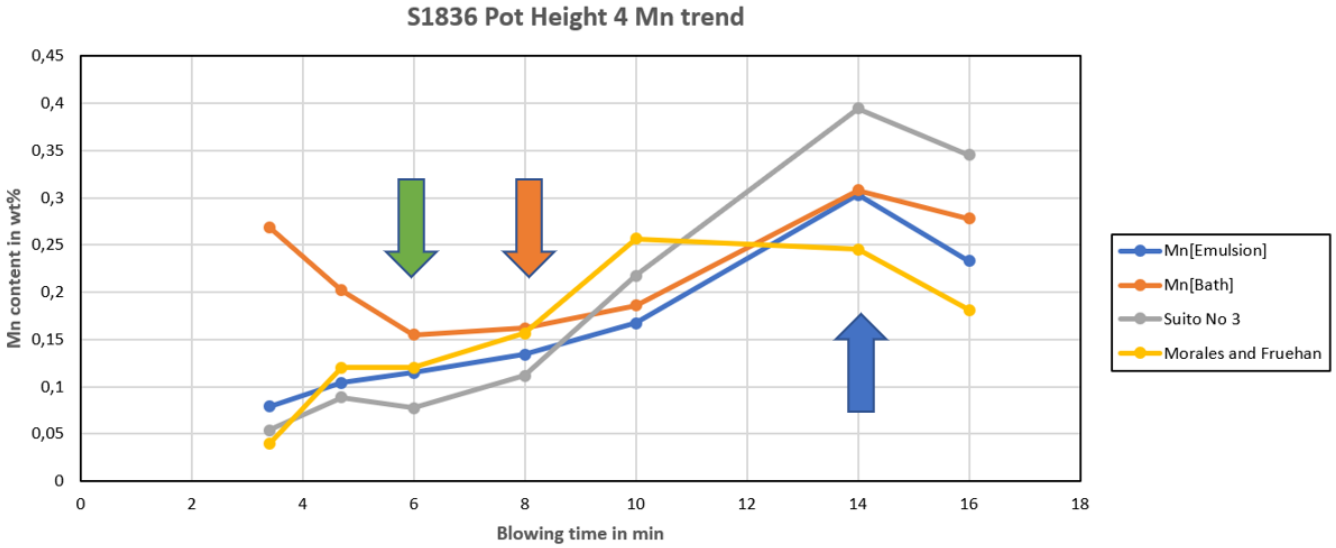

Figure 7.3: Manganese partition ratio values compared with measured IMPHOS manganese partition ratio values along the time of heat S1836 in minutes. With a temperature adjustment of +50K.

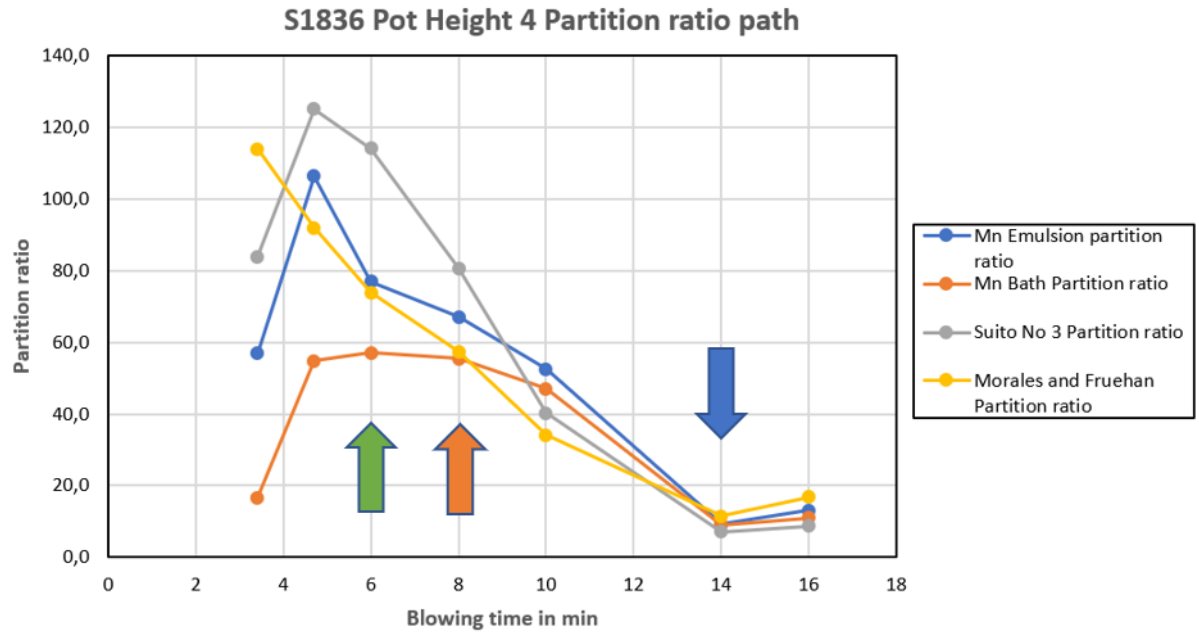

Figure 7.4: Manganese partition ratio values compared with measured IMPHOS manganese partition ratio values along the time of heat S1836 in minutes. With a temperature adjustment of +50K.

In the top figure the manganese equilibrium from both models are found to be higher during the reversion phase of the manganese in the hot metal bath and emulsion. The second oxidation stage (blue arrow) is described more accurately by Morales and Fruehan but not by Suito No 3 model, than the found curves for the original temperature of the hot metal bath. Furthermore the partition ratio shows aswell the same trend

but lower values for the oxidation potential along the whole duration of the blow.

7.1.2. Cup height 5

To identify any significant differences in manganese distribution between different IMPHOS cup heights, data from cup height 5 is also used to calculate the manganese equilibrium behaviour and partition ratio. The manganese equilibrium trend calculated for both thermodynamic models with data from cup height 5 can be found in figure 7.5. The calculated manganese partition ratio can be found in figure 7.6.

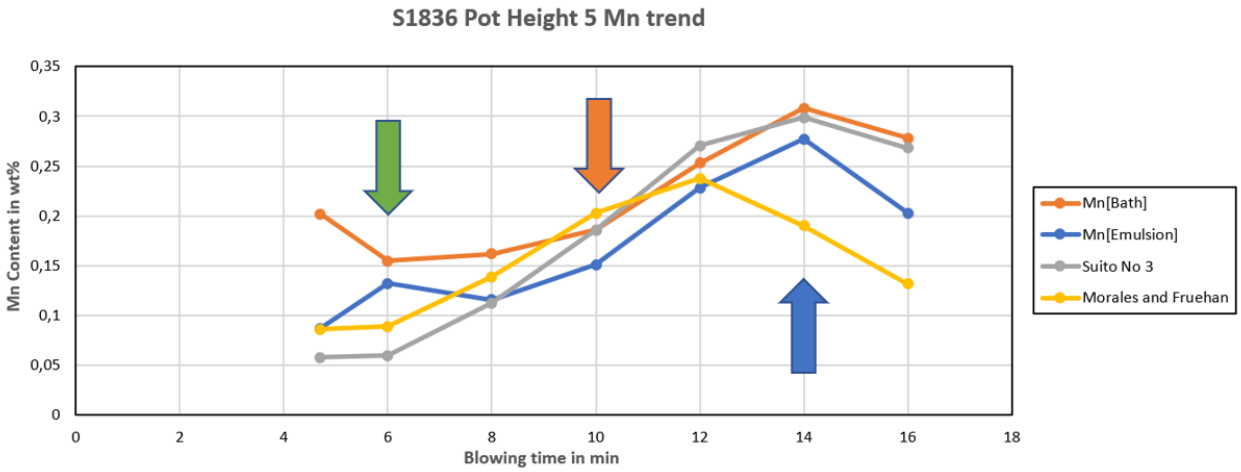

Figure 7.5: Manganese partition ratio values compared with measured IMPHOS manganese partition ratio values along the time of heat S1836 in minutes.

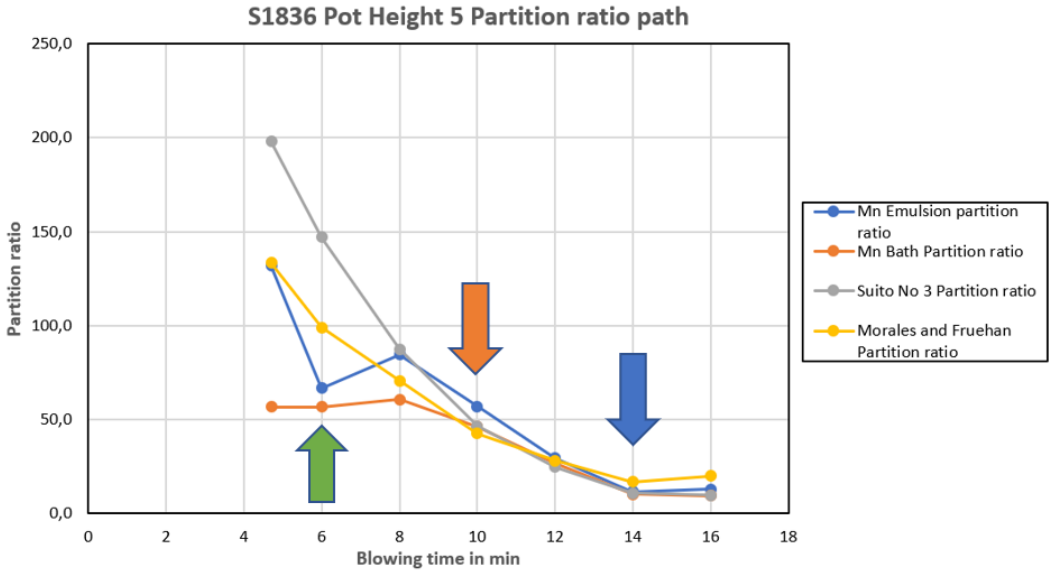

Figure 7.6: Manganese partition ratio values compared with measured IMPHOS manganese partition ratio values along the time of heat S1836 in minutes.

For both the manganese equilibrium as the partition ratio similar curves are found at cup height 5 as in cup height 4. The influence of the different slag content data from both cups is minimal on the final calculation. An important observation is that the missing data point at cup height 5 is after 2 minutes, so the first 4 minutes no accurate calculation can be made. At 12 minutes cup height 5 contains an extra data point, which makes the calculation of the equilibrium and partition ratio more accurate between 10 and 14 minutes in comparison with cup height 4. From 7.5 it can be seen that Suito no 3 model has higher values for the equi-

librium between 8 and 16 min which means it can predict the manganese reversion from 8 min(red arrow), but not the measured IMPHOS value around 6 min(green arrow). After 14 min(blue arrow) the equilibrium value for Suito is still higher than the metal bath, which means that this model is not able to predict the 2nd oxidation phase of manganese. The Morales and Fruehan model is better in predicting the 2nd oxidation phase of manganese. The found equilibrium values are lower after 14 min than the measured equilibrium values in IMPHOS.

Just as for cup height 4, At cup height 5 the slag data is also for a thermodynamic analysis with a temperature increase of 50 K. The calculated manganese equilibrium for these temperatures at cup height 5 can be found in figure 7.7. Furthermore the calculated partition ratio for this temperature can be found in figure 7.8.

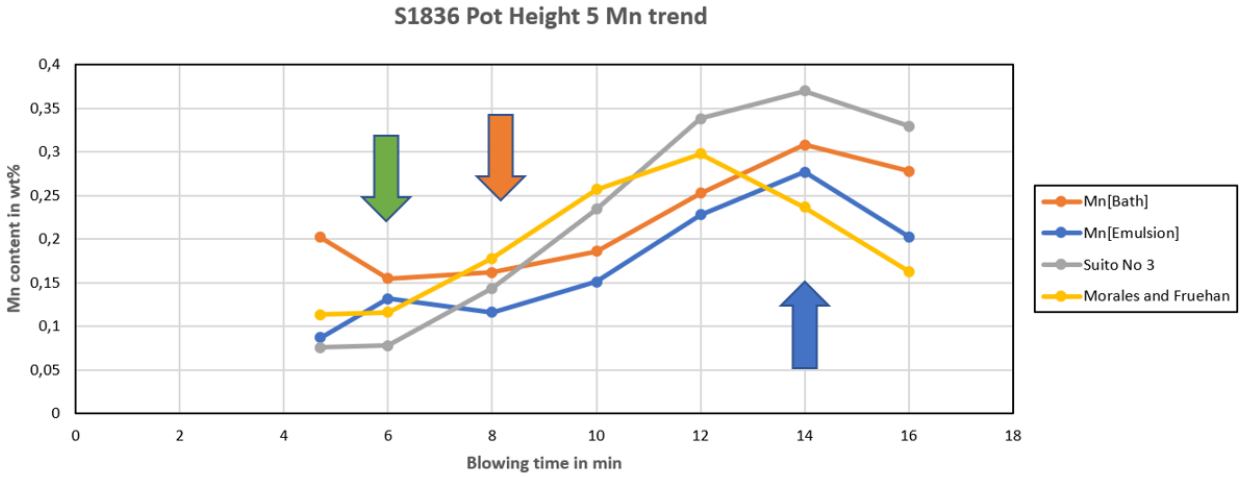

Figure 7.7: Manganese partition ratio values compared with measured IMPHOS manganese partition ratio values along the time of heat S1836 in minutes. With a temperature adjustment of +50K.

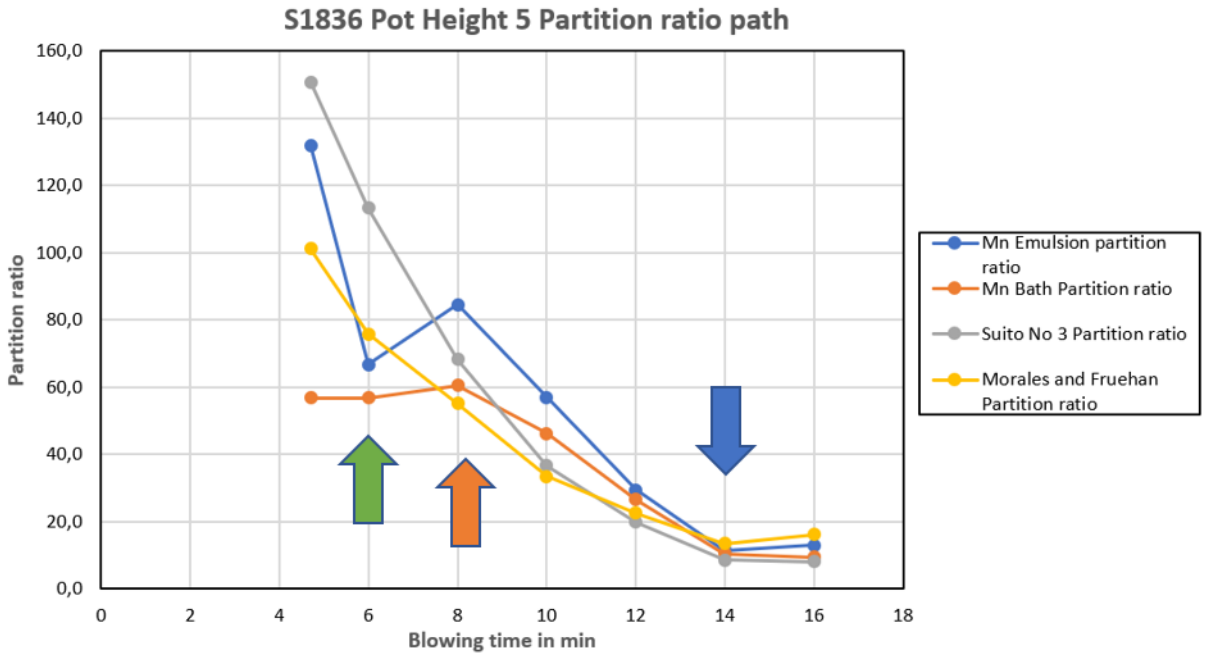

Figure 7.8: Manganese partition ratio values compared with measured IMPHOS manganese partition ratio values along the time of heat S1836 in minutes. With a temperature adjustment of +50K.

Similar cup height 4 both heights show the same behaviour for the manganese equilibrium and the oxidation

potential when the temperature used is higher. The manganese equilibrium peaks are higher for both models and the oxidation potential is lower for both models with adjusted temperature. The behaviour of the curves is the same for both cup heights, their is a difference in the maximum partition ratio. The maximum partition ratio at time of oxidation is higher for cup height 5 compared to cup height 4 for the Suito no 3 model. For the Morales and Fruehan model the observed partition ratio is the same. This is caused by a slightly higher oxide content in cup height 5 leading to a small decrease of the calculated manganese equilibrium content for the Suito no 3 model.

7.1.3. Influence of basicity and iron oxide content

As described in paragraph 2.2.2 besides temperature, the manganese distribution can also be influenced by the slag basicity (B2) from equation 2.1 or the iron oxide content in the slag. The iron content in the slag is also used in calculating the equilibrium manganese content for both the Suito no 3 and Morales and Fruehan model. Figure 7.9 shows the manganese distribution for different calculated B2 values during the heat.

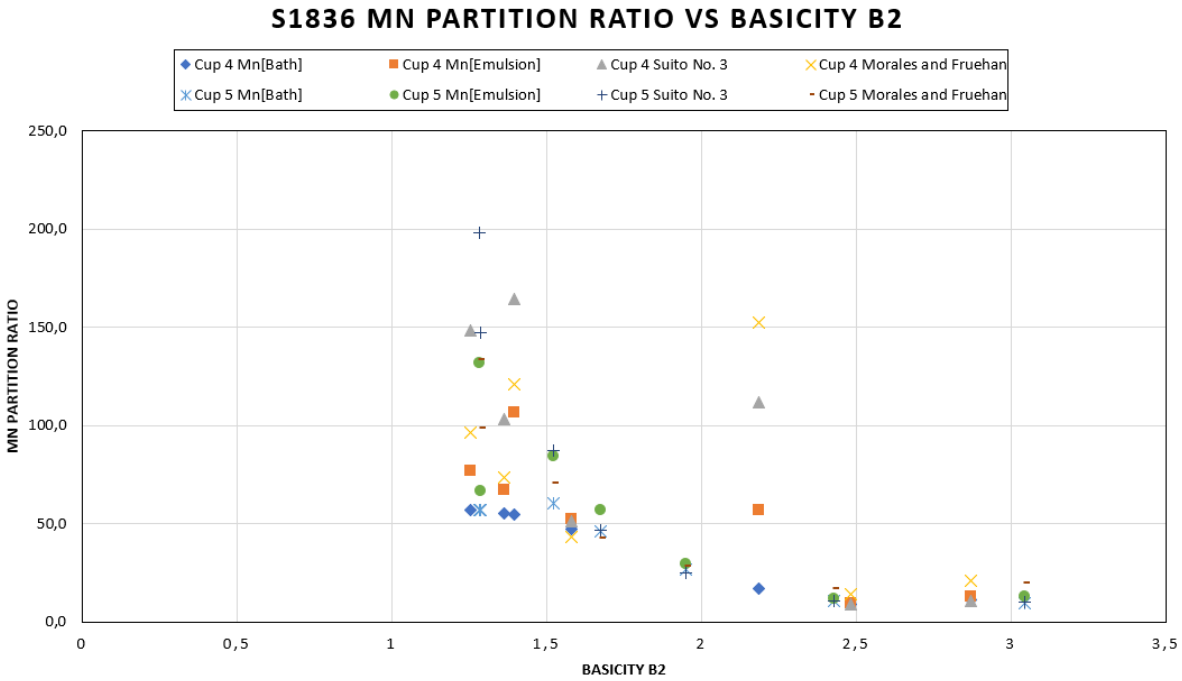

Figure 7.9: Manganese partition ratio values against the calculated slag basicity.

In the figure the most clear observation is the lower oxidation potential at higher B2 values. At lower Basicity values the observed oxidation potentials are higher with more variation. The manganese partition ratio versus the iron oxide content can be found in figure 7.10.

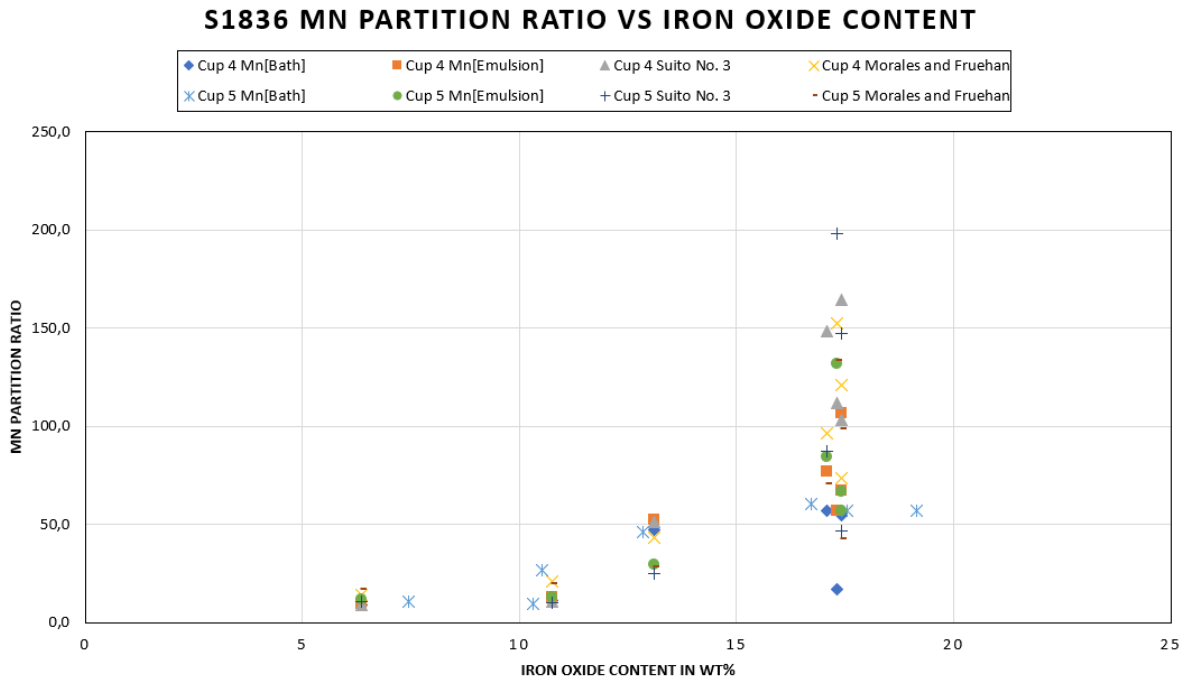

Figure 7.10: Manganese partition ratio values against the iron- oxide content in the slag.

In the figure it can be seen that the manganese oxidation potential is higher at higher FeO contents within the slag. At lower FeO contents the oxidation potential is also lower.

7.2. IMPHOS heats S1844 and S1845

For IMPHOS heats S1844 and S1845 the same analysis was done as described in the previous paragraph. The heats were analysed for the manganese equilibrium values for both thermodynamic models with data from cup height 4 and 5. The results for both heats were similar to the results from S1836 and can be found in Appendix C.

7.3. Data analysis conclusions

The following can be concluded from the results of the thermodynamic data analysis:

- Suito No 3 model shows more accurate prediction of the manganese reversion phase for the IMPHOS data than Morales and Fruehan model. Morales gives a better prediction of the 2nd oxidation phase of manganese. Both models were not capable of finding the exact point in time where the manganese reversion starts.
- Observed behaviour for manganese equilibrium and partition ratio is the same for cup height 4 and 5, cup height 5 has a slightly higher manganese partition ratio for Suito No 3 model.
- Local inaccuracies occur between cup height 4 and 5 because of the different positions of missing data points along time.
- A temperature increase of 50 K to better estimate the higher temperature of the slag within the converter, leads to a better observed approximation of manganese equilibrium behaviour and partition ratio for the IMPHOS data.
- Higher manganese oxidation potentials were found at lower B2 basicity values (<2) this is in line with the research of Suito & Inoue (1984*b*).
- Higher manganese oxidation potentials were found at higher Fe_tO values. (>15 wt%) This is logical considering the behaviour of manganese is highly influenced by equation 2.16.

8

Results: Kinetic Model for Manganese in the Converter

This chapter presents the result from the kinetic modelling for the prediction of the manganese refining path as explained in chapter 5. The kinetic model was evaluated with data from IMPHOS heats S1836, S1844, S1845 as heats with a significant reversion of manganese during the heat, and with heat S1841 as reference heat were no manganese reversion was observed. The 2 different thermodynamic models analysed in the previous chapter are used as input data for calculating the Mn equilibrium at slag-metal interface. Metal and slag data from 2 different IMPHOS cup heights 4 and 5 are used to compare them within the model. Furthermore 3 different droplet size distributions are made with the Rosin-Rammler-Sperling method to investigate how droplet size and distribution affect the results.

The kinetic model is made in python with, the goal of the modelling is to understand dynamic factors influencing the refining path of manganese in the emulsion zone. These factors are:

- Droplet size dimensions
- Droplet size distribution
- Mass transfer parameter
- Residence time

The model is evaluated to check the sensitivity of every calculation per droplet size class and to check how the total macroscopic change of manganese mass transfer influences the manganese content in the bath. The used time step in the model is 1s.

To evaluate the sensitivity of the model calculations per droplet size class the following figures are created:

- Droplet generation rate (Rb) per droplet size class
- Mass transfer parameter(K) per droplet size class
- Manganese mass transfer per droplet size class

To evaluate the total macroscopic change of manganese mass transfer the following figures are created:

- Total mass transfer of manganese
- Total mass of manganese in the hot metal bath
- Scrap melting rate
- Iron transfer rate from bath to slag

- Carbon transfer rate from bath to gas
- Total mass of the hot metal bath
- Manganese content in the hot metal bath

8.1. Sensitivity of the kinetic model calculation

8.1.1. Droplet generation rate

The droplet generation rate for heat S1836 as calculated with equation 5.8 can be found in figure 8.1.

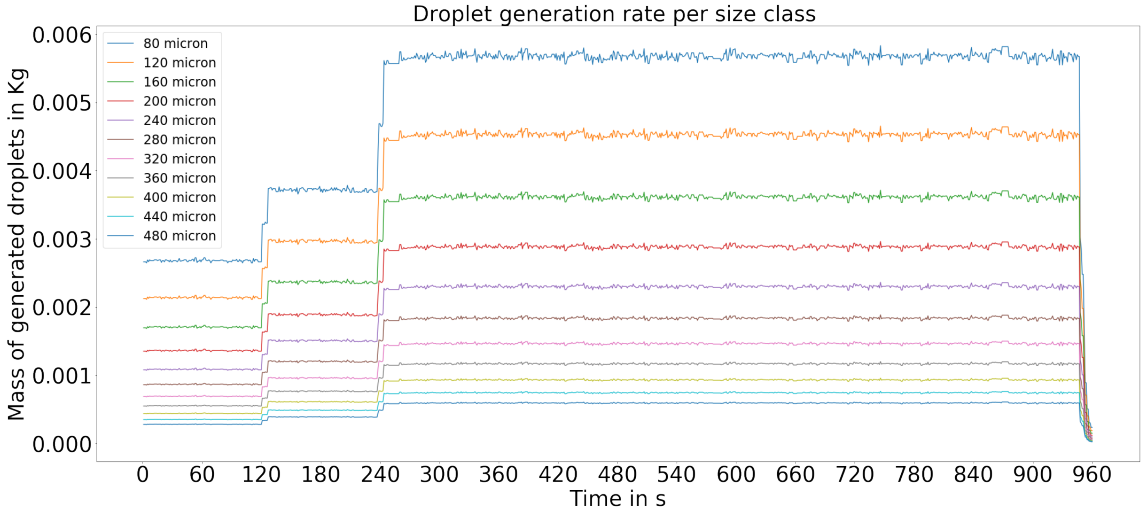

Figure 8.1: Droplet generation rate for different droplet size classes, heat S1836-cup height 4-Suito number 3 model, droplet size 20-500 micron.

In the figure it can be seen that the droplet generation rate per droplet size class, has 3 different shifts over the total 960 s of the heat. The first shift occurs at 120 s and is because the first adjustment of the lance height position, where the lance height position is lowered. The 2nd shift occurs at 240s where the lance height position is lowered again. The final major change can be seen at the end of the heat where the lance height is raised again. Furthermore in the figure it can be seen that for the smallest size classes the most droplets are generated. In the RRS distributions the smallest droplet sizes contribute also the most to the overall droplet population. How sensitive the droplet generation rate is for lance height position can be seen in 8.2.

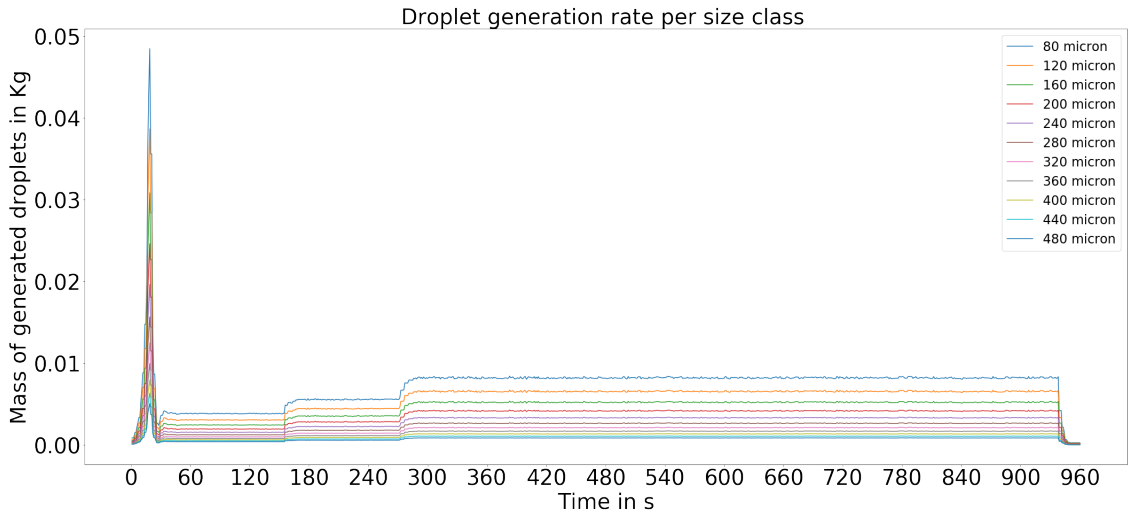

Figure 8.2: Droplet generation rate for different droplet size classes, heat S1844-cup height 4-Suito number 3 model, droplet size 20-500 micron.

For S1836 a more gradual interval for lance height position was selected , while for S1844 the lance height position was used immediatly from the start of the heat. After 30 seconds the lance height is first lowered until 120 cm. Afterwards its immediatly raised again until 180 cm, after which the normal lance height gradual lance height position is used as seen in the droplet generation rate of S1836. The peak at 30s in S1844 shows how fast the droplet generation can change for a very drastic change of lance height position.

8.1.2. Mass transfer parameter K

The mass transfer parameter K per droplet size class for heat S1836 and S1844 can be seen in figure 8.3 and 8.4.

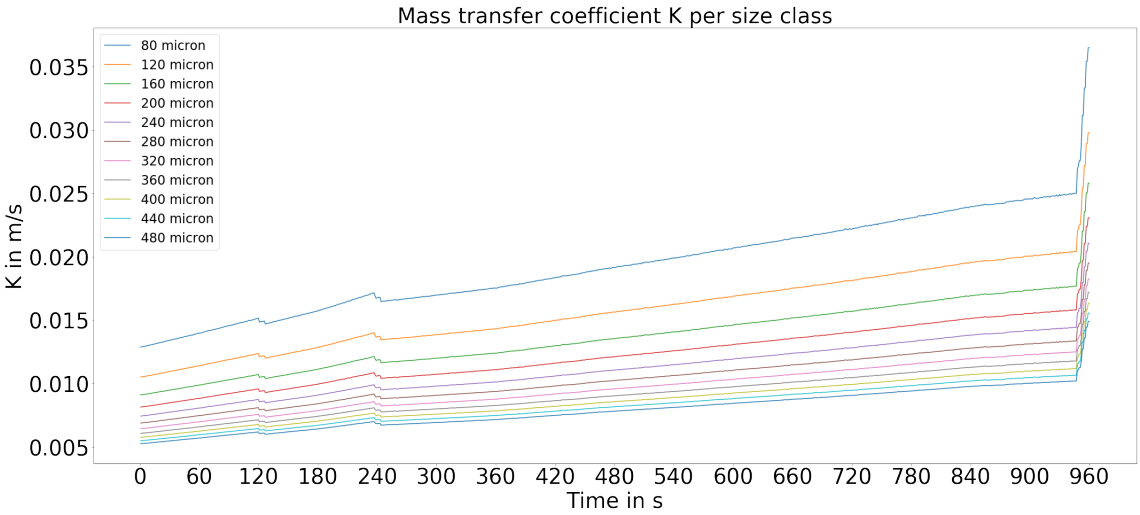

Figure 8.3: Mass transfer parameter K for different droplet size classes, heat S1836-cup height 4-Suito number 3 model, droplet size 20-500 micron.

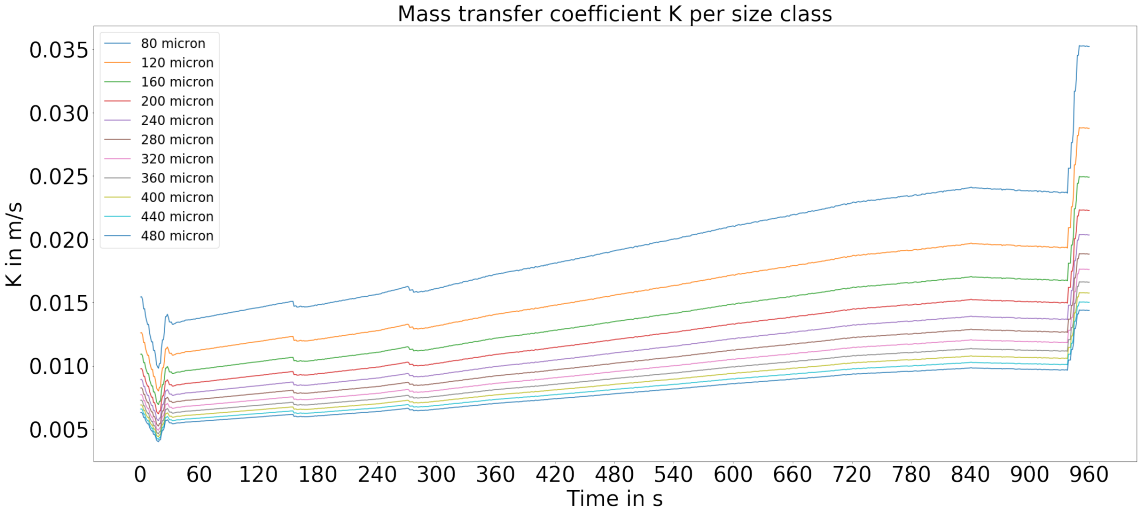

Figure 8.4: Mass transfer parameter K for different droplet size classes, heat S1844-cup height 4-Suito number 3 model, droplet size 20-500 micron.

In the top figure it can be seen that the 2 shifts of the droplet generation rate at 120 and 240 s also influences the mass transfer parameter K at this time. This is because the droplet generation rate influences the ejection velocity of the droplets from the hot metal bath, used in Higbie's penetration theory from equation 5.10. In the bottom figure the peak after 30 seconds caused by the drastic change in lance height position also influences the mass transfer parameter for heat S1844. Due to the influence of the droplet size in the denominator of 5.10 the smallest droplet size classes show the highest mass transfer parameter values. For smaller droplets

the ratio of surface area to its volume is also bigger than for bigger droplets. The relation between droplets generation rate and ejection velocity is clear: if more droplets are ejected, the ejection velocity of the droplets will be lower causing a decrease in the mass transfer coefficient K due to less friction between the droplets surface and the surrounding slag. The mass transfer parameter is increasing over time while the droplet generation rate is constant, because of the increasing temperature and a changing slag viscosity leading to an overall higher diffusivity.

8.1.3. Manganese mass transfer per droplet size class

The manganese mass transfer in kg per droplet size class over time for heat S1836 can be seen in figure 8.5. The mass transfer per droplet size class for heat S1844 can be seen in 8.6.

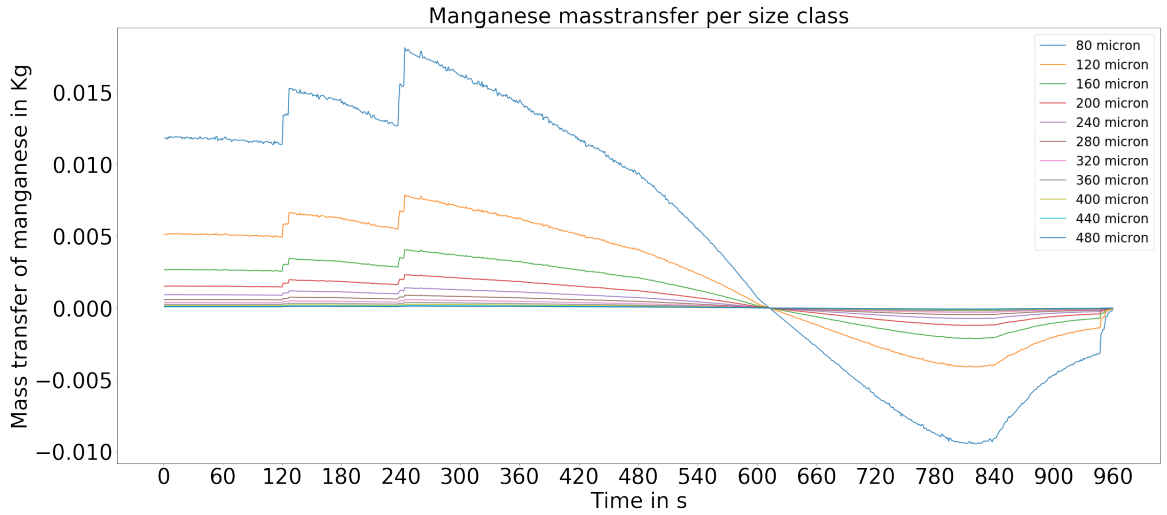

Figure 8.5: Manganese mass transfer in kg for different droplet size classes, heat S1836-cup height 4-Suito number 3 model, droplet size 20-500 micron.

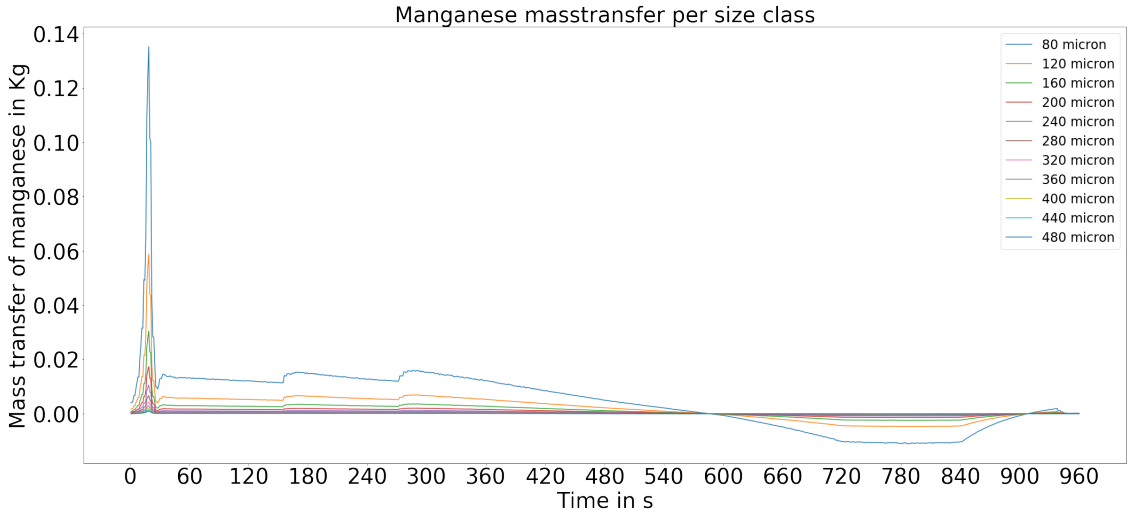

Figure 8.6: Manganese mass transfer in kg for different droplet size classes, heat S1844-cup height 4-Suito number 3 model, droplet size 20-500 micron.

In the figures above it can be seen that the mass transfer is positive until 600 s which means the first 10 min net amount of manganese in the hot metal bath is decreasing. After 600 s the net mass transfer of manganese is negative which means the total amount of manganese is increasing in the hot metal bath and the reversion is happening. Because of the highest amount of droplets generated for the smallest droplet size class and the highest value for kinetic mass transfer parameter, the masstransfer for this size class is the highest. In the bottom figure the standard peak due to lance height at 30 s is higher again than the rest of the heat. For droplet generation rate the same high peak was noticed while the kinetic mass transfer parameter had a small dip. This means that the higher droplet generation rate still leads to a significantly short increase of the manganese mass transfer.

8.2. Macroscopic change of manganese in the kinetic model

8.2.1. Manganese mass transfer

The total manganese mass transfer rate over time for heat S1836 can be seen in figure 8.7.

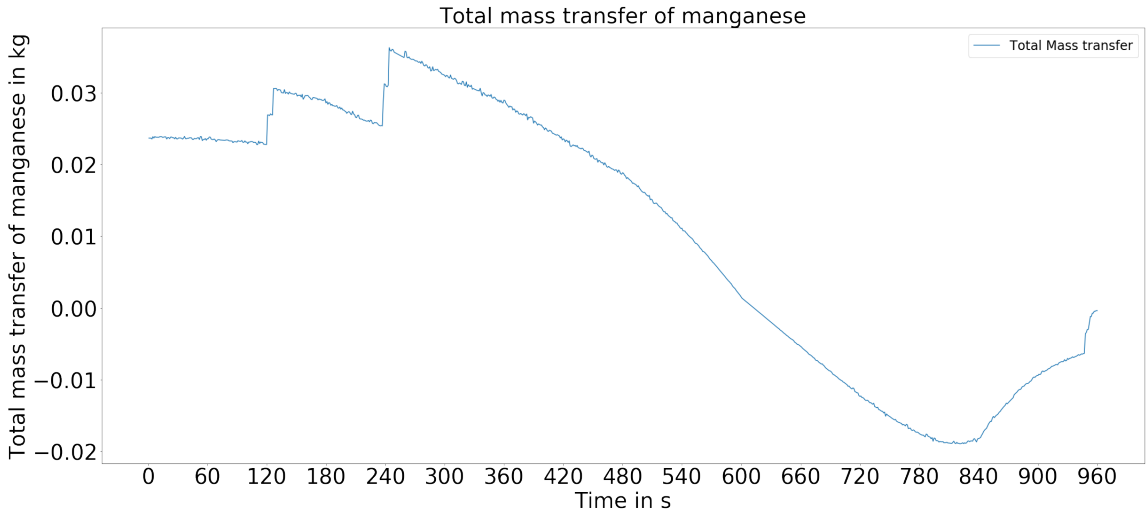

Figure 8.7: Total manganese mass transfer rate in kg, heat S1844-cup height 4-Suito number 3 model, droplet size 20-500 micron.

The total manganese mass transfer rate shows the same profile as in figure 8.5. The 2 changes in lance height position are influencing the total mass transfer rate per s at 120 s and 240 s. Until 600 s the net amount of manganese in the hot metal bath is decreasing after which reversion happens. Figure 8.8 shows the total change of manganese mass in the hot metal bath in kg for heat S1836.

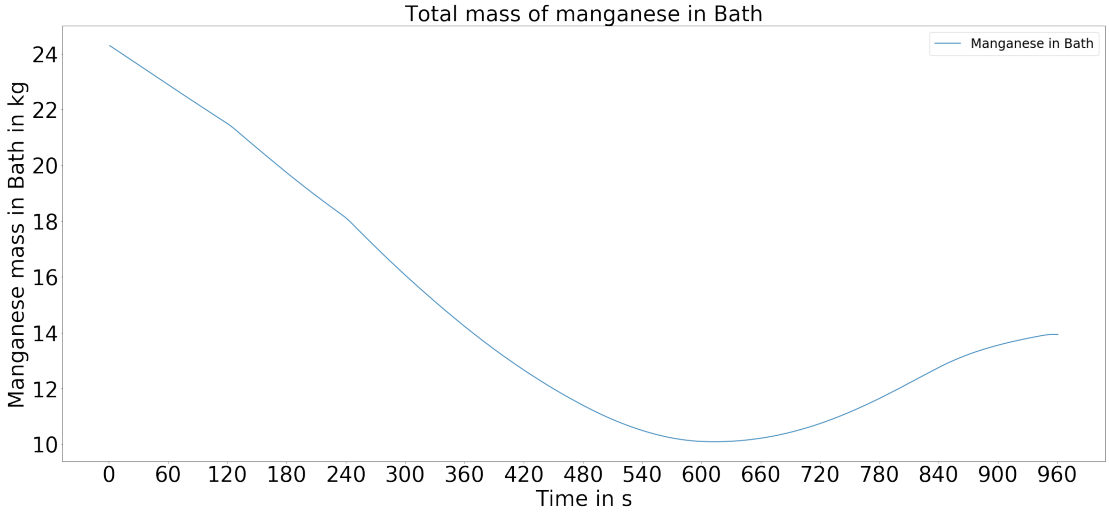

Figure 8.8: Total manganese mass in the hot metal bath in kg, heat S1836-cup height 4-Suito number 3 model, droplet size 20-500 micron.

In this figure it can be seen that the manganese mass in the hot metal bath for this heat starts of with 24 kg, it decreases until 600 s into the heat to a value of 10 kg with a wt% of 0.18, after which reversion occurs until the final amount of manganese in the hot metal bath is reached with a value of 14 kg and a wt% of 0.24.

8.2.2. Total mass change of the hot metal bath

In this model the total mass of the hot metal bath is not only influenced by the manganese mass transfer, due to the standard value of 700 kg scrap added to the hot metal at the start of the IMPHOS heat the total mass of the bath increases until all the scrap is molten into the metal bath. From Hewage et al. (2016) it was calculated that scrap is melting with a constant rate of 110 kg/min in the hot metal bath. This means a constant scrap melting rate of 1.83 kg/s for all IMPHOS heats. For every heat 700 kg of scrap is added, this means that the scrap is depleted into the hot metal bath around 380 s. The total mass change of the hot metal bath is also dependant on the iron transfer into the emulsion and the carbon transfer from the hot metal bath to the gas phase. Weight percentages of iron oxide and carbon content are combined with the molar fractions and the slag weight to calculate the total mass transfer rate for both, the separate datapoints have to be interpolated for this over 960s. The mass transfer rate for iron in S1836 can be seen in figure 8.9. The mass transfer rate for carbon transfer can be seen in figure 8.10.

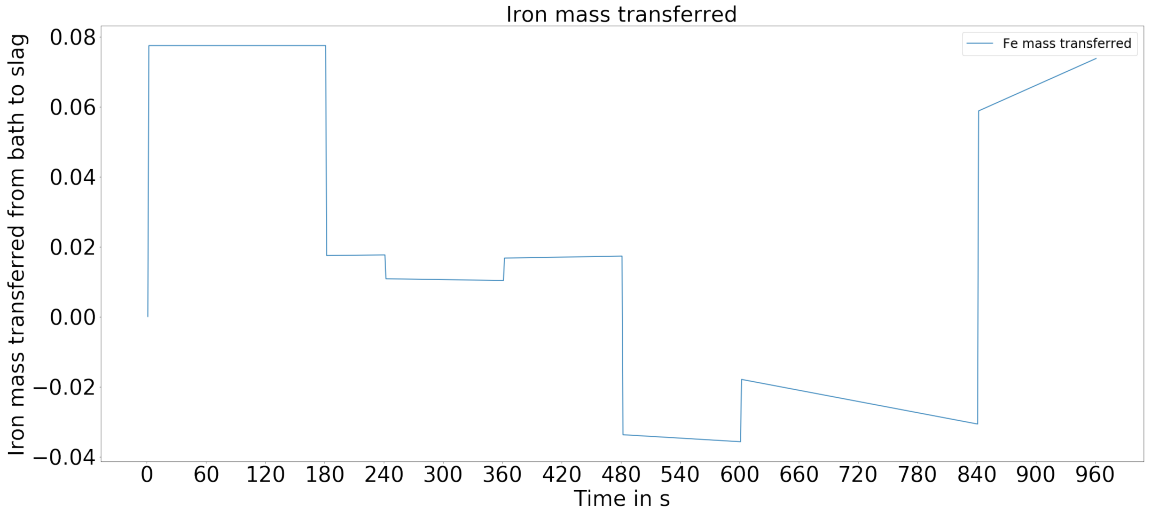

Figure 8.9: Iron mass transfer rate in kg , heat S1836-cup height 4-Suito number 3 model, droplet size 20-500 micron.

In figure 2.10 and 2.11 the different intervals from the data interpolation are clearly visible, The iron first oxides fast after which it also reverts back into the metal bath. The carbon transfer is slow in the beginning which is supported by Jalkanen & Holappa (2013). After 6 min the silicon is depleted and the carbon transfer rate is increasing. The bend lines in the figures are caused by the missing datapoints for the respective cup height 4.

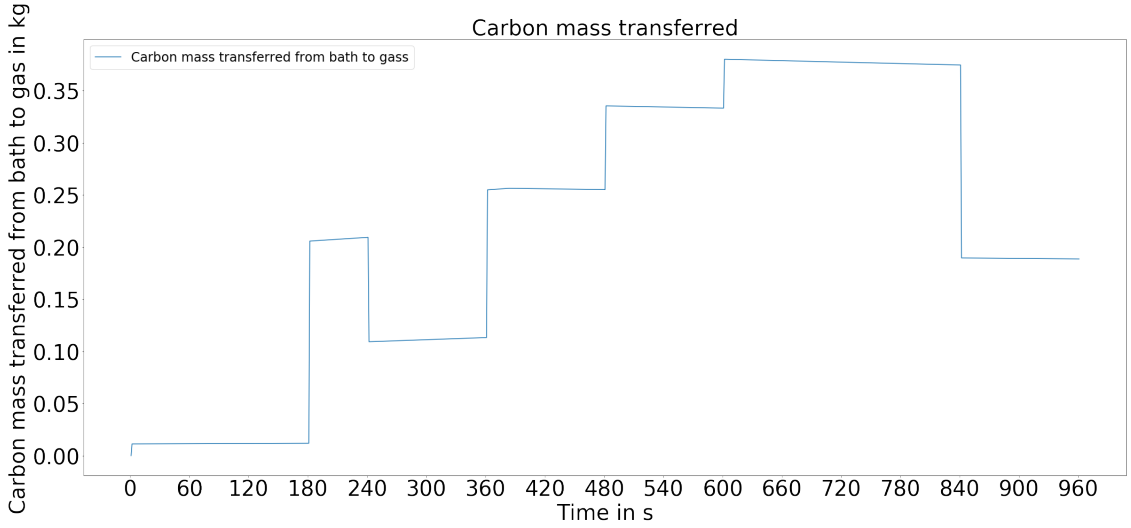

Figure 8.10: Carbon mass transfer rate in kg , heat S1836-cup height 4-Suito number 3 model, droplet size 20-500 micron.

For every time step the new total mass of the hot metal bath is then calculated by subtracting the manganese transfer, iron transfer and carbon transfer and adding the molten scrap per s. The total mass change for heat S1836 can be seen in figure 8.11.

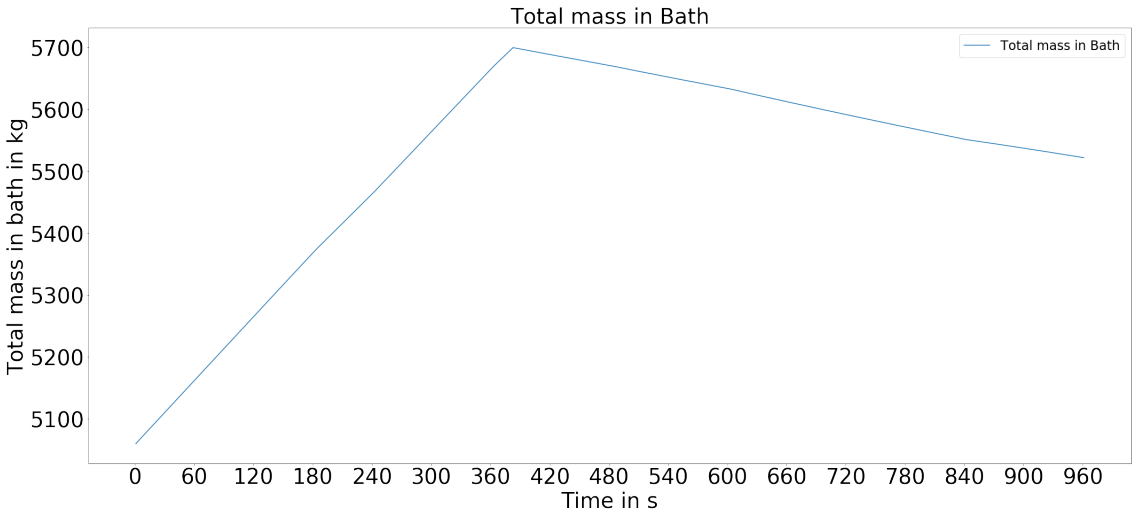

Figure 8.11: Total mass hot metal bath in kg , heat S1836-cup height 4-Suito number 3 model, droplet size 20-500 micron.

It can be seen that the mass of the bath is increasing until all scrap is melted around 380 seconds. After which the net mass change is negative because of the carbon iron and manganese leaving the bath. after 600 seconds when manganese reversion occurs the curve is flattening a bit. For this heat the total weight of the hot metal bath starts at 5060 kg after all scrap is melted the weight of hot metal bath lies around 5700 kg.

8.2.3. Change of manganese content in the hot metal bath

By dividing the manganese mass in the hot metal bath in the next time step by the new total mass of the hot metal bath, the new manganese content in weight percentage in the hot metal bath can be calculated. The weight percentage of manganese in the hot metal bath over time for heat S1836 can be found in figure 8.12.

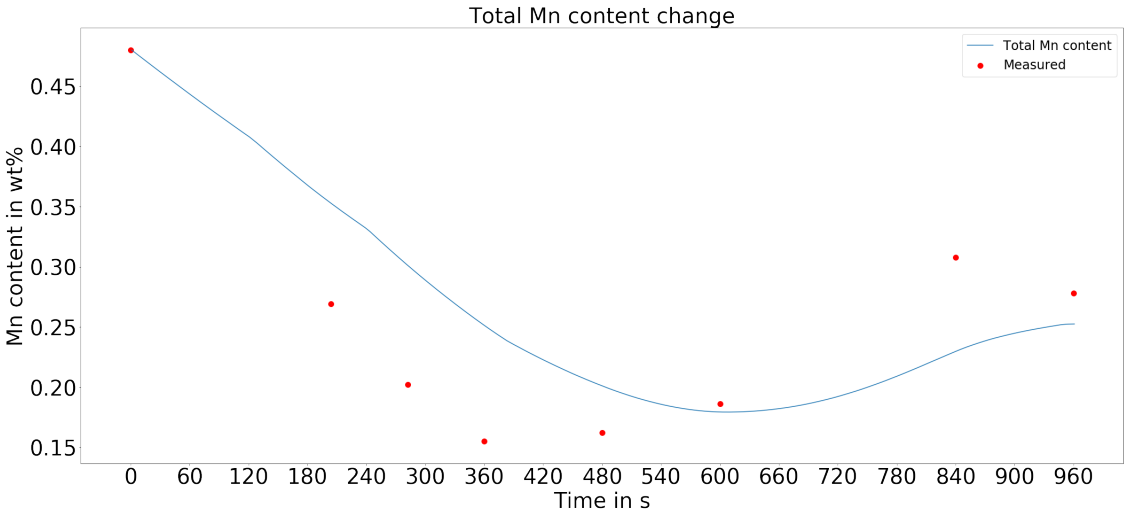

Figure 8.12: Total manganese content change over time in wt% , heat S1836-cup height 4-Suito number 3 model, droplet size 20-500 micron.

In the figure it can be seen that the model predicts the primary oxidation phase of manganese a bit too slow, also the reversion of manganese starts later than the observed IMPHOS data points indicated by the red dots within the figure. The reason for the slow primary oxidation rate can be the lack of slag data at the start of the heat. For this model the starting slag composition is assumed to be the same as the same data point after 2 min. The other important influence is the inaccuracy of the Mn equilibrium prediction of the reversion of manganese in IMPHOS as seen in chapter 7. From Hewage et al. (2016) it was concluded that the manganese reversion was very hard to predict with first order kinetic modelling. The heats without manganese reversion are by literature easy to estimate therefore this kinetic model was also run with data from heat S1841. The weight percentage of manganese in the hot metal bath over time for heat S1841 can be found in figure 8.13.

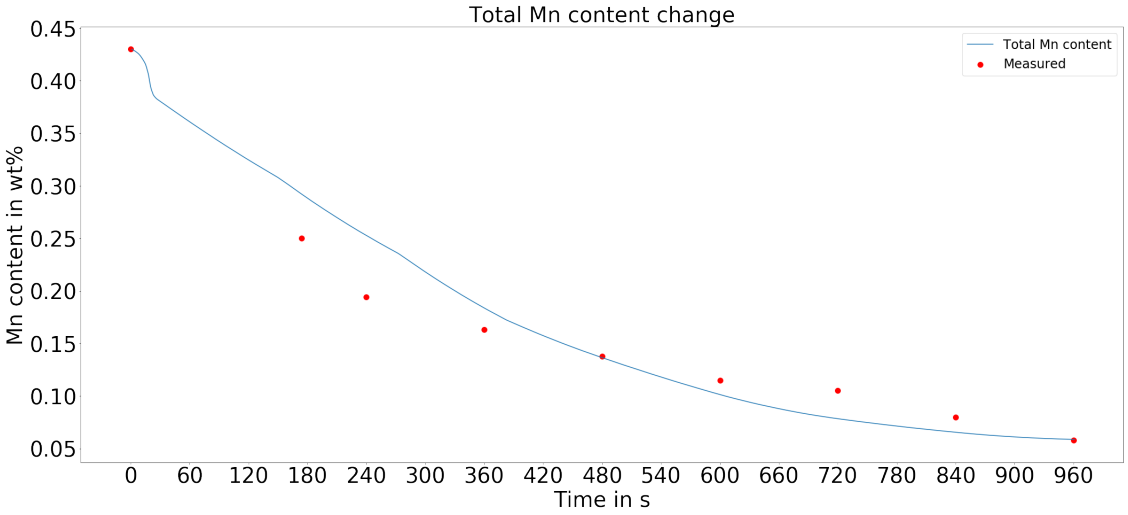

Figure 8.13: Total manganese content change over time in wt% , heat S1841-cup height 4-Suito number 3 model, droplet size 20-500 micron.

In this figure the sudden drop in the beginning of the curve is due to the lance height position used for heat s1841, the same sudden drop in lance height position was observed in S1844 in the beginning of this chapter.

It can be seen that the actual data of manganese content in the hot metal bath is better predicted by the model without manganese reversion than heats with manganese reversion.

8.3. Influence and comparison of model input data on the results

The kinetic model is run for 4 heats with 2 different thermodynamic models using data from 2 different cup heights, with 3 different droplet distributions. This paragraph describes the differences between results of the different input data used. 48 runs were done and 528 figures were created. Some additional figures resulting from the kinetic model can be found in appendix D.

8.3.1. Droplet size distribution

The kinetic model was analysed for 3 droplet size distributions 20-500 micron, 20-1000 micron, 20-2000 micron. The influence of increasing droplet size range for heat S1844 can be found in figure 8.14.

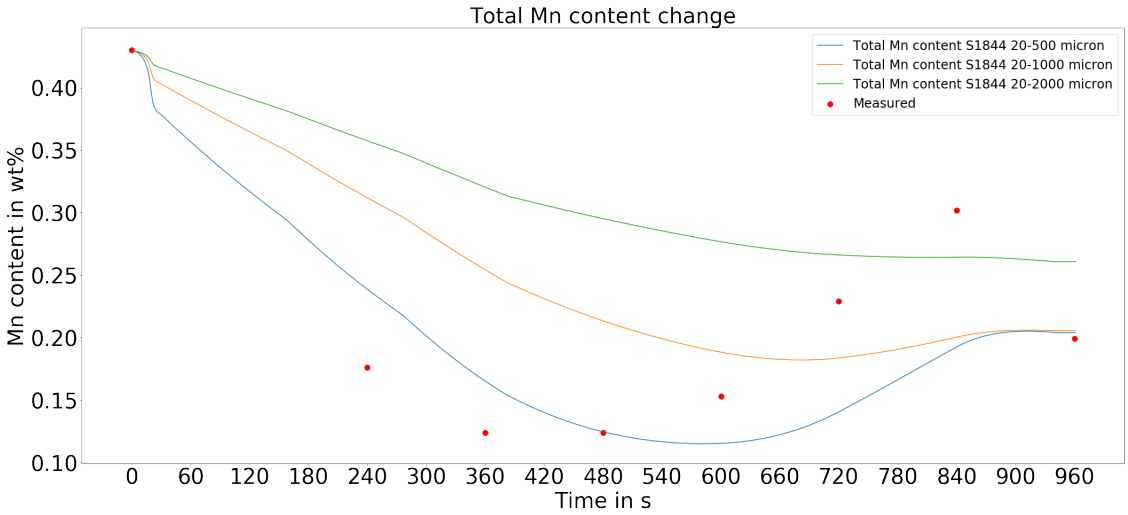

Figure 8.14: Total manganese content change over time in wt% , heat S1844-cup height 4-Suito number 3 model, droplet size 20-500 micron, 20-1000 micron and 20-2000 micron.

Comparing the 2 figures it can be seen that the model calculations with the smallest droplet size range 20-500 micron, are more accurate than the model with a size range of 20-1000 micron. This is because the average droplet size parameter d in equation 5.10 is increasing in the denominator, leading to an overall lower mass transfer parameter K. According to Obasohan (2015) the most droplets encountered under a microscope for heat S1837 and S1840 were smaller than 100 micron, over a total size range of 16-6500 micron. The manganese content for droplet size range of 20-2000 micron is more flat and less accurate than the 20-500 micron run and the 20-1000 micron run.

8.3.2. IMPHOS cup height data

The model is evaluated with slag data from 2 different cup heights 4 and 5 within the IMPHOS converter. The results for both cup heights can be seen in figure 8.15.

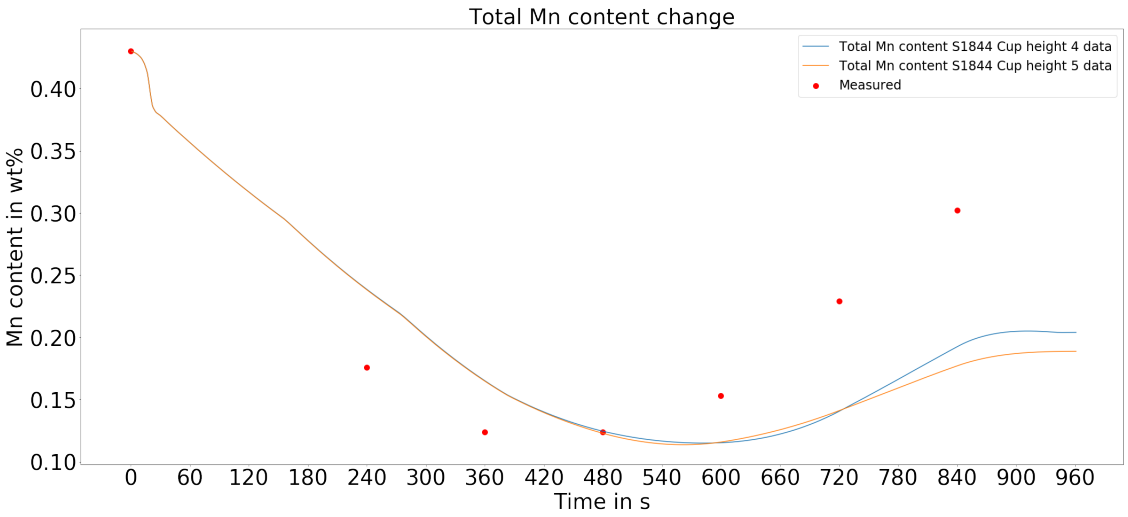

Figure 8.15: Total manganese content change over time in wt% , heat S1844-cup height 4 and 5-Suito number 3 model, droplet size 20-500 micron.

Comparing height 4 and height 5 no significant differences in the resulting manganese weight percentages in the hot metal bath over time are found. This supports the conclusion from the data analysis in chapter 7.

8.3.3. Thermodynamic equilibrium model

The kinetic model is evaluated with both Suito no 3 model and the Morales and Fruehan model for the thermodynamic calculation of the manganese equilibrium value. This value is used as input in to calculate the manganese masstransfer in equation 5.1. The resulting manganese weight content over time for heat S1844 with both models can be seen in figure 8.16.

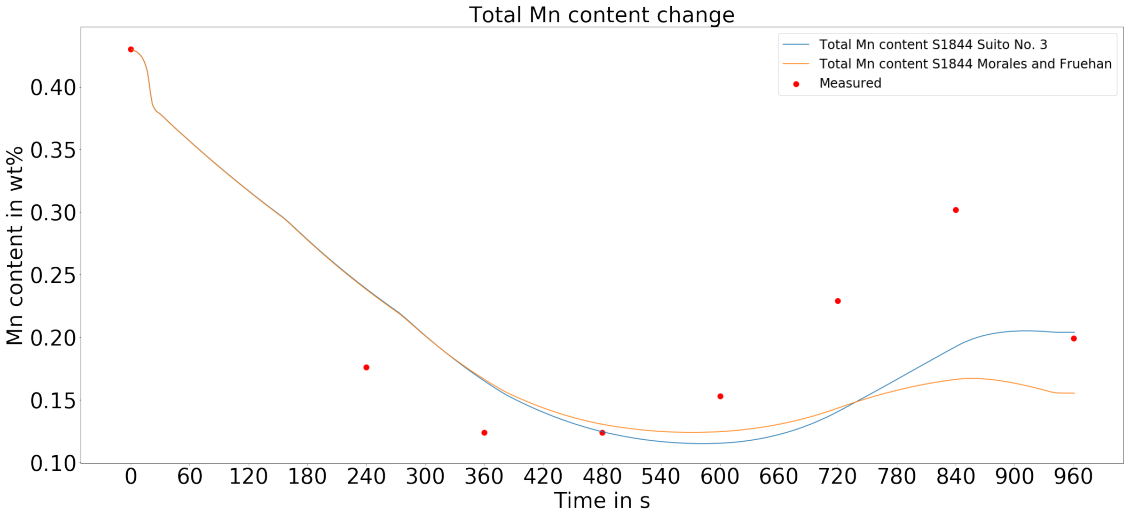

Figure 8.16: Total manganese content change over time in wt% , heat S1844-cup height 4-Suito number 3 model and Morales and Fruehan model, droplet size 20-500 micron.

From the figure it can be concluded that both thermodynamic models show the same behaviour in predicting the primary oxidation phase of manganese during the first 6 min of the heat. For the reversion of manganese the Suito no 3 model is more accurate than the Morales and Fruehan model. This is supported by the findings of the thermodynamic data analysis in chapter 7.

8.4. Kinetic model conclusion

The following can be observed from the results of the kinetic model for the prediction of the manganese refining path:

- The smallest droplet size classes contributes the most to the generation of droplets and the kinetic masstransfer.
- Kinetic model is able to predict manganese reversion for small droplet size classes. For bigger droplet size distributions the solution is diverging.
- Slag data difference between IMPHOS cup height 4 and 5 is negligible for kinetic modelling.
- The use of the Suito No 3 model is better to predict manganese reversion than the Morales and Fruehan model.
- More research should be done on droplet residence time and implemented in this kinetic model.

9

Results: IMPHOS Sample analysis

This chapter describes the results of the physical sample analysis performed on heat S1836 cup height 2. The methods are described in chapter 6. The metal samples were checked for homogeneity of manganese, phosphorus and carbon with Spark OES analysis and checked on their bulk chemical content with Spark OES and ICP analysis. Cup height 2 samples were never analysed before in IMPHOS and can be compared with the cup height 1 analysis done 10 years ago, to identify any deviations within the hot metal bath.

9.1. IMPHOS heat S1836 cup height 2 homogeneity analysis

This paragraph describes the homogeneity analysis performed on S1836 cup height 2. For the homogeneity analysis sample dips 1,3,4 and 7 were used, to sketch a representative image along the whole 16 minutes of the blow. The homogeneity of the metal sample for dip 1 (2 minutes into the blow) can be seen in figures 9.1 , 9.2 , 9.3. the spark OES was not calibrated for the homogeneity analysis so the results should be used as indication.

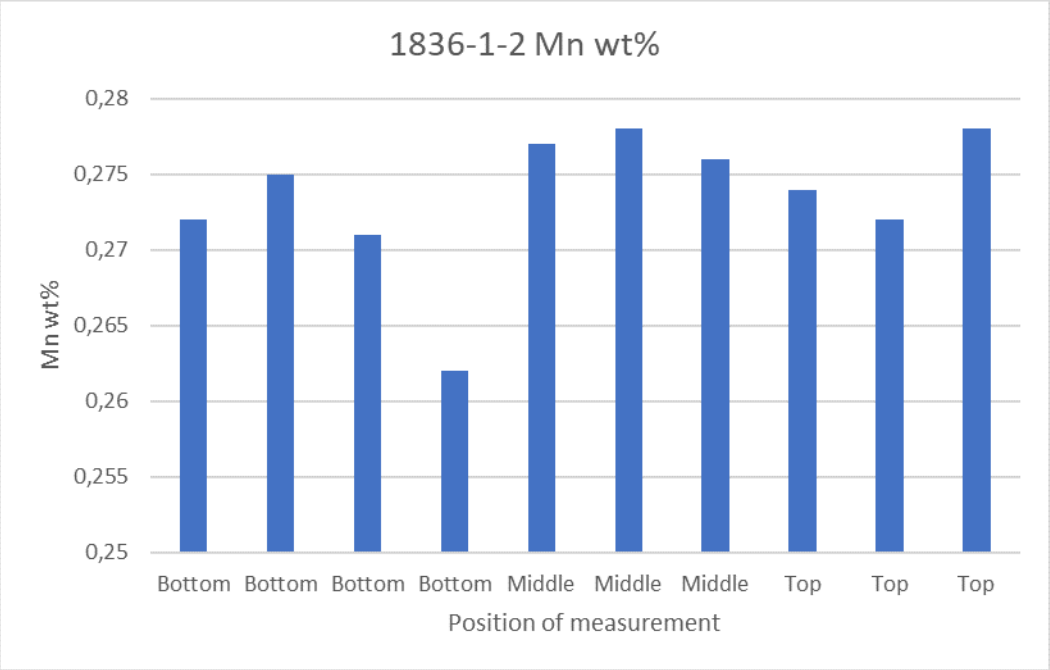

Figure 9.1: Weight percentages of manganese throughout sample S1836-1-2, measurements are taken from left to right at the indicated position.

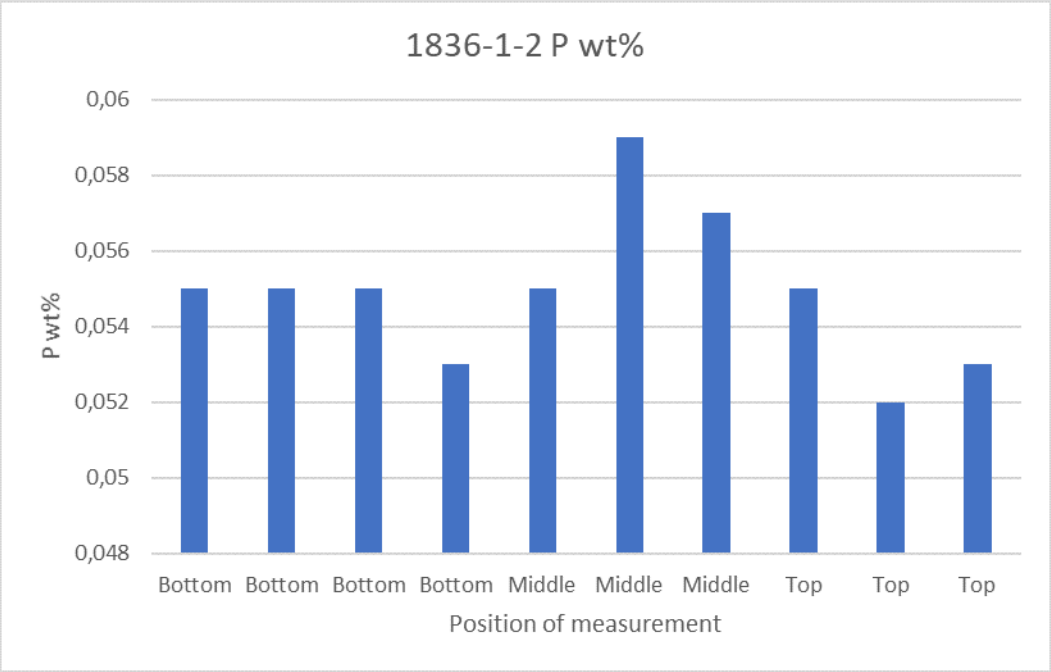

Figure 9.2: Weight percentages of phosphorus throughout sample S1836-1-2, measurements are taken from left to right at the indicated position.

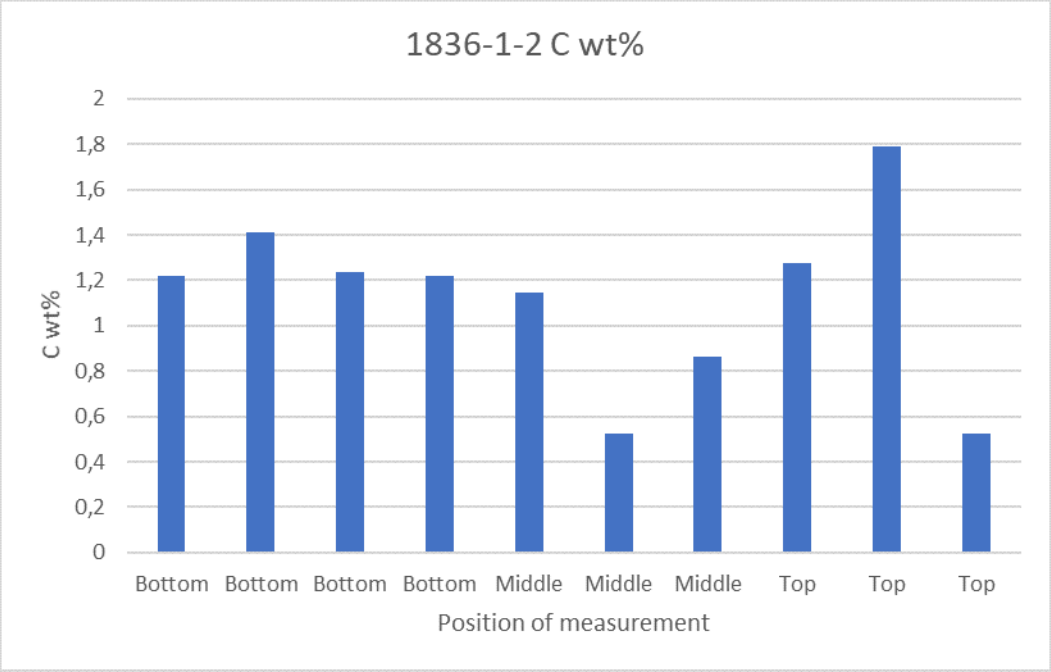

Figure 9.3: Weight percentages of carbon throughout sample S1836-1-2, measurements are taken from left to right at the indicated position.

In the figures local deviation for all three elements can be seen throughout the sample. This sample heterogeneity is probably caused by solidification when the samples were taken from the metal bath. The outside of the sample cools down first and preserve therefore more original content from the metal bath. Due to the cooling from outside to the inside the elements precipitates and this precipitation is pushed to the middle of the sample and higher concentration of elements can normally be found there. Also measurement errors can be noticed e.g. 4th measurement of the bottom. These errors are caused by small holes within the sam-

ple(see chapter 6) therefore the spark was not correctly placed on the sample leading to lower concentrations of phosphorus and manganese at this position.

The following 3 figures 9.4, 9.5, 9.6 are showing the found weight percentages of manganese , phosphorus and carbon 14 minutes into the blow.

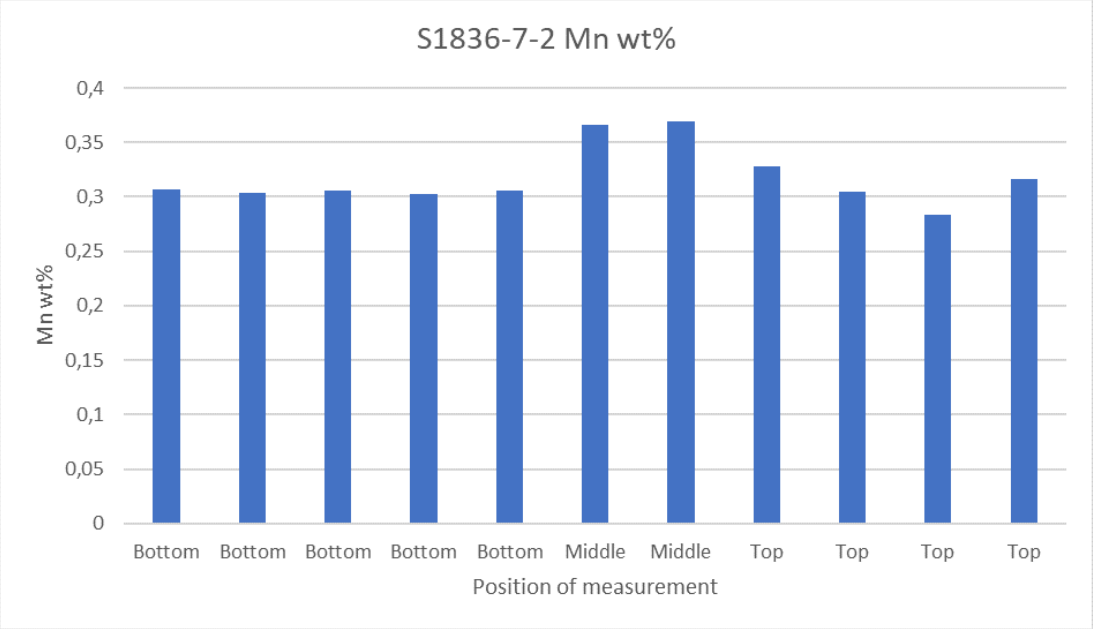

Figure 9.4: Weight percentages of manganese throughout sample S1836-7-2, measurements are taken from left to right at the indicated position.

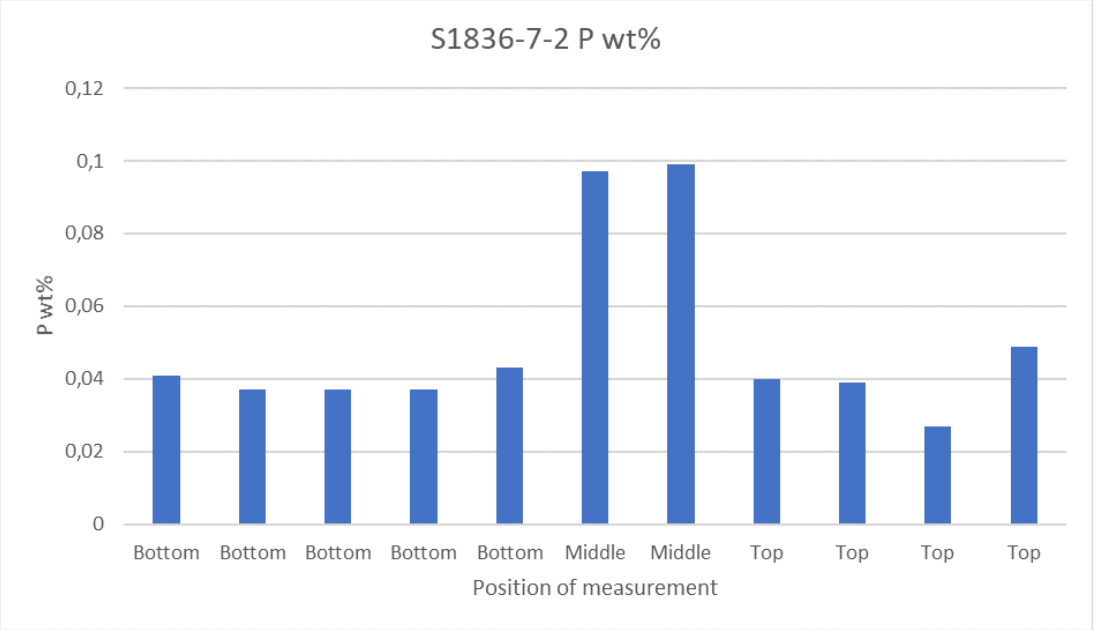

Figure 9.5: Weight percentages of phosphorus throughout sample S1836-7-2, measurements are taken from left to right at the indicated position.

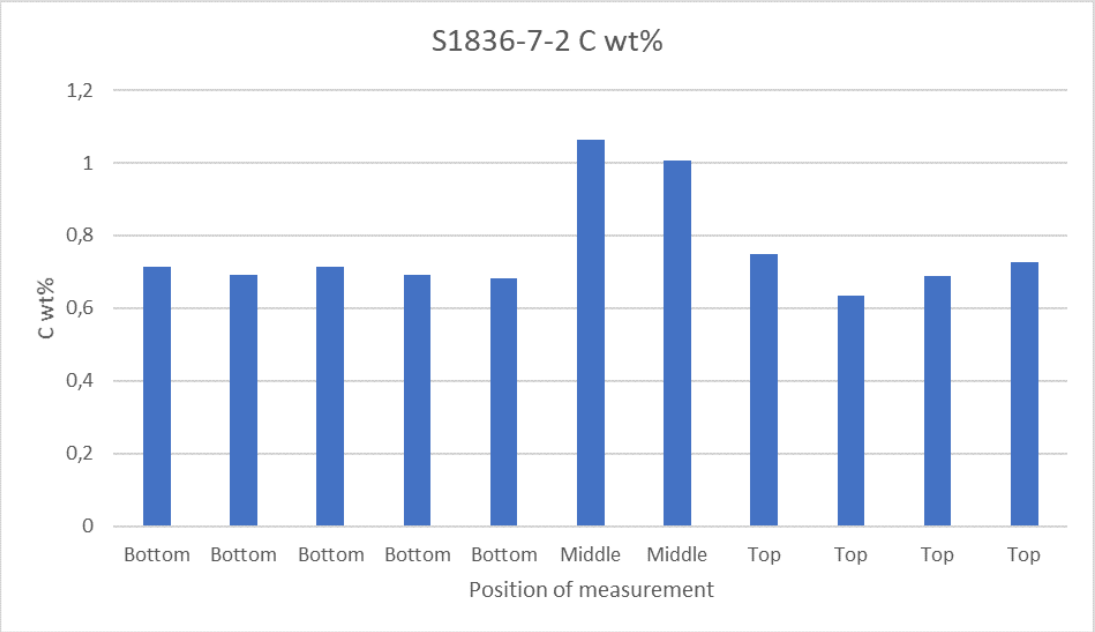

Figure 9.6: Weight percentages of carbon throughout sample S1836-7-2, measurements are taken from left to right at the indicated position.

It can be seen after 14 minutes into the blow that the precipitated concentration is higher in the middle of the sample. Compared to 2 minutes into the blow, the measurements on the outsides of the sample are more homogeneous 14 min into the blow. This indicates a more homogeneous metal bath after 14 minutes than after 2 minutes. Why the peaks of phosphorus and carbon are higher in the middle measurements than manganese, is out of scope for this research and therefore not explained in this report. The homogeneity analysis is also performed for dip sample 3 and 4 , the results from this analysis can be found in Appendix E.

The main goal of the sample analysis is to obtain the bulk chemical content of S1836 cup height 2 and to compare the values with the original analysis at S1836 cup height 1. From the homogeneity analysis it becomes clear, that within the samples taken from the hot metal bath local deviations occur and all measurements done with calibrated spark OES and ICP analysis should be averaged out, in order to find the most approximate value of the original metal content.

9.2. IMPHOS heat S1836 bulk chemical content

The bulk chemical content of heat S1836 was analysed for manganese, phosphorus, sulphur, silicon and carbon at cup height 2. The methods used were Spark OES, ICP analysis and Eltra analysis(only for carbon and sulphur). The results from Spark OES are more used as indication, because of the holes encountered in the cut samples that were used for this bulk chemical content analysis. These holes lead some time to inaccuracies in the sample measurement. According to the responsible TATA steel lab worker the ICP analysis is more reliable for this bulk content analysis, however this method was not used 10 years ago.

The results for manganese and silicon for cup height 2 were in the same range of results as the cup height 1 analysis. This can be seen in figure 9.7 and 9.8.

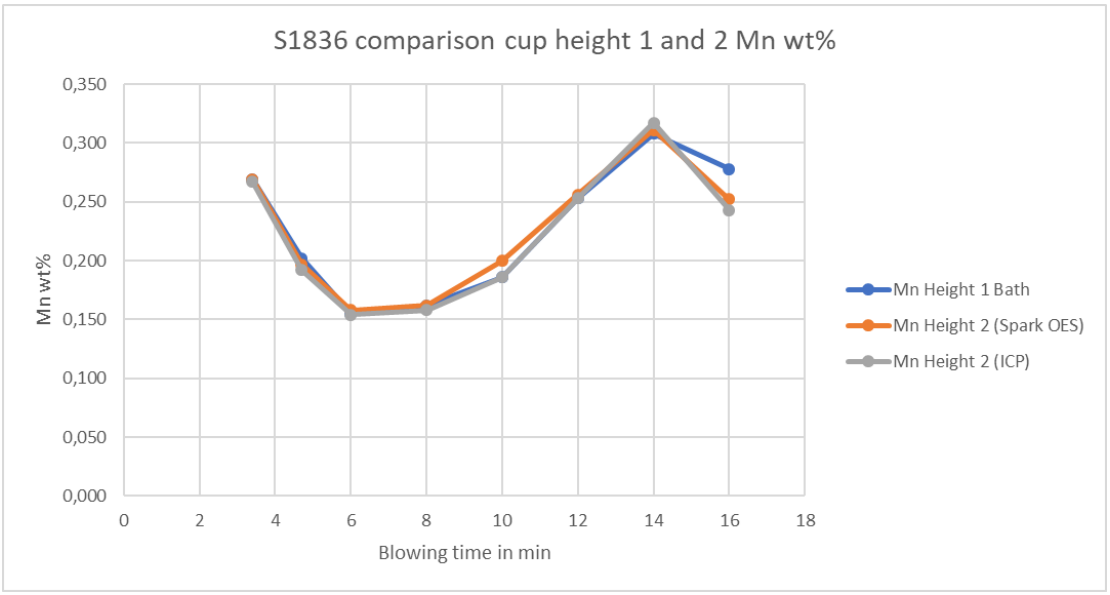

Figure 9.7: Weight percentages of manganese in heat S1836 cup height 2 compared with old cup height 1 measurements

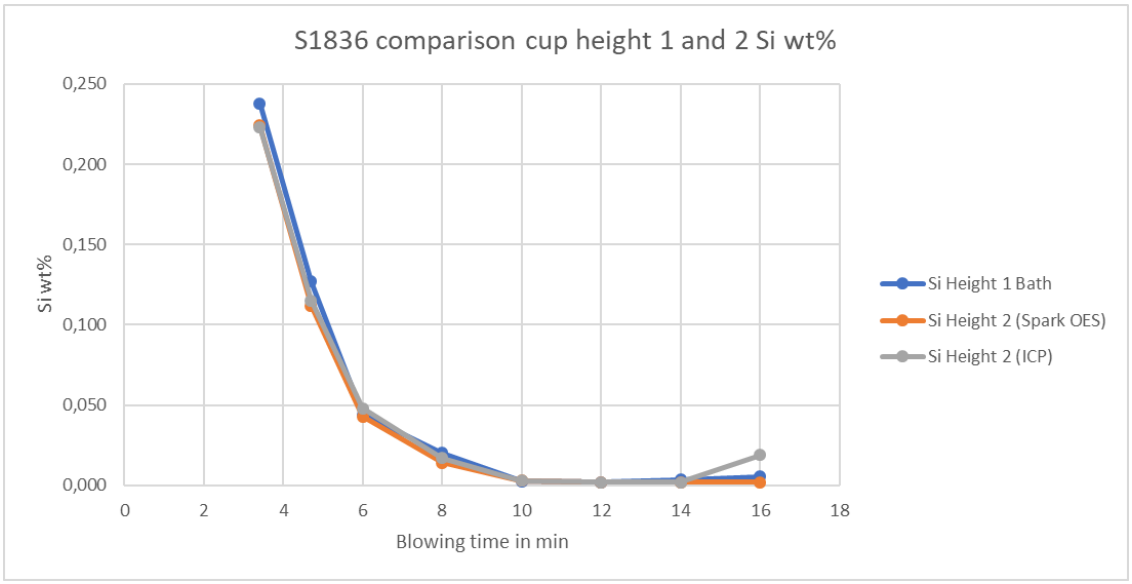

Figure 9.8: Weight percentages of silicon in heat S1836 cup height 2 compared with old cup height 1 measurements

For manganese it can be observed that the final value after 16 minutes is lower for the current Spark OES analysis and ICP analysis compared with the old value measured at cup height 1. Both curves are following the original curves very accurate over the heat, therefore it was concluded that the old measurement at 16 min is a measurement error.

For silicon the only remarkable observation can be made at 16 min into the blow, where the current ICP analysis performed at cup height 2 gives a strange measurement error. At this point the silicon is suddenly 0.019% were the previous measurements were at 0.002%.

The results for carbon , phosphorus and sulphur all showed some deviations in comparison with the old S1836 cup height 1 results. This can be seen in figures 9.9, 9.10, 9.11.

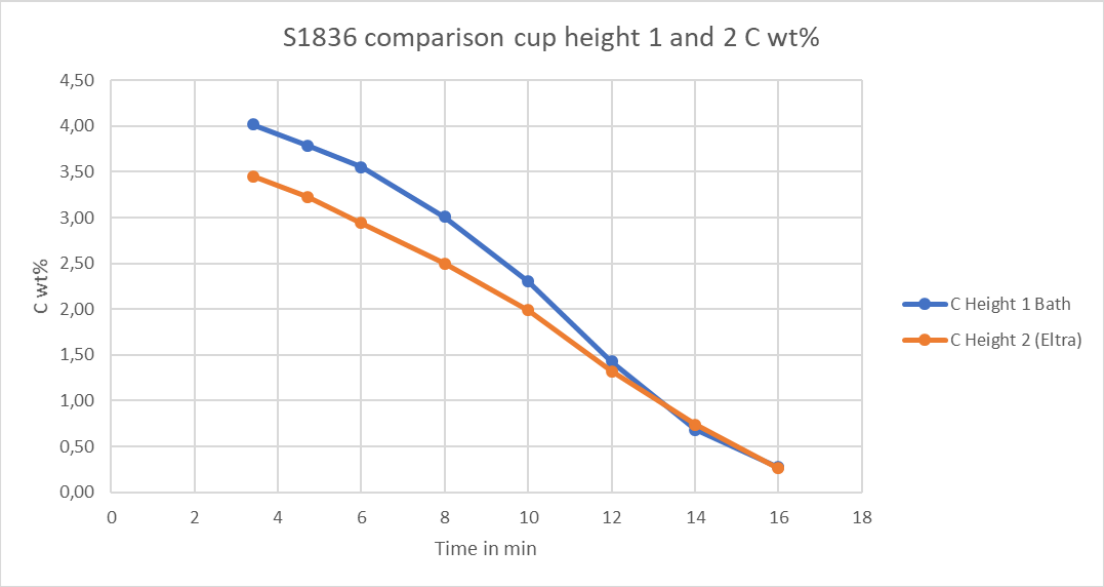

Figure 9.9: Weight percentages of carbon in heat S1836 cup height 2 compared with old cup height 1 measurements

For carbon a structural deviation of 0.5% is observed between the new Eltra measurement at cup height 2 and the old Leico measurement at cup height 1 from 3.5 minutes until 10-12 minutes into the blow were deviation disappears. The reason for this might be complicated and is covered more in the discussion in chapter 10.

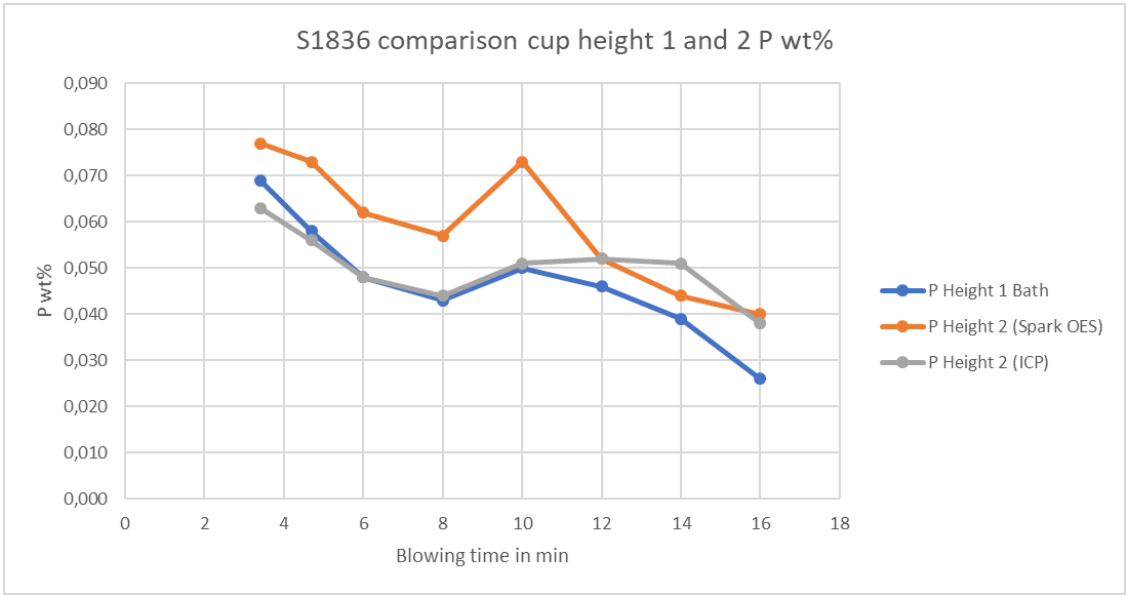

Figure 9.10: Weight percentages of phosphorus in heat S1836 cup height 2 compared with old cup height 1 measurements

For phosphorus the found weight percentages of the spark OES analysis are structurally deviating from the old measurements. They can be marked as unreliable in combination with the advice to use Spark OES as indicative for the cup height 2 analysis. The more trustworthy ICP analysis however follows the old measurements until 10 min into the blow. After 10 min the found values are higher than the cup height 1 Spark OES analysis from 10 years ago. More about this deviation can be found in chapter 10.

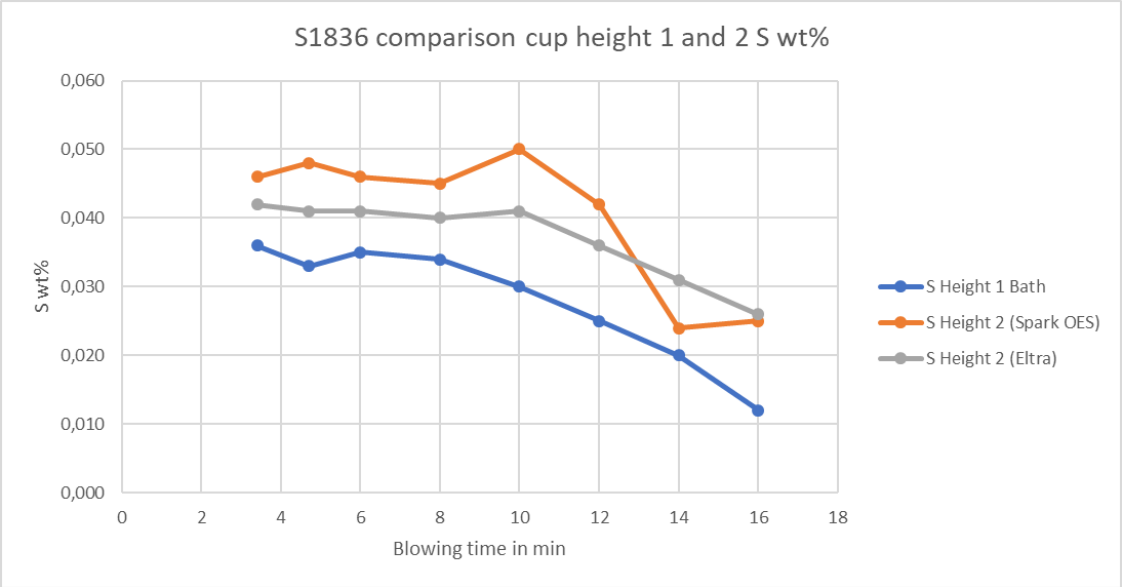

Figure 9.11: Weight percentages of sulphur in heat S1836 cup height 2 compared with old cup height 1 measurements

For sulphur the found values were overall observed as too high for both the Spark OES and Eltra analysis. The conclusion is that the overall analysis is not accurate for sulphur and therefore should not be trusted.

9.3. IMPHOS sample Analysis conclusion

The following can be observed from the IMPHOS sample analysis results:

- IMPHOS samples taken from the hot metal bath are not homogeneous due to solidification from the outside of the sample to the inside. Bulk chemical analysis measurements should be taken as an average, to get the best representation of the chemical content within the sample.
- Silicon and manganese are not showing any deviations in the top part of the hot metal bath compared to the bottom part of the bath.
- Carbon and Phosphorus are showing deviations with an error around 10 percent between the top part and bottom part of the metal bath.
- The sulphur measurements are structurally deviating. This is probably caused by big errors in the measurements. These sulphur measurements should not be trusted.

Part V

Discussion, Recommendations and Conclusion

10

Discussion

The goal of this study is to gain a better understanding of the manganese refining path. Manganese highly influences the slag viscosity. According to Rout et al. (2018) Low slag viscosity due to high MnO contents can lead to slopping, refractory lining consumption and yield losses. In contrary, low MnO and FeO content slag can lead in combination with high silicon, to a very dry slag because silicon also influences the activity of MnO as found by Vargas-Ramirez et al. (2002) and Jamieson & Coley (2017). By adjusting the lance height, the slag viscosity can be influenced. In order to monitor and adjust the lance height during the heat, more understanding about the in-situ behaviour of the slag and metal composition is necessary over time. In modern steelmaking there is a growing need for more dynamic models, to make the steelmaking process more efficient. Dynamic models use these in-situ measurement of metal and slag composition, to change process variables such as the lance height position during the blow.

In order to understand the behaviour of manganese in the converter process, a clear overview of the manganese reactions happening in the converter is necessary. Rout et al. (2018) showed that manganese reactions are taking place in 3 different zones within the converter. The jet impact zone, the slag-metal interface zone, and the emulsion zone. This previous research showed that reactions between metal droplets and the slag in the emulsion zone, contributes the most to the manganese mass transfer in the reversion phase. The current work focuses on the influence of manganese mass transfer in the converter emulsion zone on the manganese refining path during the blow. The contribution of the other 2 zones of the converter are out of scope for this study. The following 3 paragraphs discuss the results obtained for the present study.

10.1. Thermodynamic analysis

First thermodynamic data analysis is done to analyse the manganese distribution within the IMPHOS heats S1836, S1844 and S1845 with two different Mn equilibrium distribution ratio correlations. One model by Suito & Inoue (1995) taking into account the dynamic composition of multiple oxides in the slag as presented in equation 4.1 to calculate the apparent equilibrium value for manganese. The 2nd model by Morales & Fruehan (1997) uses a temperature relation from equation 4.2 to calculate the apparent equilibrium. The manganese instantaneous equilibrium content is then found by filling in the apparent equilibrium in 2.13, which includes the MnO and FeO content in the slag.

The results from the data analysis has shown the expected behaviour of manganese in both the metal bath and the emulsion as can be seen in figure 7.1 and 7.5. For the 2 different IMPHOS cup heights that were analysed no clear differences were found, this is probably due to too small deviations in the slag and metal composition between cup height 4 and 5. When the temperature is raised with 50 K both instantaneous equilibrium concentrations show a more accurate behaviour regarding the shift in oxidation and reduction in comparison with the original data as seen in 7.3 and 7.7. This is due to the temperature of the slag is probably slightly higher than the hot metal bath as described in Deo & Boom (1993). The used value of 50 K is an assumption, more thermodynamic research should be done to identify the exact temperature difference between the IMPHOS slag and hot metal bath. The accuracy of the data analysis is influenced by missing

data points within cup height 4 and 5. Both cup heights contain 6 or 7 datapoints instead of 8, due to either wrong measurements or problems retrieving the physical sample content. The manganese partition ratio gave higher values over time when the IMPHOS slag contained more FeO. The manganese partition ratio was also higher over time when a lower slag basicity (B2) value were measured. This can be seen in figure 7.9 and in figure 7.10. This finding is also observed in existing literature from Suito & Inoue (1984*b*). The thermodynamic equilibrium models from literature are often made in laboratory setups. In these setups different temperature ranges and slag compositions are used then for the current IMPHOS research. The models reasonably capture the change in the state of oxidation and reduction of manganese after the temperature was raised with 50K. A more accurate prediction of the IMPHOS slag temperature may be useful to predict the exact manganese equilibrium value.

10.2. Kinetic modelling

In figures 8.1 and 8.3 from the kinetic model it became clear, that for the smallest droplets size classes, the highest amount of droplets were generated and the highest mass transfer coefficient was found. This leads to the highest amount of manganese mass transfer for these small size classes in 8.5 compared to the bigger size classes.

The kinetic mass transfer coefficient is highly influenced by droplet size. Bigger droplets will have a bigger surface area, but a smaller surface area to volume ratio. This reduces the mass transfer coefficient along droplet boundaries. In this research the droplet size was assumed to be the same during the heat, furthermore, the total average size of the droplets was taken as a constant. In reality droplets swell and may increase the volume due to internal nucleation of CO bubbles. This changes the droplet size during their transition within the emulsion. According to Rout et al. (2017) and Gu et al. (2017) the mass transfer parameter of phosphorus is a factor $10^{-}2$ lower for a carbon containing droplet. Furthermore, it was found that the stirring effect of CO bubbles also influences the surface renewal of the droplets. Future improvements for this model are a more accurate description of droplet behavior and transport within the slag. Rout (2018) used 2 dimensional ballistic motion to calculate the residence time of the metal droplets, making use of the droplet velocity and the drag force coefficients acting on droplets within the slag.

More model limitations, as described in paragraph 5.6, are influencing the current micro kinetic behaviour in the results. The hot atmosphere temperature effect is not taken into account for the calculation of the blowing number, leading to a smaller droplet generation rate around a magnitude 2 smaller than described in Subagyo et al. (2005). For the overall droplet size distribution 3 different size classes were used with 12 different size classes in the range from 20-500 micron, 20-1000 micron and 20-2000 micron with the RRS distribution method. The RRS distribution for all the size classes didn't fully add up to 100 percent so a correction factor was used to make up for the total amount of droplets that were generated in kg/s. The 20-500 micron size range gave the most reasonable prediction for the manganese concentration in the hot metal bath compared to the original measured values in IMPHOS. Obasohan (2015) already observed that the most metal droplets in IMPHOS, encountered under a microscope, were in a range smaller than 100 micron and within a total range of 16-6500 micron. This research combined with research by Rout et al. (2018) and unpublished SEM-EDS microscopy work by J.Small, showed that smaller droplets had more manganese content during the reversion phase of manganese around 6-14 min. The model showed that the droplets, which were smaller than 100 micron, contributed the most to oxidation and reversion behavior of manganese in the emulsion, this can be explained by the bigger total amount of reaction surface area of smaller droplets, where mass transfer can occur along the droplet boundaries. For industrial applications the control of the manganese droplet size can potentially be controlled by adjusting the lance height position. By adjusting the lance height to a higher position, the oxygen velocity at the jet impingement point decreases. This lead to a lower tangential flow velocity within the hot metal bath. Less splashing occurs and less droplets are ejected in the slag emulsion. The downside of raising the lance height position is that it will lead to a lower decarbonization rate. This results in a less efficient carbon removal from the hot metal.

In order to obtain a more detailed droplet distribution, SEM-EDS characterisation of the IMPHOS heats in this study is necessary. SEM-EDS microscopy can potentially also lead to new insights of metal transport along and across droplet boundaries.
By comparing the model prediction of the manganese content in the hot metal bath with the original IM-

PHOS measurements, it can be seen that the most accurate results were obtained with the smallest droplet size class and Suito's thermodynamic model. The dynamic slag composition used by Suito, is more accurately describing the manganese distribution than the temperature correlation proposed by Morales. This can be seen in figure 8.16. Despite the model limitations with this model setup, the manganese reversion can be seen after 8-10 min in figure 8.15. The same trend is observed between results with data from cup height 4 and 5. Therefore the conclusions from the data analysis in chapter 7 are justified. The Suito no 3 model can predict more accurately the manganese equilibrium behavior during the refining period of the IMPHOS heats. Furthermore the deviation in input data between cup height 4 and 5 is too small to cause any noticeable differences in the kinetic model. However, doing SEM-EDS analysis can lead in the future to a more accurate droplet size distribution between the two heights. This can lead to changes in the obtained droplet generation rate and kinetic mass transfer parameter at these heights. These changes will influence the manganese content in the droplets at these heights. This deviation in chemical content of different droplet sizes for different cup heights was already described in Millman et al. (2011).

The current model under predicts the primary oxidation during initial period of Mn refining. This is mainly due to the missing data in the first 2 min of the heat, were the slag composition is basically unknown. This under prediction is also caused by the inaccuracy of the prediction of the manganese thermodynamic distribution. Another reason for this slow trend, is the negligence of the manganese transfer within the jet impact zone in the model. Rout et al. (2018) stated that direct oxidation of Mn by O_2 also influences the manganese kinetics in the primary oxidation phase. The curve follows the typical behaviour of manganese as in figure 3.7 from Hewage et al. (2016), but the curve is delayed compared to the original measured datapoints from the heats. The results for this model, show indicative good predicted manganese behaviour for smaller droplet sizes. A dynamic droplet generation rate calculation from Subagyo et al. (2005) was applied incorporating changing lance height position within the heat. Furthermore manganese mass transfer parameter k was calculated with Higbie's penetration theory. The diffusivity was taken as a dynamic parameter dependant on changing viscosity, calculated with the modified Urbain model explained in Kondratiev & Jak (2001) which is mainly dependant on slag composition. The diffusivity is also dependant on the dynamic change of temperature of the hot metal bath in the heat. The droplet ejection velocity used is dependant on the dynamic variation of the droplet generation rate. The only parameter which is assumed constant for this research is the average droplet size and shape. Still, the model was able to predict the manganese oxidation and reversion reasonably for small droplet sizes. To make the models prediction more accurate over time, the change of droplet size and shape due to the droplets bloating behaviour needs to be implemented. This causes the droplets to grow and is leading to a larger surface area and lower mass transfer coefficient according to Gu et al. (2017). Rout et al. (2018) already showed in his model that smaller droplets experienced more reversion, or have more conversion capacity due to their surface area to volume ratio. If metal droplets are rising or falling due to bloating, they also experience more dynamic changes at the droplet-slag interface. This is due to the change of slag temperature and a changing slag FeO content between dense and foamy slag (Gu et al. 2017). The aspect of bloating and residence time of metal droplets in the slag-metal emulsion, need to be incorporated in the prediction model to get an accurate prediction of the oxidation and reversion of manganese.

10.3. Sample analysis

To examine the quality of the original hot metal datapoints used to validate the model, physical sample research was performed on S1836 cup height 2. All original hot metal datapoints were measured at cup height 1. The metal bath is assumed to be homogeneous in the original research. Due to a lack of time and resources cup height 2 samples were never investigated as explained in Millman et al. (2011). Selecting the cup samples for this research was quite difficult. Most preserved samples were stored in containers at the Tata Ijmuiden site. The exact documentation of the volume of these containers is outdated. For heat S1836 cup height 2, all 18 samples over the 16 min of measurements were still preserved. Sample preparation took 2 months due to a lack of time and resources, which limited the final evaluation of the sample analysis performed on the samples.

The homogeneity analysis over 4 different samples showed deviations within the sample. This is probably due to solidification from the outside to the inside of the sample. This can be seen in figures 9.1 and 9.4. The homogeneity of the original hot metal bath can be derived more from the outside sample measurement than

the inside. This is because precipitated elements will move to the core of the sample due to cooling from the outside to the inside of the samples, the outside measurements showed less homogeneity than the last dip measurement at 16 min. Due to the variable content within the sample, the final bulk chemical analysis measurements were averaged. This was done to approximate the original content as much as possible with Spark OES and ICP analysis.
The samples were prepared for bulk chemical analysis the same way as in Millman et al. (2011). The samples were analysed with Spark OES and ICP analysis. The results from the Spark OES were used as indicative, due to holes in some prepared samples, as can be seen in figure 6.8. The ICP analysis is more trustworthy due to less surface sensitivity for this type measurement. Comparing the results from cup height 2 with the old results for cup height 1, the chemical content of manganese and silicon were similar, except an incorrect data point at 16 min for the original manganese content. The silicon content also contained an incorrect data point at 16 min for the ICP analysis done. These findings can be seen in figure 9.7 and 9.8. A constant lower carbon content was found at cup height 2 for the first 10 minutes of the blow. For phosphorus, the content was found to be higher after 10 minutes at cup height 2 than at cup height 1. This occurs during the reversion phase of phosphorus. The observed deviations are 10 percent and are therefore probably not caused by equipment calibration errors. It shows local deviations in chemical gradients within the hot metal bath. This can be seen in figure 9.9 and 9.10. This phenomena is already shown by Rote & Flinn (1972), where in a pilot size converter probes were inserted through the side of the vessel. The deviation in chemical gradient was found to be higher for a shallow penetration of the oxygen into the metal bath. The metal bath gradient was deviating for carbon, sillicon, manganese and phosphorus. In this research the deviation for carbon is probably due to the oxygen impingement in the top of the metal bath, were the carbon reacts first with the oxygen in the jet impact zone and forms CO gas. The 6t MEFOS converter uses an oxygen flow of 17 Nm^3/min, while in comparison a full scale 330t converter in Ijmuiden blows 910 N/m^3 of O_2 into the bath. This is 50 times as much oxygen for a converter which is 50 times larger. So the MEFOS pilot converter uses a normal oxygen flow rate compared to an industrial scale converter. This should theoretically lead to enough turbulent flow within the bath, to avoid local deviations within the bath. For manganese, sillicon and sulphur no structural deviations were observed in this research, this is probably due to the short distance between the cup heights 1 and 2. The difference in position of the sample measurements is too small to identify deviations at the low weight percentages of these 3 elements. It is expected, that when carbon shows deviations in the hot metal bath, sillicon will also show deviations at the start of the blow. This is mainly due to its fast reaction with oxygen. From this research it cannot be explained why carbon shows deviation and sillicon not. Also, when phosphorus content at this height in the top part of the metal bath is higher during the reversion phase, it is normally expected that manganese is also higher in the top part of the hot metal bath due to metal droplets falling back in the metal bath. This research couldn't explain why this higher content is only found for phosphorus and not for manganese. IMPHOS cup height 2 can be close to the hot spot within the converter, According to Uchida (2018) a higher concentration of phosphorus at height 2 may be due to the reversion of phosphorus as a result of high temperature prevailing at jet impact zone. Also from the research performed by Rote & Flinn (1972) in combination with the results from the current sample research of heat S1836, were the error between the 2 sample height values was around 10 percent, It may be believed that there were slight deviations in the IMPHOS hot metal bath content. However, to confirm structural observed deviations between cup height 1 and 2 within the hot metal bath, more research is necessary on cup height 2 samples from IMPHOS heats. This research is essential in order to get more confirmation about local carbon and phosphorus deviations within the hot metal bath.

11

Conclusion

11.1. Thermodynamic analysis

- The thermodynamic analysis showed that the Suito No. 3 model was more accurate than the Morales and Fruehan model, in predicting the manganese reversion behaviour for the IMPHOS data set. The Morales and Fruehan model was better in predicting the 2nd oxidation phase of manganese for IMPHOS data.
- The importance of temperature on the manganese distribution is seen, by raising the temperature with 50 K compared to the original measured temperature of the hot metal bath. This resulted in a more accurate manganese reversion behaviour compared to the original temperature value.
- The influence from IMPHOS cup height 4 and 5 slag data on the thermodynamic behaviour of manganese was evaluated. No significant differences were observed. After the thermodynamic data analysis the hypothesis was made, that the difference in cup height data won't influence the results of the kinetic model for the respective heights.

11.2. Kinetic modelling

- The best kinetic model results were found with as input Suito no 3 model, with the smallest droplet size range used for all 4 heats evaluated. The inaccuracy of the thermodynamic model negatively influences the predicted oxidation and reversion in the model results.
- Transient model parameters such as the dimensionless blowing number, diffusivity, slag composition , temperature and lance height position are taken into account for the kinetic model. While the droplet size was taken as an average over time. These predictions show a good agreement with the change in the originally obtained hot metal Mn concentration during refining, which were measured during the IMPHOS project. The oxidation and reversion of Mn are well captured in the model.
- The model prediction showed that, small sized droplets, smaller than 100 micron contributed the most to the oxidation and reversion behaviour of manganese in the emulsion. This can be explained by the larger total amount of reaction surface area of smaller droplets, where mass transfer can occur along the droplet boundaries.

11.3. Sample analysis

- The samples taken by the hot metal bath are not homogeneous. This inhomogeneity is caused by the slow cooling of metal by air. This will lead to precipitated elements being pushed inwards towards the core of the sample. The hot metal content measurements during bulk chemical analysis at various locations of the IMPHOS samples should be taken as an average.
- The sample evaluation of S1836 cup height 2 was compared with the original cup height 1 analysis. A deviated carbon and phosphorus content was found with an error of 10 percent. This can indicate deviations within a distance around 20 cm in the hot metal bath of the 6t converter used in IMPHOS.

This is probably because of the direct oxidation of oxygen with the hot metal bath at the jet impact zone. A higher concentration of phosphorus at height 2 may be due to the reversion of phosphorus as a result of high temperature prevailing at jet impact zone. However, further data analysis with more height 2 samples is necessary to confirm this finding.

12

Recommendations

Based on the discussion and conclusion in chapter 10 and 11 the following recommendations can be made, to utilise the IMPHOS samples for future research. This future research will be vital in understanding more about the manganese refining path.

- SEM-EDS characterization for emulsion samples should be done on more IMPHOS samples, to illustrate metal concentration differences between single droplets over time of a heat. From this SEM-EDS analysis, a more accurate droplet size distribution for different cup heights within the IMPHOS heats can be found.
- More manganese equilibrium distribution ratio correlations should be tested with different temperature inputs. This is done in order to find the ideal temperature range of the IMPHOS slag to describe the manganese distribution. According to literature a higher exact temperature within the range of 50K-100K is necessary for a more accurate description of the manganese oxidation and reversion.
- A time varying droplet shape and size should be implemented in the kinetic model. Furthermore the model should be evaluated with a more dynamic step size, together with 2 dimensional ballistic motion of ejected metal droplets within the slag emulsion. This will lead to a better simulation of the effect of droplet residence time on the manganese concentration of the droplets and the hot metal bath. This is done for a more accurate description of the bloating behaviour of the metal droplets within the slag emulsion.
- The influence of the temperature effect caused by a hot atmosphere, should be implemented in the kinetic model. This is done in order to obtain a better estimation of the dimensionless blowing number. This updated blowing number can be used then for a more accurate calculation of the amount of metal droplets generated in the kinetic model.
- New extensive documentation has to be done of the current physical IMPHOS samples stored in the red containers at Tata steel Ijmuiden. The current documentation is outdated, and over 10 years time, a lot of samples and data were lost because of logistical inefficiency. Finding out what samples are still not evaluated and in possession of Tata steel Ijmuiden, can speed up SEM research of the physical samples for IMPHOS based research in the future.
- More cup height 2 samples from IMPHOS should be physically analyzed on their bulk chemical content. This should be done to confirm the observed deviation of chemical gradient for carbon and phosphorus in the hot metal bath during heat S1836.

Bibliography

Daines, W. & Pehlke, R. (1971), 'Kinetics of manganese oxide reduction from basic slags by carbon dissolved in liquid iron', *Metallurgical and Materials Transactions B* **2**, 1203–1211.

Deo, B. & Boom, R. (1993), *Fundamentals of Steelmaking Metallurgy*, New York, N.Y. : Prentice Hall, pp. 106–163.

Dogan, N. (2011), Mathematical Modelling of Oxygen Steelmaking, PhD thesis, Swinburne University of Technology, Melbourne, Australia.

Duan, S., Guo, X., Guo, H. & Guo, J. (2016), 'A manganese distribution prediction model for $CaO-SiO_2-FeO-MgO-MnO-Al_2O_3$ slags based on IMCT', *Ironmaking and Steelmaking* **44**, 168–184.

Duan, S., Li, C., Guo, X., Guo, H., S.W., H. & Yang, W. (2017), 'Thermodynamicaanalysis for the oxidation behaviour of manganese in iron based melts during demanganisation processes', *Ironmaking and Steelmaking* **46:8**, 755–760.

Gu, K., Dogan, N. & Coley, K. (2017), 'Dephosphorization kinetics between bloated metal droplets and slag containing FeO: The influence of CO bubbles on the mass transfer of phosphorus in the metal', *Metallurgical and Materials Transactions B* **48**, 2984–3001.

Hewage, A., Rout, B., Brooks, G. & Naser, J. (2016), 'Analysis of steelmaking kinetics from IMPHOS pilot plant data', *Ironmaking and Steelmaking* **43**, 358–370.

Higbie, R. (1935), 'The rate of absorption of a pure gas into a still liquid during short periods of exposure', *Trans. AIChE* **31**, 365–389.

Huang, Y., Guoping, X., Junshi, W., Yinfeng, W. & Hui, C. (2012), 'An overview of utilization of steel slag', *Procedia Environmental Sciences* **16**, 791–801.

Huiting, S. & Forssberg, E. (2003), 'An overview of recovery of metals from slags', *Waste management (New York, N.Y.)* **23**, 933–49.

Jalkanen, H. & Holappa, L. (2013), *Converter Steelmaking*, Vol. 3, Aalto University, Department of Chemistry, chapter 1.4, pp. 223–270.

Jamieson, B. & Coley, K. (2017), 'Kinetics of silicothermic reduction of manganese oxide for advanced high-strength steel production', *Metallurgical and Materials Transactions B* **48**, 1613–1624.

Jung, S. (2003), 'Equilibria of manganese and sulfur between liquid iron and $CaO-SiO_2-Fe_tO-MgO-MnO$ slags saturated with $2CaO*SiO_2$ and MgO', *ISIJ International* **43**, 216–223.

Kaar, S., Krizan, D., Schneider, R., Beal, C. & Sommistsch, C. (2019), 'Effect of manganese on the structure-properties relationship of cold rolled AHHS treated by a quenching and partitioning process', *Metals* **9,1122**, 1–15.

Kadrolkar, A. & Dogan, N. (2019), 'Model development for refining rates in oxygen steelmaking: Impact and slag-metal bulk zones', *Metals* **9:3**, 309.

Kato, Y. & Okuda, H. (2003), 'Reaction model for carbon, manganese, and oxygen in bottom blowing with mixed gas in final stage of steel refining in converter', *ISIJ International* **43:11**, 1710–1714.

Kawai, Y., Shinozaki, N. & Mori, K. (1982), 'Rate of transfer of manganese across metal-slag interface and interfacial phenomena', *Canadian Metallurgical Quarterly* **21**, 385–391.

Kim, S., Takekawa, J., Shibata, H., Yamaguchi, K. & Kang, Y. (2013), 'Thermodynamic assesment of MnO and FeO acticvities in $FeO-MnO-MgO-P_2O_5-SiO_2-CaO$ molten slag', *ISIJ International* **53**, 1325–1333.

Kondratiev, A. & Jak, E. (2001), 'Review of experimental data and modeling of the viscosities of fully liquid slags in the $Al_2O_3 - CaO - 'FeO' - SiO_2$ system', *Metallurgical and Materials Transactions B* **32:6**, 1015–1025.

Lytvynyuk, Y., Schenk, J. & Hiebler, M. (2013), 'Application of thermodynamic and kinetic model for converter steelmaking to optimise manganese yield in crude steel', *Berg Huettenmaenn Monatsh* **158**, 457–458.

Meraikib, M. (1993), 'Manganese distribution between a slag and a bath of molten sponge iron and scrap', *ISIJ International* **33**, 352–360.

Miller, T., Jimenez, J., Sharan, A. & Goldstein, D. (1998), *Steelmaking and Refining Volume*, The AISE Steel Foundation, chapter 9, pp. 475–524.

Millman, M., Kapilashrami, A., Bramming, M. & Malmberg, D. (2011), *IMPHOS: improving phosphorus refining*, European Commission, Research Fund for Coal and Steel, Project number: RFSR-CT-2006-00006.

Morales, A. & Fruehan, R. (1997), 'Thermodynamics of MnO, FeO, and phosphorus in steelmaking slags with high MnO contents', *Metallurgical and Materials Transactions B* **28**, 1111–1118.

Obasohan, E. (2015), Study of Oxidation Steelmaking Reactions of Blast Furnace Hot-metal, PhD thesis, The University of Sheffield, Faculty of Engineering, Department of Materials Science and Engineering, Sheffield, UK.

Oeters, F. (1994), 'Metallurgy of steelmaking', *Verlag Stahleisen* pp. 316–377.

Rote, F. & Flinn, R. (1972), 'Experimental observations of chemical and thermal gradients in an experimental BOF', *Metallurgical and Materials Transactions B* **3**, 1373–1384.

Rout, B. (2018), Modelling of Dephosphorization in Oxygen Steelmaking, PhD thesis, Swinburne University of Technology, Faculty of Science, Engineering and Technology, Melbourne, Australia.

Rout, B., Brooks, G., Akbar Rhamdhani, M. & Li, Z. (2016), 'Modeling of droplet generation in a top blowing steelmaking process', *Metallurgical and Materials Transactions B* **47:1**, 3350–3361.

Rout, B., Brooks, G., Li, Z. & Rhamdhani, M. (2017), 'Transient behaviour of dephosphorization kinetics in oxygen steelmaking', *AISTech 2015* pp. 3225–3237.

Rout, B., Brooks, G., Rhamdani, M., Li, Z., Schrama, F. & Van der Knoop, W. (2018), 'Dynamic model of basic oxygen steelmaking process based on multizone reaction kinetics: Modelling of manganese removal', *Metallurgical and Materials Transactions B* **49**, 2191–2208.

Shin, D., Ueda, S., Gao, X. & Kitamura, S. (2019), 'Separation of phosphorus and manganese from steelmaking slag by selective reduction.', *Metallurgical and Materials Transactions B* **50**, 1248–1259.

Subagyo, Brooks, G. & Coley, K. (2005), 'Residence time of metal droplets in slag-metal-gas emulsions through top gas blowing', *Canadian Metallurgical Quarterly* **44:1**, 119–130.

Subagyo, Brooks, G., Coley, K. & Irons, G. (2003), 'Generation of droplets in slag metal emulsions through top gas blowing', *ISIJ International* **43:7**, 983–989.

Suito, H. & Inoue, R. (1984*a*), 'Manganese equilibrium between molten iron and MgO saturated $CaO-Fe_tO-SiO_2-MnO$ slags', *ISIJ International* **24**, 257–265.

Suito, H. & Inoue, R. (1984*b*), 'Thermodynamic considerations on manganese equilibria between liquid iron and FetO-MnO-MOx (MOx equals $P_2O_5, SiO_2, Al_2O_3, MgO, CaO$) slags.', *ISIJ International* **24**, 301–307.

Suito, H. & Inoue, R. (1995), 'Thermodynamic assessment of manganese distribution in hot metal and steel', *ISIJ International* **35**, 266–71.

Takaoka, T., Sumi, I., Kikuchi, Y. & Kawai, y. (1993), 'Manganese reaction rate in combined blowing with less slag', *ISIJ International* **33**(1), 98–103.

Turkdogan, E. (1996), *Fundamentals of Steelmaking*, Pennsylvania State University, Institute of Materials, chapter 8, pp. 209–244.

Turkdogan, E. & Pearson, J. (1953), 'Activities of constituents of iron and steelmaking slags', *J. Iron Steel Inst.* **175**, 398–401.

Uchida, Y.-i. (2018), 'Reaction near hotspot in refining of molten iron during supplying top-blown oxygen and powder additives', *7th International Congress on Science and Technology of Steelmaking*. pp. 1–8.

van Elk, E., Knaap, M. & Versteeg, G. (2007), 'Application of the penetration theory for gas-liquid mass transfer without liquid bulk: Differences with system with a bulk', *Chemical Engineering Research and Design* **85:4**, 516–524.

Vargas-Ramirez, M., Romero-Serrano, A., Chavez-Alcala, F., Zeifert, B. & Hallen-Lopez, M. (2002), 'Reduction of MnO from molten slags with liquid steel of high carbon content', *Steel Research* **73:9**, 378–384.

Wang, Z., Chang, J., Ju, Q., Xie, F., Wang, B., Li, H., Wang, B., Lu, X., Fu, G. & Liu, Q. (2012), 'Prediction model of end-point manganese content for BOF steelmaking process', *ISIJ International* **52:9**, 1585–1590.

Williams, R. (2016), *Control and Analysis in Iron and Steelmaking*, Elsevier, chapter 1, pp. 1–9.

Zhou, Z., Zhou, K., Hou, X. & Luo, H. (2005), 'Arc/spark optical emission spectrometry: Principles, instrumentation, and recent applications', *Applied Spectroscopy Reviews* **40:2**, 165–185.

A

Appendix A

Table A.1: RRS distribution 1 , 20-500 micron

Size Class	Average droplet size in m	RRS fraction	n	d'
1	0.00004		2.72	0.48
2	0.00008	0.1613		
3	0.00012	0.1287		
4	0.00016	0.1027		
5	0.00020	0.0819		
6	0.00024	0.0654		
7	0.00028	0.0521		
8	0.00032	0.0416		
9	0.00036	0.0332		
10	0.00040	0,0265		
11	0.00044	0,0211		
12	0.00048	0,0169		
Total		0.7314		

Table A.2: RRS distribution 2 , 20-1000 micron

Size Class	Average droplet size in m	RRS fraction	n	d'
1	0.000061		1.74	0.59
2	0.000143	0.1841		
3	0.000225	0.1432		
4	0.000307	0.1115		
5	0.000389	0.0867		
6	0.000471	0.0675		
7	0.000553	0.0525		
8	0.000635	0.0409		
9	0.000717	0.0318		
10	0.000799	0,0247		
11	0.000881	0,0193		
12	0.000963	0,0150		
Total		0.7772		

Table A.3: RRS distribution 1 , 20-2000 micron

Size Class	Average droplet size in m	RRS fraction	n	d'
1	0.0001025		1.61	1
2	0.0002675	0.1981		
3	0.0004325	0.1518		
4	0.0005975	0.1163		
5	0.0007625	0.0891		
6	0.0009275	0.0689		
7	0.0010925	0.0523		
8	0.0012575	0.0401		
9	0.0014225	0.0307		
10	0.0015875	0,0235		
11	0.0017525	0,0180		
12	0.0019175	0,0138		
Total		0.8026		

B

Appendix B

Time in min	Temp in K	FeOtot wt%	CaO wt%	SiO2 wt%	MgO wt%	Al2O3 wt%	P2O5 wt%
00:00	1577	17,31254	44,88253	20,53484	2,454655	2,007325	1,113438
00:03	1691	17,31254	44,88253	20,53484	2,454655	2,007325	1,113438
00:04	1731	17,40833	34,41128	24,64172	1,26242	0,820358	1,428517
00:06	1769	17,07594	32,62319	26,02913	2,42523	4,132689	1,635543
00:08	1823	17,42515	33,66609	24,72015	2,326148	3,113429	1,750591
00:10	1872	13,10439	39,44287	24,97964	2,112917	1,559702	1,333435
00:14	1956	6,349558	52,21395	21,01712	5,604448	1,617004	1,302344
00:16	1990	10,74145	52,53991	18,29369	5,246091	2,155374	1,467148

MnO wt%	C wt%	Si wt%	Mn wt%	P wt%	S wt%	Cr wt%	Cu wt%	Slag weight in Kg
4,494964	4,06	0,64	0,48	0,086	0,0513	0,03	0,0062	0
4,494964	4,02	0,238	0,269	0,069	0,036	0,03	0,0062	230
11,06031	3,79	0,127	0,202	0,058	0,033	0,03	0,0062	246
8,844819	3,55	0,044	0,155	0,048	0,035	0,031	0,0062	272
8,976518	3,01	0,02	0,162	0,043	0,034	0,033	0,0064	300
8,763463	2,3	0,003	0,186	0,05	0,03	0,033	0,0065	308
2,809763	0,68	0,003	0,308	0,039	0,02	0,036	0,0082	373
3,046459	0,27	0,005	0,278	0,026	0,012	0,034	0,01	432

Figure B.1: Table containing the chemical input data for heat S1836 cup height 4

Time in min	Temp in K	FeOtot wt%	CaO wt%	SiO2 wt%	MgO wt%	Al2O3 wt%	P2O5 wt%
00:00	1577	19,15872	31,91278	24,83584	1,237461	1,126953	1,448187
00:04	1691	19,15872	31,91278	24,83584	1,237461	1,126953	1,448187
00:06	1731	17,54896	32,97989	25,62906	2,254378	4,077287	1,685777
00:08	1769	16,71925	35,97271	23,61319	1,606698	1,138921	2,043611
00:10	1823	12,84396	40,569	24,21237	2,00274	1,110353	1,225501
00:12	1872	10,52156	45,60687	23,38888	2,533045	1,785194	1,160376
00:14	1956	7,452909	51,40741	21,1629	5,491981	1,724136	1,344123
00:16	1990	10,322	52,68945	17,31313	7,349268	1,733487	1,39749

MnO wt%	C wt%	Si wt%	Mn wt%	P wt%	S wt%	Cr wt%	Cu wt%	Slag weight in Kg
11,47719	4,06	0,64	0,48	0,086	0,0513	0,03	0,0062	0
11,47719	3,79	0,127	0,202	0,058	0,033	0,03	0,0062	244
8,801001	3,55	0,044	0,155	0,048	0,035	0,031	0,0062	276
9,807147	3,01	0,02	0,162	0,043	0,034	0,033	0,0064	315
8,607327	2,3	0,003	0,186	0,05	0,03	0,033	0,0065	318
6,696889	1,43	0,002	0,253	0,046	0,025	0,035	0,0078	333
3,181739	0,68	0,003	0,308	0,039	0,02	0,036	0,0082	371
2,630393	0,27	0,005	0,278	0,026	0,012	0,034	0,01	456

Figure B.2: Table containing the chemical input data for heat S1836 cup height 5

Time in min	Temp in K	FeOtot wt%	CaO wt%	SiO2 wt%	MgO wt%	Al2O3 wt%	P2O5 wt%
00:00	1669	29,55	31,78	19,53	3,45	2,28	1,82
00:04	1699	29,55	31,78	19,53	3,45	2,28	1,82
00:06	1751	35,96	30,77	15,92	3,39	1,09	1,83
00:08	1798	37,46	30,23	14,83	3,07	1,64	1,86
00:10	1841	39,05	23,2	18,89	4,16	3,47	1,85
00:12	1879	39,44	30,08	13,06	4,52	2,32	1,43
00:14	1913	43,04	28,37	12,17	4,1	2,75	1,38
00:16	1943	42,62	29,27	10,57	6,56	2,15	1,18

MnO wt%	C wt%	Si wt%	Mn wt %	P wt%	S wt%	Cr wt%	Cu wt%	Slag weight in Kg
5,51	3,78	0,61	0,43	0,093	0,05	0,032	0,0038	0
5,51	3,7	0,169	0,194	0,058	0,033	0,032	0,0038	246
4,96	3,29	0,084	0,163	0,044	0,035	0,031	0,004	361
4,96	2,74	0,028	0,138	0,028	0,029	0,029	0,0042	430
4,16	2,33	0,0047	0,115	0,027	0,028	0,028	0,0044	354
3,94	1,39	0,001	0,105	0,023	0,025	0,026	0,0045	519
3,55	0,68	0,001	0,08	0,016	0,019	0,02	0,0044	562
3,55	0,028	0,001	0,058	0,017	0,022	0,018	0,0045	652

Figure B.3: Table containing the chemical input data for heat S1841 cup height 4

Time in min	Temp in K	FeOtot wt%	CaO wt%	SiO2 wt%	MgO wt%	Al2O3 wt%	P2O5 wt%
00:00	1669	29,39376	31,05835	20,18888	3,002428	2,537101	1,902826
00:04	1699	29,39376	31,05835	20,18888	3,002428	2,537101	1,902826
00:06	1751	35,67339	28,46462	17,19076	3,604868	1,989605	1,724325
00:08	1798	37,54349	30,60545	14,46257	3,291966	1,53301	1,861512
00:10	1841	40,18696	27,90184	13,73695	3,97548	2,594885	1,502302
00:12	1879	40,47077	30,11499	12,53456	4,268957	2,193372	1,425692
00:14	1913	44,94651	27,5305	11,41731	4,318222	2,775252	1,221111
00:16	1943	42,85571	28,23967	11,57017	5,598872	2,535177	1,212476

MnO wt%	C wt%	Si wt%	Mn wt%	P wt%	S wt%	Cr wt%	Cu wt%	Slag weight in Kg
5,563327	3,78	0,61	0,43	0,093	0,05	0,032	0,0038	0
5,563327	3,7	0,169	0,194	0,058	0,033	0,032	0,0038	238
5,40352	3,29	0,084	0,163	0,044	0,035	0,031	0,004	334
4,849184	2,74	0,028	0,138	0,028	0,029	0,029	0,0042	441
4,706949	2,33	0,0047	0,115	0,027	0,028	0,028	0,0044	486
3,919478	1,39	0,001	0,105	0,023	0,025	0,026	0,0045	541
3,400649	0,68	0,001	0,08	0,016	0,019	0,02	0,0044	599
3,55137	0,028	0,001	0,058	0,017	0,022	0,018	0,0045	596

Figure B.4: Table containing the chemical input data for heat S1841 cup height 5

Time in min	Temp in K	FeOtot wt%	CaO wt%	SiO2 wt%	MgO wt%	Al2O3 wt%	P2O5 wt%
00:00	1583	20,38695	38,0241	20,72622	1,315422	1,183546	2,474687
00:04	1702	20,38695	38,0241	20,72622	1,315422	1,183546	2,474687
00:06	1775	24,64381	31,73026	20,90793	1,355016	1,402865	2,550664
00:08	1847	19,4878	34,59056	22,31937	3,201357	1,857358	1,966614
00:10	1911	16,33666	37,46516	22,99496	6,395194	3,236193	1,369159
00:12	1961	11,68605	44,1939	23,35568	5,100444	1,579858	1,263887
00:14	1988	8,888162	50,02183	21,81009	5,043334	1,704321	1,384761
00:16	1987	17,06433	45,88661	17,20039	6,451259	1,032784	1,755733

MnO wt%	C wt%	Si wt%	Mn wt%	P wt%	S wt%	Cr wt%	Cu wt%	Slag weight in Kg
7,093547	3,97	0,62	0,43	0,098	0,052	0,028	0,0035	0
7,093547	3,73	0,102	0,176	0,06	0,043	0,029	0,0036	263,5691
8,099837	3,32	0,028	0,124	0,045	0,039	0,028	0,0036	301,0354
7,126614	2,76	0,013	0,124	0,05	0,036	0,029	0,0038	291,6089
5,917222	1,99	0,0042	0,153	0,058	0,034	0,031	0,0039	289,551
4,921154	0,88	0,0043	0,229	0,054	0,027	0,033	0,0067	287,5048
3,132415	0,311	0,0047	0,302	0,047	0,025	0,035	0,0059	310,3328
3,705273	0,025	0,0023	0,199	0,023	0,02	0,032	0,0041	381,6839

Figure B.5: Table containing the chemical input data for heat S1844 cup height 4

Time in min	Temp in K	FeOtot wt%	CaO wt%	SiO2 wt%	MgO wt%	Al2O3 wt%	P2O5 wt%
00:00	1583	20,13295	38,07676	21,16314	1,288315	1,49572	2,457254
00:04	1702	20,13295	38,07676	21,16314	1,288315	1,49572	2,457254
00:06	1775	25,04292	31,51845	20,59862	1,303656	1,184078	2,563468
00:08	1847	20,45087	31,96316	23,36617	2,441598	2,055856	2,055856
00:10	1911	15,50306	38,4205	23,02615	5,652529	2,527665	1,369152
00:12	1961	12,20283	42,85105	23,73416	4,720215	1,956173	1,304115
00:14	1988	10,71402	48,22504	21,49879	5,097188	2,001476	1,474772
00:16	1987	16,99097	46,00878	17,18097	6,372929	1,037168	1,763186

MnO wt%	C wt%	Si wt%	Mn wt%	P wt%	S wt%	Cr wt%	Cu wt%	Slag weight in Kg
6,865964	3,97	0,62	0,43	0,098	0,052	0,028	0,0035	0
6,865964	3,73	0,102	0,176	0,06	0,043	0,029	0,0036	258
8,267659	3,32	0,028	0,124	0,045	0,039	0,028	0,0036	306
7,82029	2,76	0,013	0,124	0,05	0,036	0,029	0,0038	279
6,286757	1,99	0,0042	0,153	0,058	0,034	0,031	0,0039	289
4,972327	0,88	0,0043	0,229	0,054	0,027	0,033	0,0067	283
3,325658	0,311	0,0047	0,302	0,047	0,025	0,035	0,0059	315
3,713079	0,025	0,0023	0,199	0,023	0,02	0,032	0,0041	400

Figure B.6: Table containing the chemical input data for heat S1844 cup height 5

Time in min	Temp in k	FeOtot wt%	CaO wt%	SiO2 wt%	MgO wt%	Al2O3 wt%	P2O5 wt%
00:00	1555	20,4	37,33	21,19	1,9	1,69	2,46
00:04	1699	20,4	37,33	21,19	1,9	1,69	2,46
00:06	1751	26,32	28,57	21,5	2,43	2,8	2,87
00:08	1798	18,5	33,61	23,14	2,76	2,1	2,06
00:10	1841	14,1	37,02	25,06	3,23	2,18	1,32
00:12	1879	10,74	43,82	23,72	5,36	1,71	1,3
00:14	1913	10,1	50,05	19,23	6,69	1,8	1,66
00:16	1943	19,56	44,14	16,04	7,62	1,5	1,79

MnO wt%	C wt%	Si wt%	Mn wt%	P wt%	S wt%	Cr wt%	Cu wt%	Slag weight in Kg
7,59	4,07	0,53	0,46	0,095	0,045	0,032	0,0038	0
7,59	3,8	0,1	0,18	0,056	0,036	0,029	0,004	215
8,18	3,41	0,02	0,13	0,039	0,039	0,028	0,004	249
8,97	2,65	0,01	0,15	0,046	0,035	0,031	0,004	241
7,97	1,92	0	0,19	0,057	0,033	0,032	0,004	227
5,17	0,93	0,01	0,25	0,048	0,026	0,034	0,006	242
3,4	0,39	0	0,29	0,035	0,017	0,034	0,006	303
3,68	0,02	0	0,15	0,019	0,025	0,034	0,006	366

Figure B.7: Table containing the chemical input data for heat S1845 cup height 4

Time in min	Temp in K	FeOtot wt%	CaO wt%	SiO2 wt%	MgO wt%	Al2O3 wt%	P2O5 wt%
00:00	1555	22,00815	37,22461	20,12191	1,978468	1,536605	2,505636
00:04	1711	22,00815	37,22461	20,12191	1,978468	1,536605	2,505636
00:06	1787	25,46403	29,76184	20,73044	2,873603	2,705622	2,765986
00:08	1857	18,1221	33,50225	23,36387	2,744196	2,177431	2,099819
00:10	1917	13,54357	38,29251	24,57387	3,261611	1,585325	1,26826
00:14	1994	10,6972	51,61705	18,4219	5,657908	1,449054	1,659825
00:16	2004	20,29273	44,71569	15,32559	7,381285	1,187243	1,752325

MnO wt%	C wt%	Si wt%	Mn wt%	P wt%	S wt%	Cr wt%	Cu wt%	Slag weight in Kg
7,630985	4,07	0,53	0,46	0,095	0,045	0,028	0,0038	0
7,630985	3,8	0,097	0,179	0,056	0,036	0,029	0,0038	229
8,215451	3,41	0,023	0,134	0,039	0,039	0,028	0,0039	260
9,025133	2,65	0,008	0,149	0,046	0,035	0,031	0,004	241
7,987382	1,92	0,003	0,19	0,057	0,033	0,032	0,004	235
3,236431	0,387	0,0048	0,286	0,035	0,017	0,032	0,004	316
3,665777	0,02	0,0001	0,15	0,019	0,025	0,032	0,004	383

Figure B.8: Table containing the chemical input data for heat S1845 cup height 5

C

Appendix C

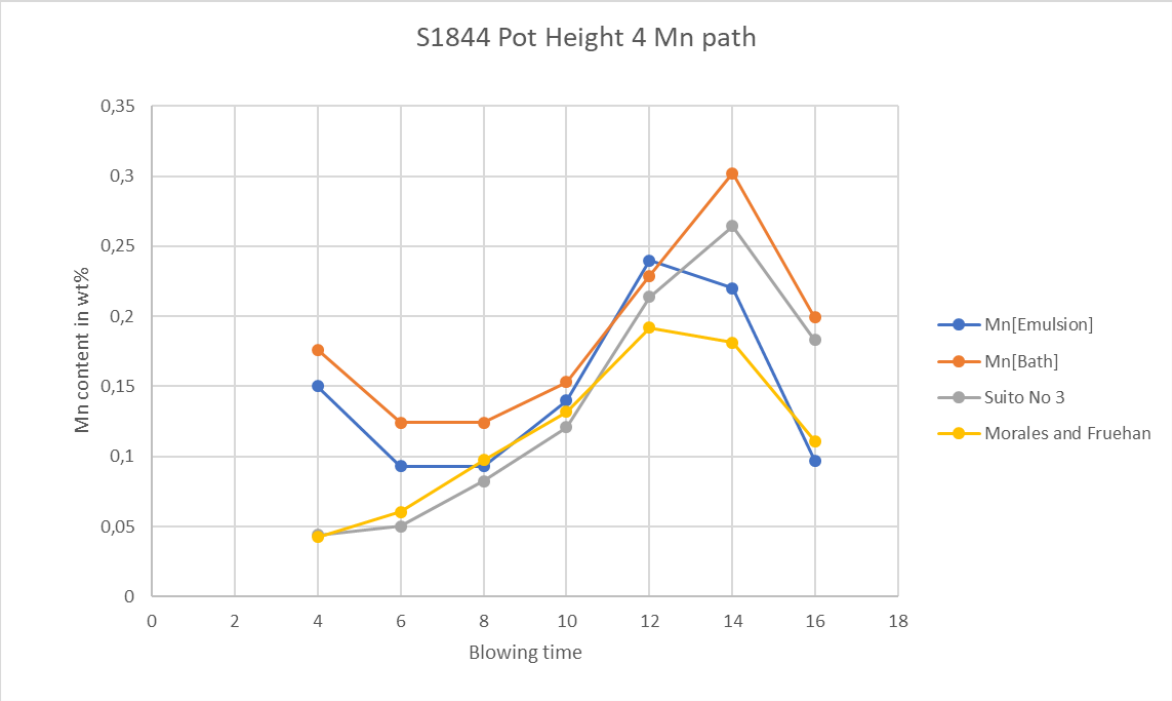

Figure C.1: Manganese equilibrium values compared with measured IMPHOS manganese values along the time of heat S1844 in minutes.

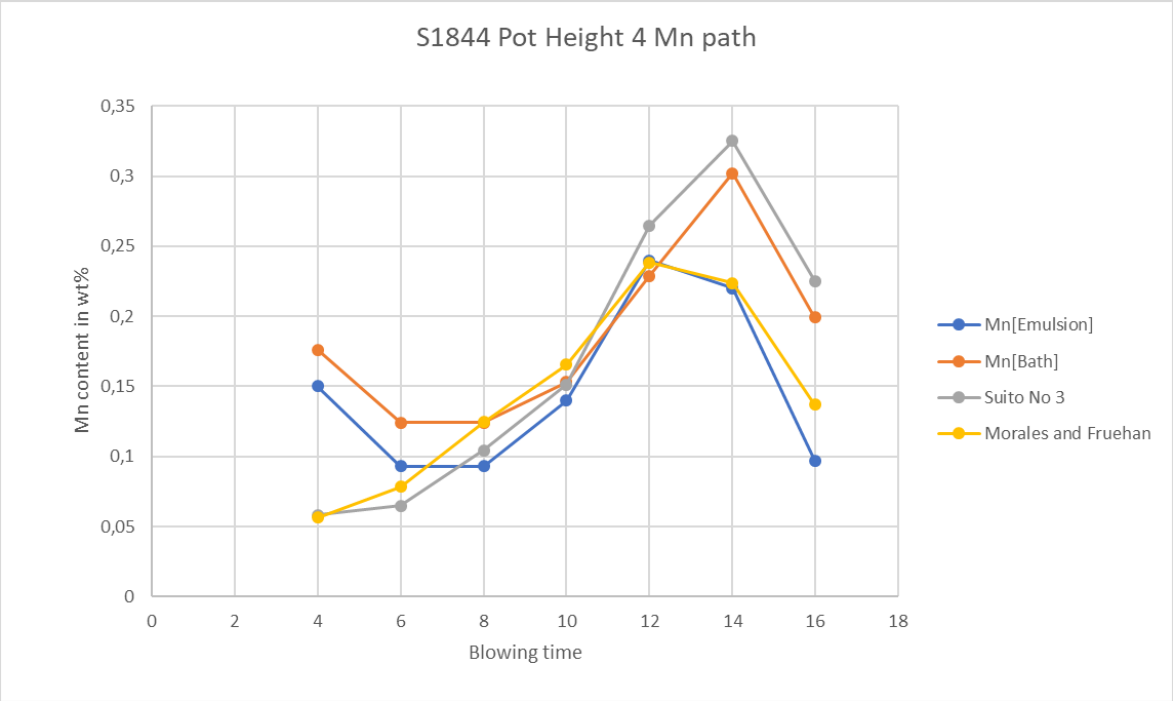

Figure C.2: Manganese partition ratio values compared with measured IMPHOS manganese partition ratio values along the time of heat S1844 in minutes. With a temperature adjustment of +50K.

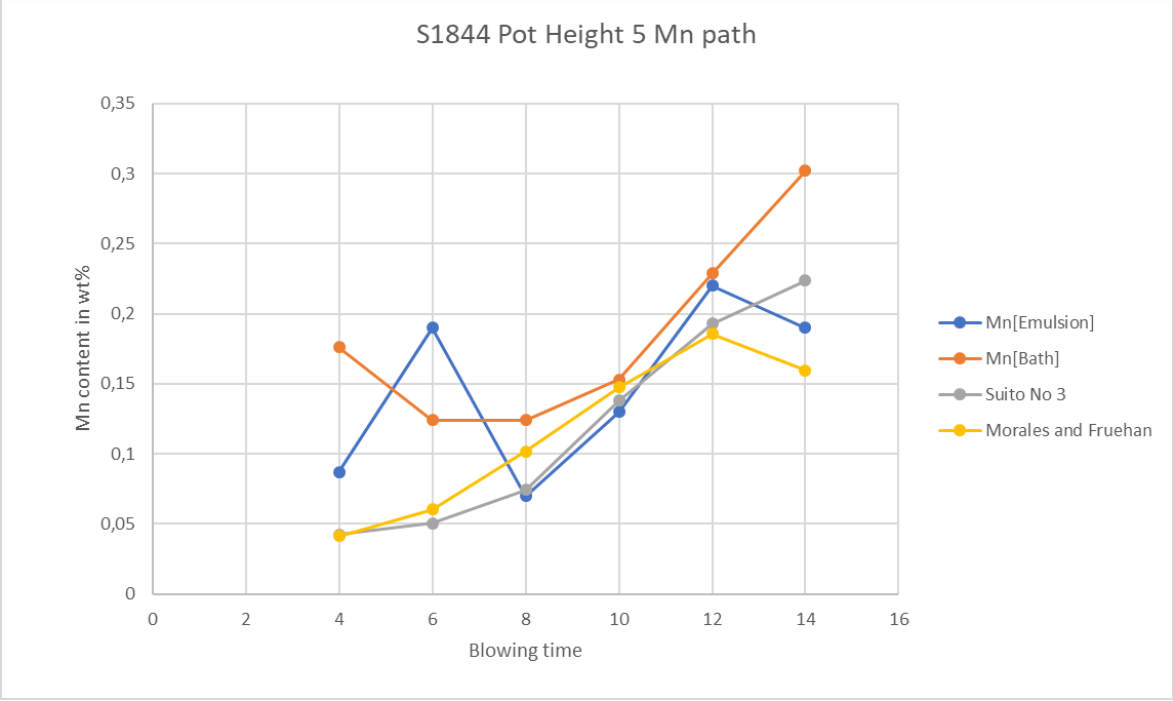

Figure C.3: Manganese equilibrium values compared with measured IMPHOS manganese values along the time of heat S1844 cup height 5 in minutes.

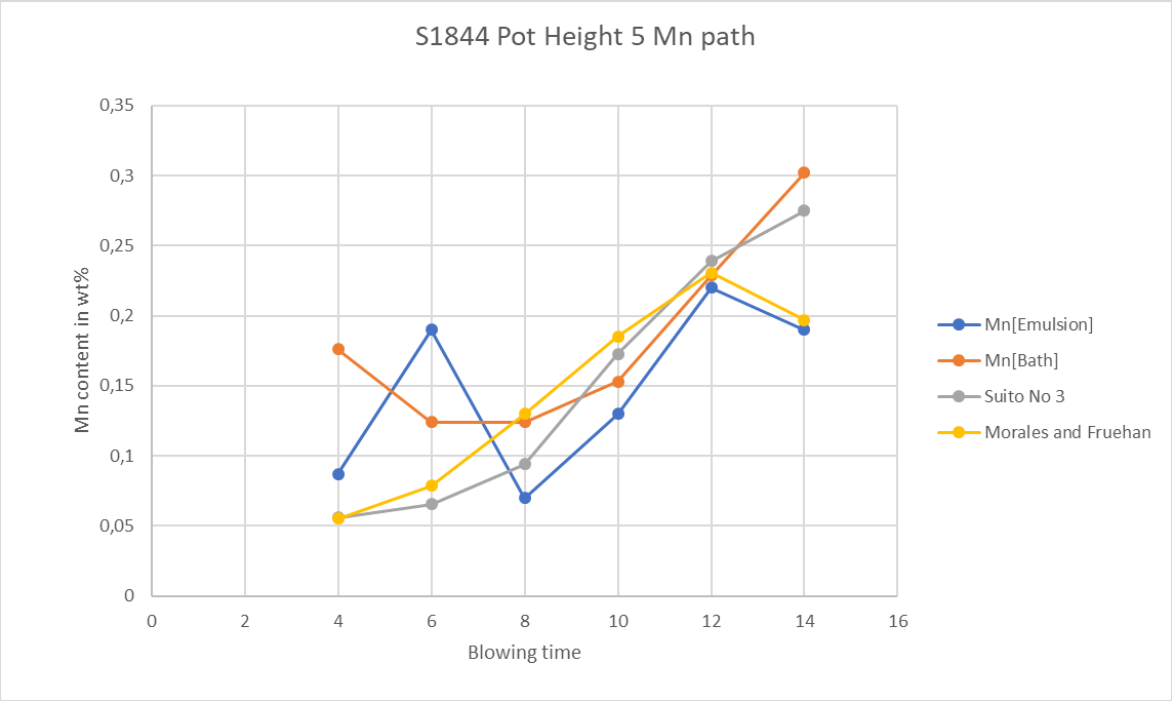

Figure C.4: Manganese partition ratio values compared with measured IMPHOS manganese partition ratio values along the time of heat S1844 cup height 5 in minutes. With a temperature adjustment of +50K.

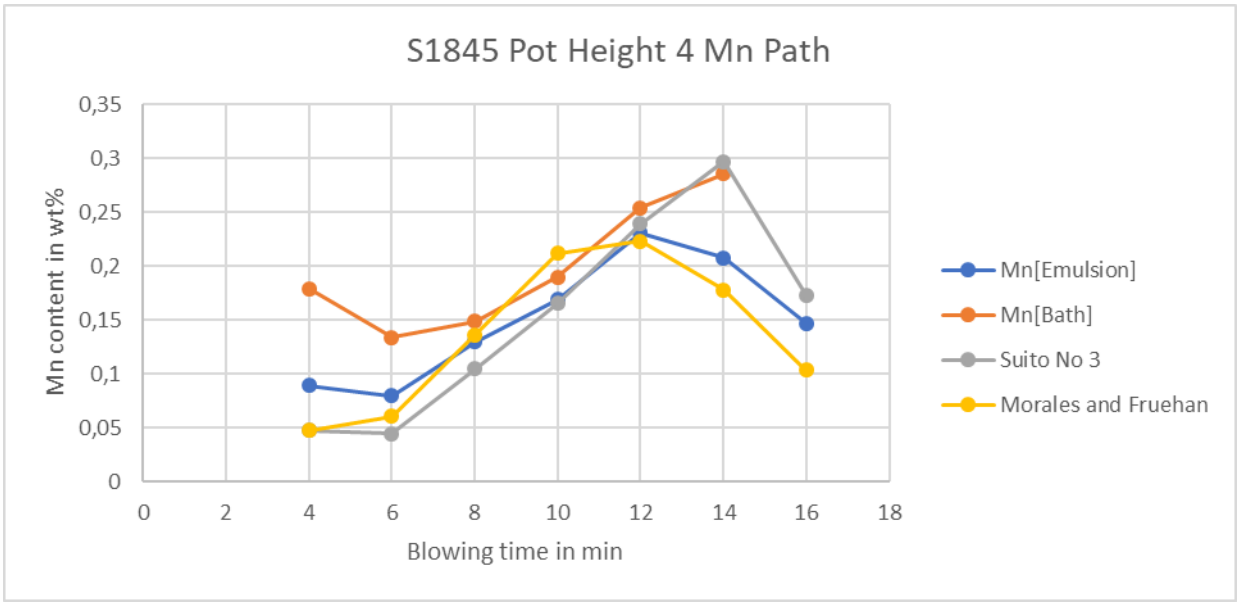

Figure C.5: Manganese equilibrium values compared with measured IMPHOS manganese values along the time of heat S1845 in minutes.

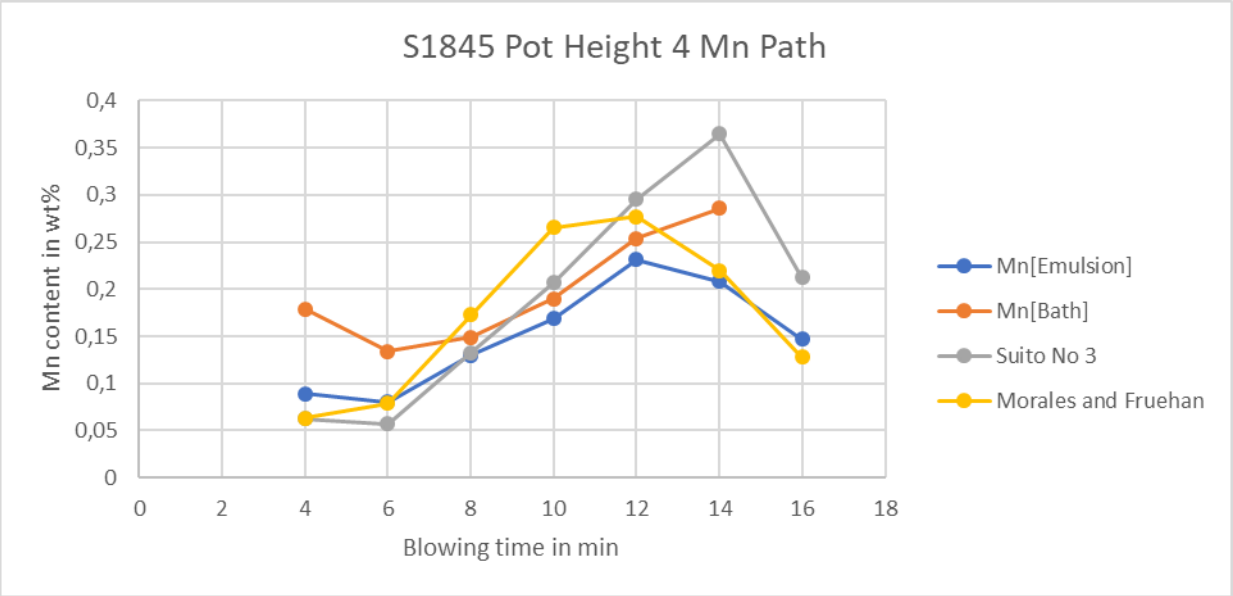

Figure C.6: Manganese partition ratio values compared with measured IMPHOS manganese partition ratio values along the time of heat S1845 in minutes. With a temperature adjustment of +50K.

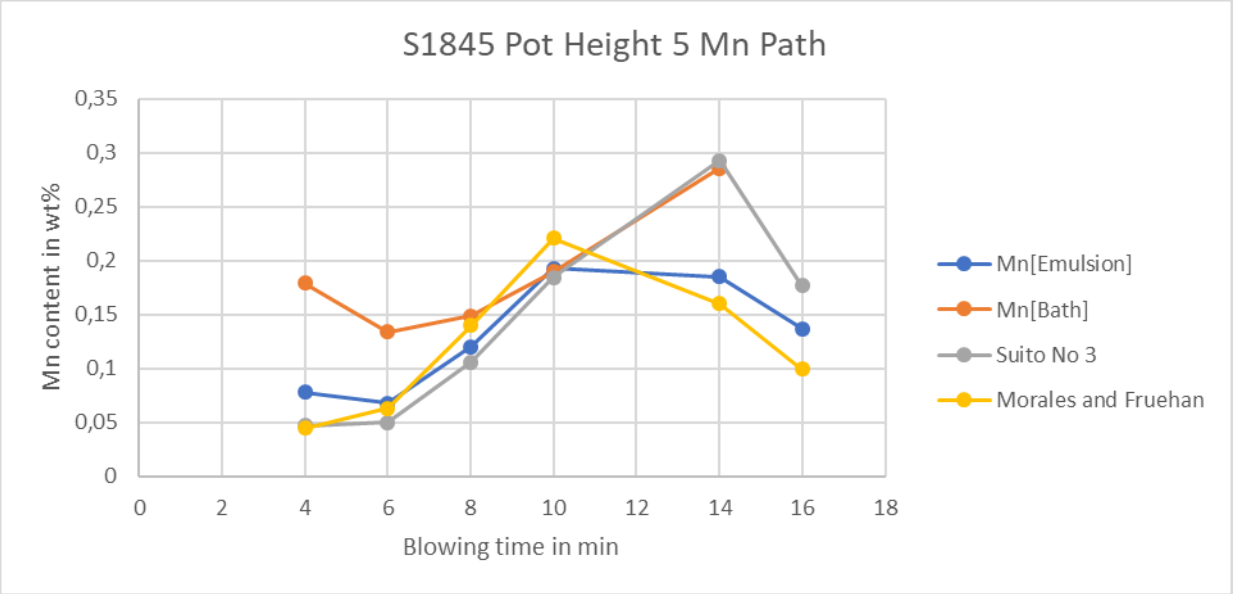

Figure C.7: Manganese equilibrium values compared with measured IMPHOS manganese values along the time of heat S1845 cup height 5 in minutes.

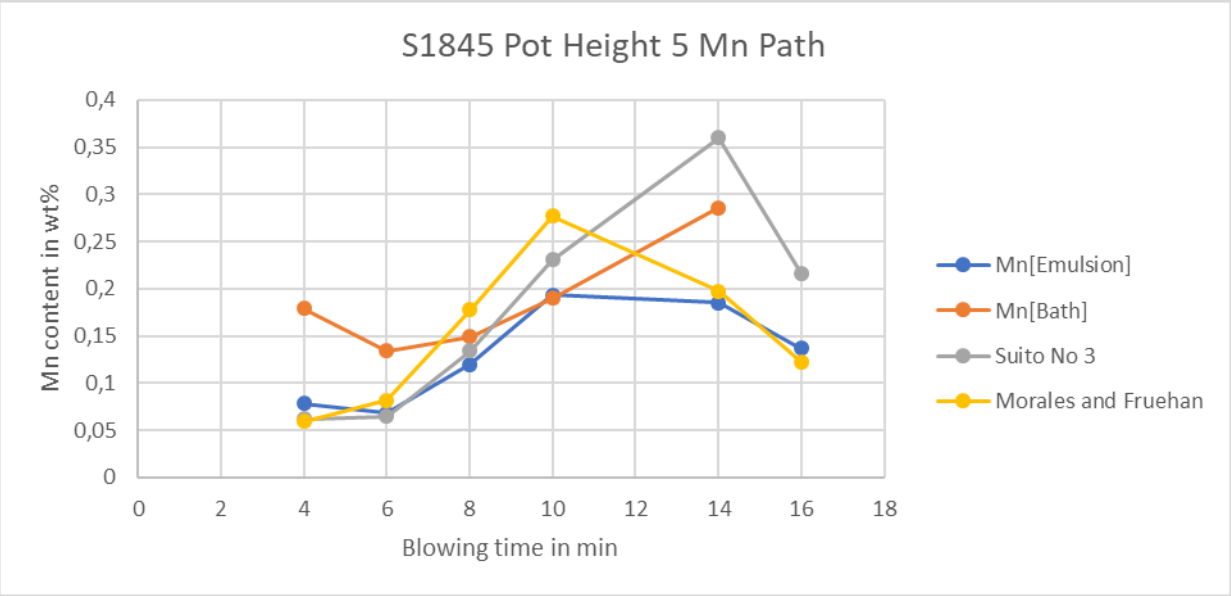

Figure C.8: Manganese partition ratio values compared with measured IMPHOS manganese partition ratio values along the time of heat S1845 cup height 5 in minutes. With a temperature adjustment of +50K.

D

Appendix D

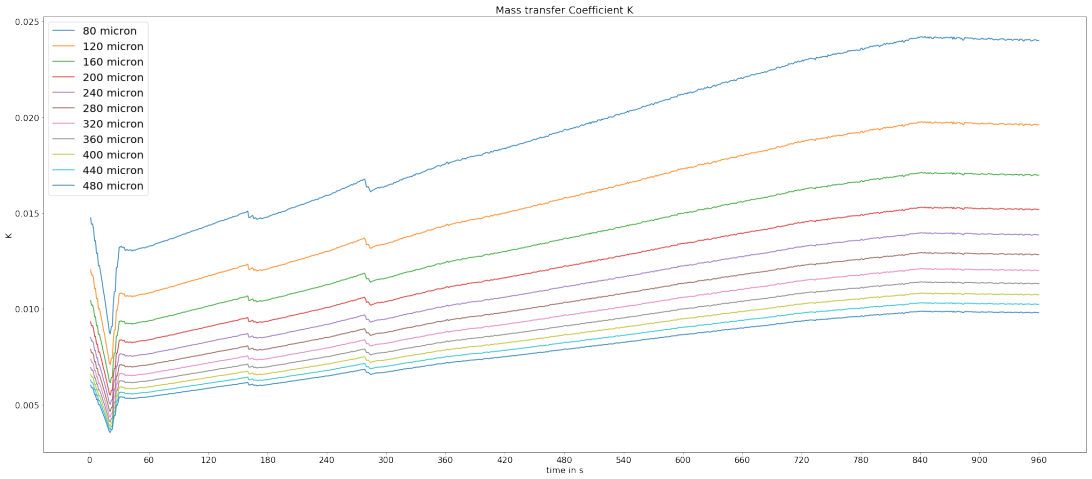

Figure D.1: Mass transfer parameter K in m/s for different droplet size classes, heat S1845-cup height 4-Suito number 3 model, droplet size 20-500 micron.

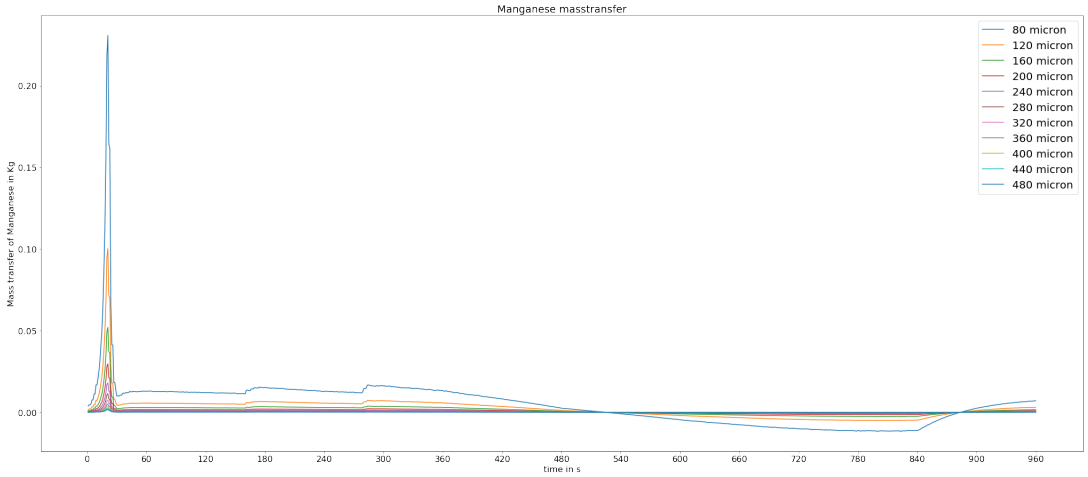

Figure D.2: Manganese mass transfer in kg for different droplet size classes, heat S1845-cup height 4-Suito number 3 model, droplet size 20-500 micron.

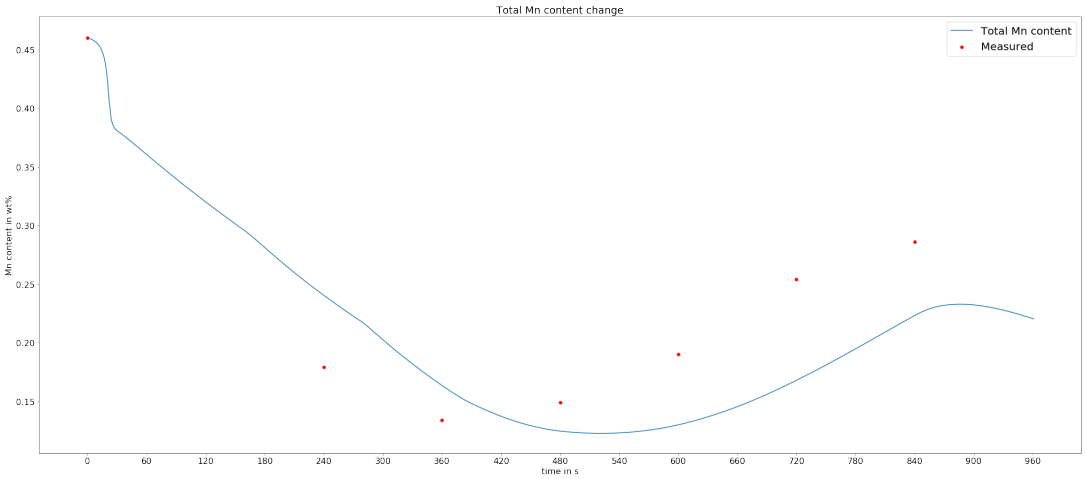

Figure D.3: Total manganese content change over time in wt% , heat S1845-cup height 4-Suito number 3 model, droplet size 20-500 micron.

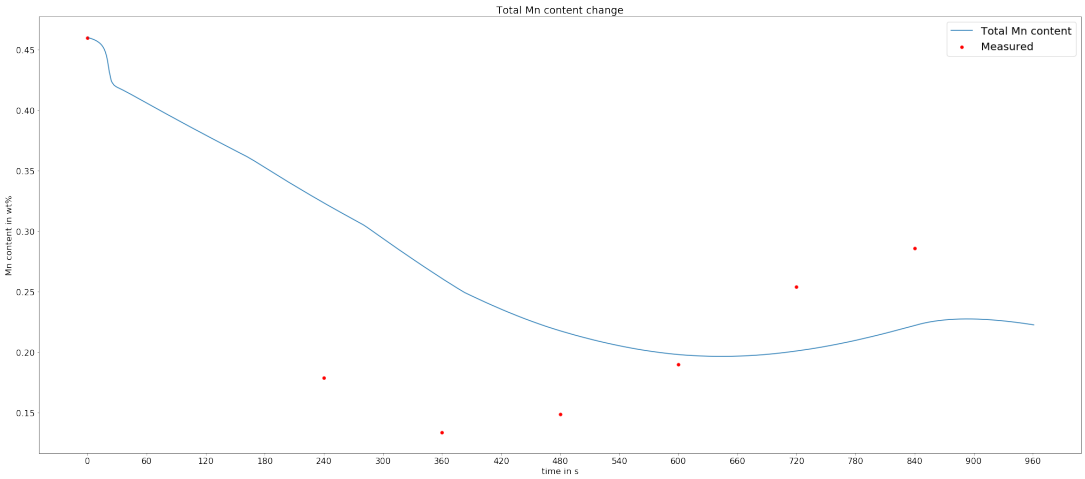

Figure D.4: Total manganese content change over time in wt% , heat S1845-cup height 4-Suito number 3 model, droplet size 20-500 micron.

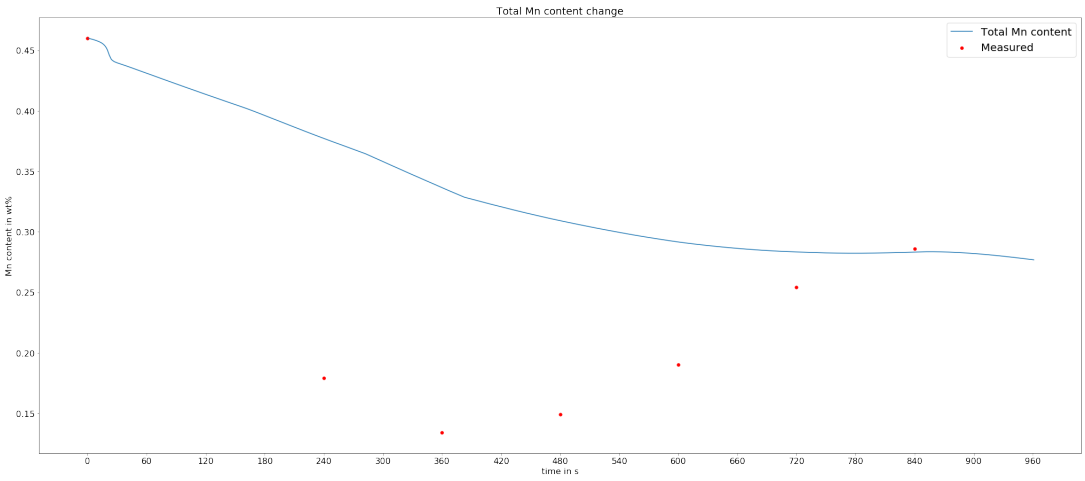

Figure D.5: Total manganese content change over time in wt% , heat S1845-cup height 4-Suito number 3 model, droplet size 20-500 micron.

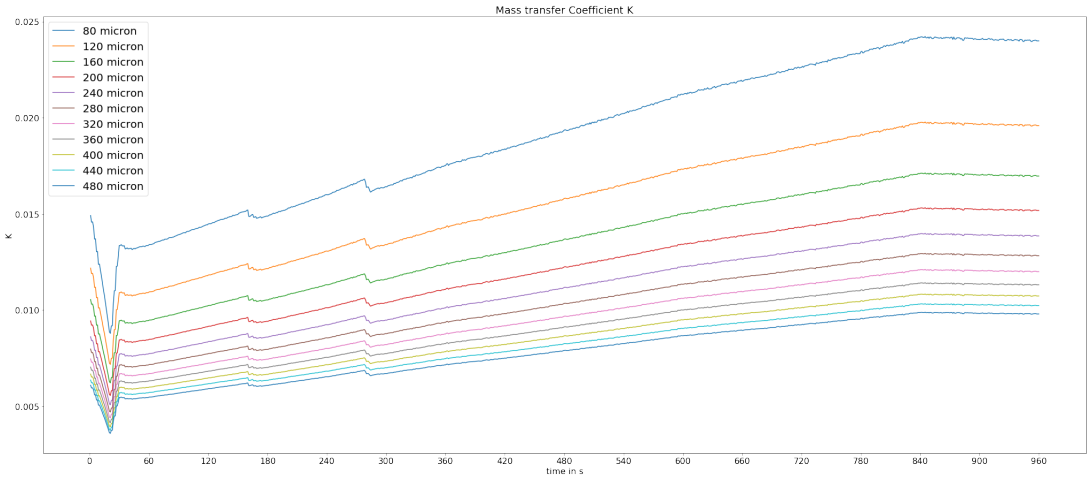

Figure D.6: Mass transfer parameter K in m/s for different droplet size classes, heat S1845-cup height 5-Suito number 3 model, droplet size 20-500 micron.

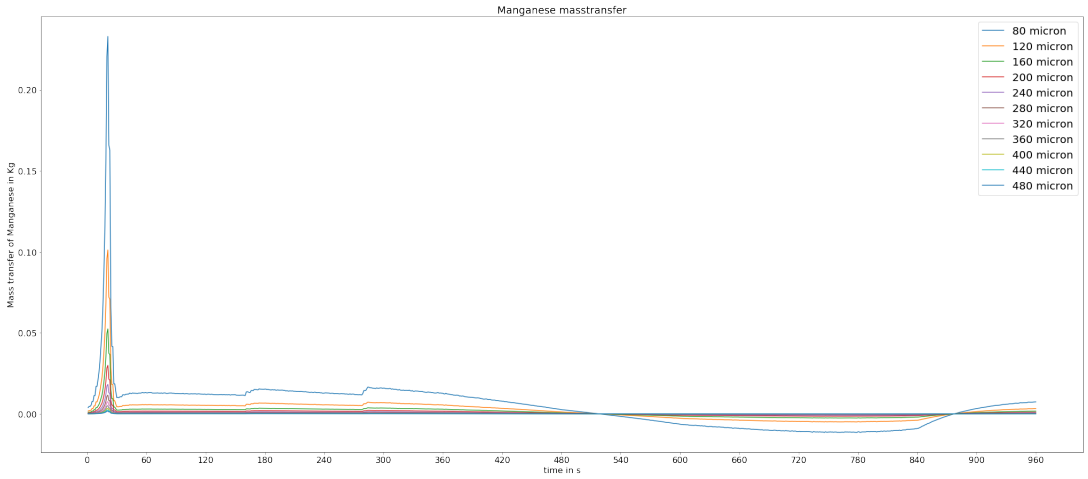

Figure D.7: Manganese mass transfer in kg for different droplet size classes, heat S1845-cup height 5-Suito number 3 model, droplet size 20-500 micron.

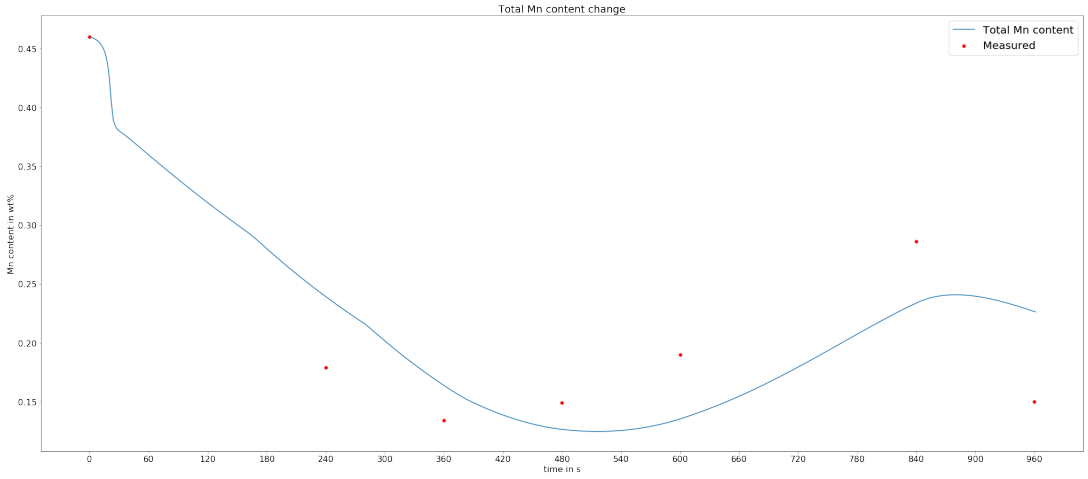

Figure D.8: Total manganese content change over time in wt% , heat S1845-cup height 5-Suito number 3 model, droplet size 20-500 micron.

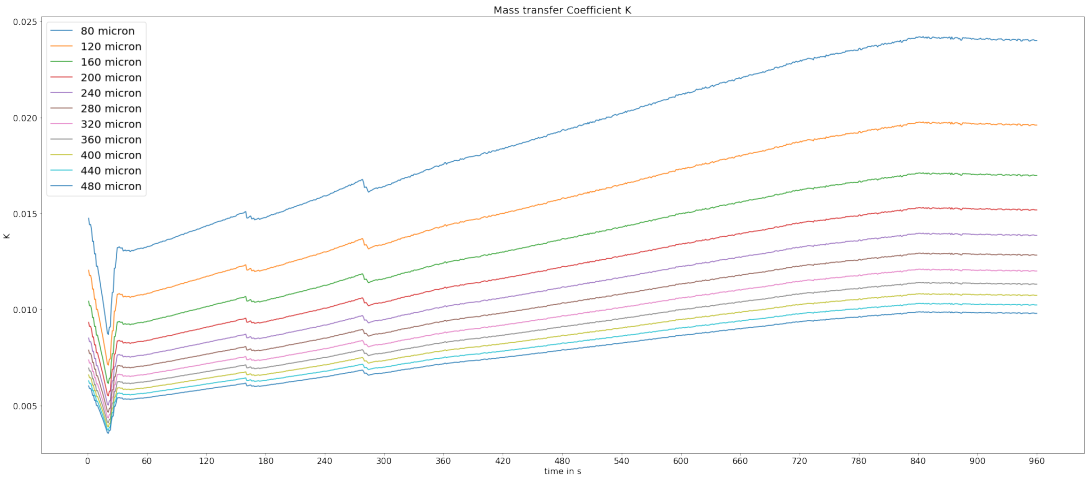

Figure D.9: Mass transfer parameter K in m/s for different droplet size classes, heat S1845-cup height 4-Morales and Fruehan model, droplet size 20-500 micron.

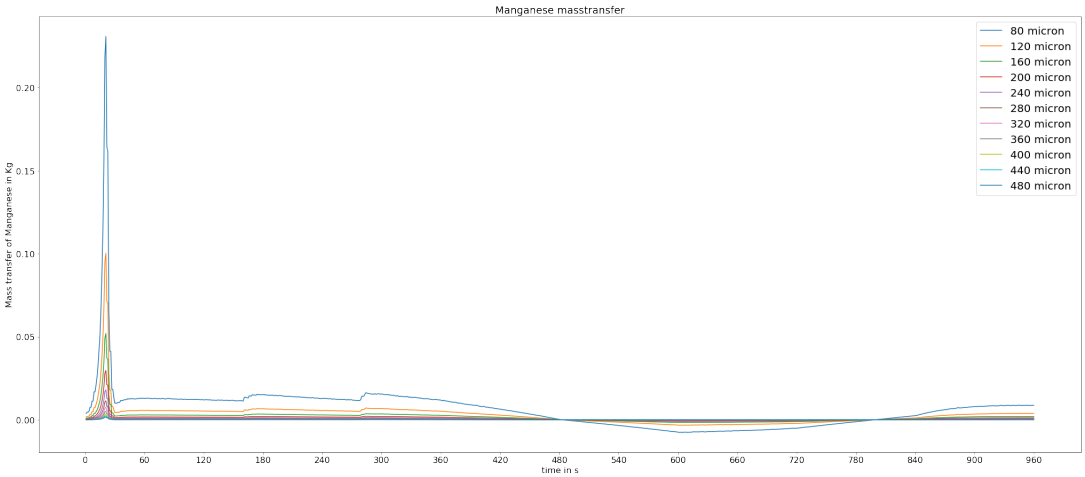

Figure D.10: Manganese mass transfer in kg for different droplet size classes, heat S1845-cup height 4-Morales and Fruehan model, droplet size 20-500 micron.

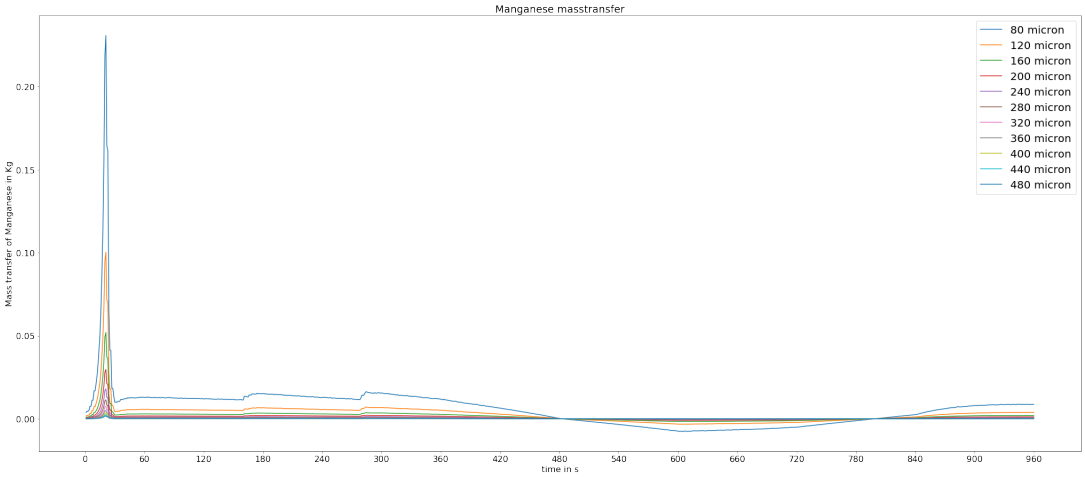

Figure D.11: Total manganese content change over time in wt% , heat S1845-cup height 4-Morales and Fruehan model, droplet size 20-500 micron.

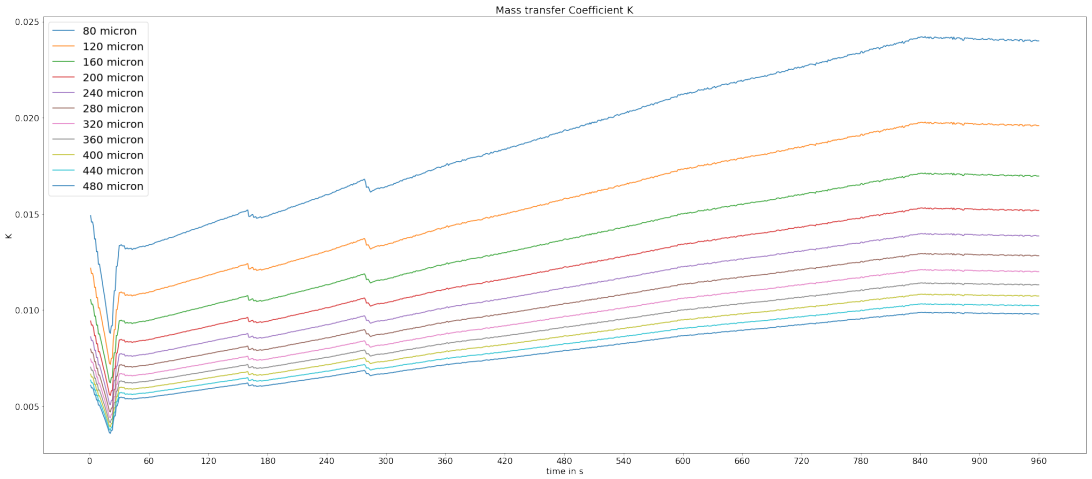

Figure D.12: Mass transfer parameter K in m/s for different droplet size classes, heat S1845-cup height 5-Morales and Fruehan model, droplet size 20-500 micron.

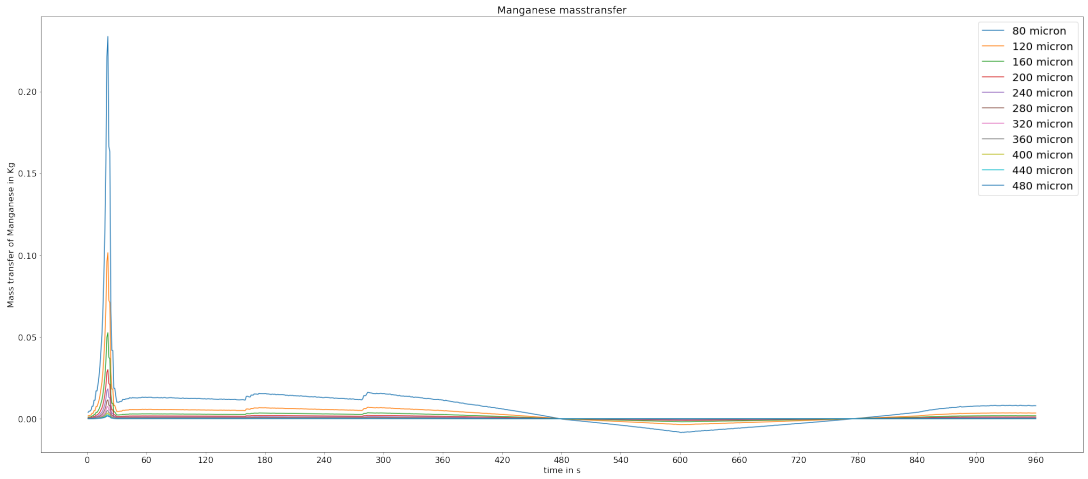

Figure D.13: Manganese mass transfer in kg for different droplet size classes, heat S1845-cup height 5-Morales and Fruehan model, droplet size 20-500 micron.

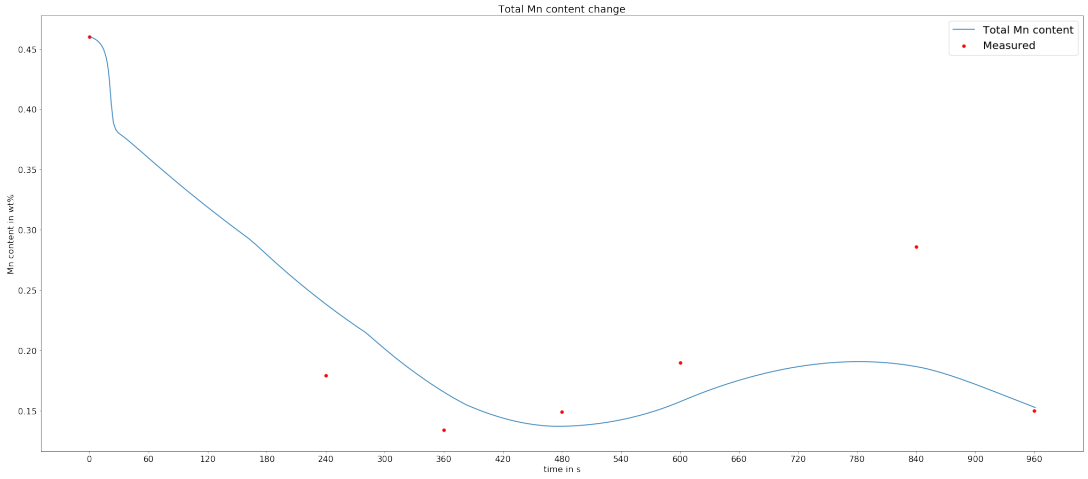

Figure D.14: Total manganese content change over time in wt% , heat S1845-cup height 5-Morales and Fruehan model, droplet size 20-500 micron.

E

Appendix E

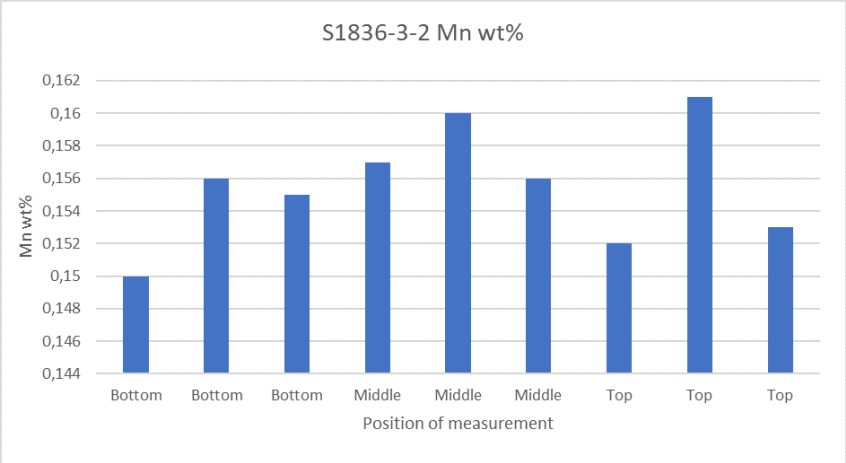

Figure E.1: Weight percentages of manganese throughout sample S1836-3-2, measurements are taken from left to right at the indicated position.

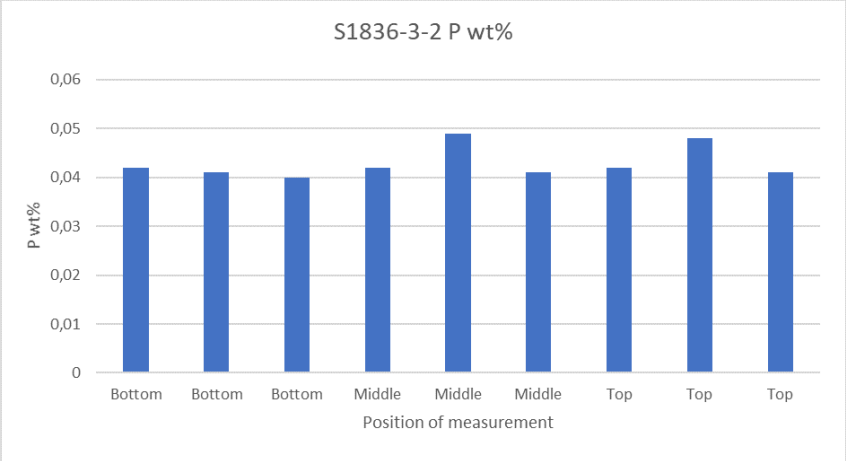

Figure E.2: Weight percentages of phosphorus throughout sample S1836-3-2, measurements are taken from left to right at the indicated position.

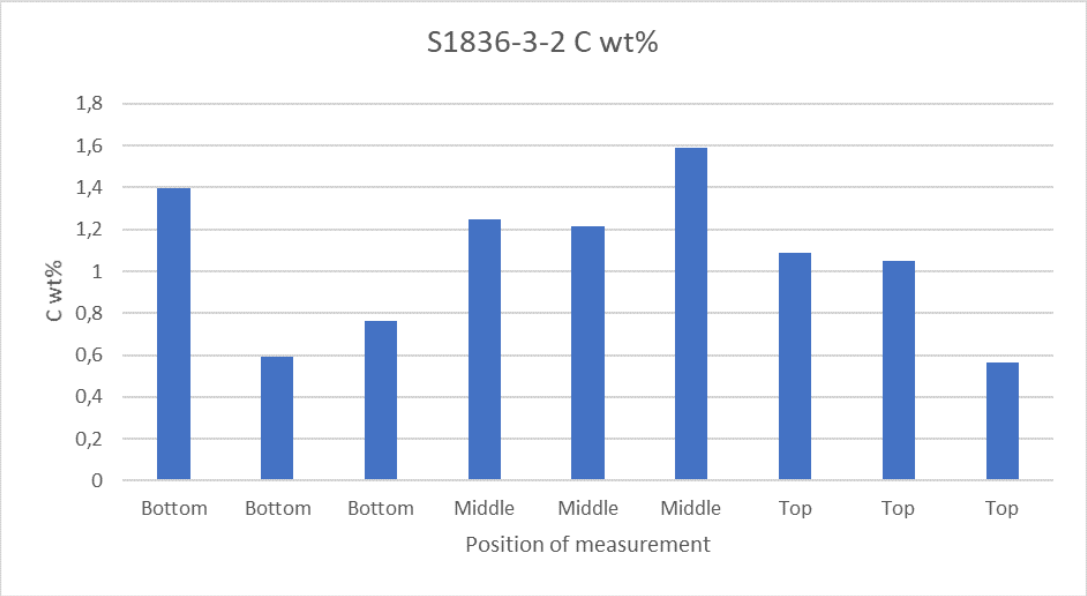

Figure E.3: Weight percentages of carbon throughout sample S1836-3-2, measurements are taken from left to right at the indicated position.

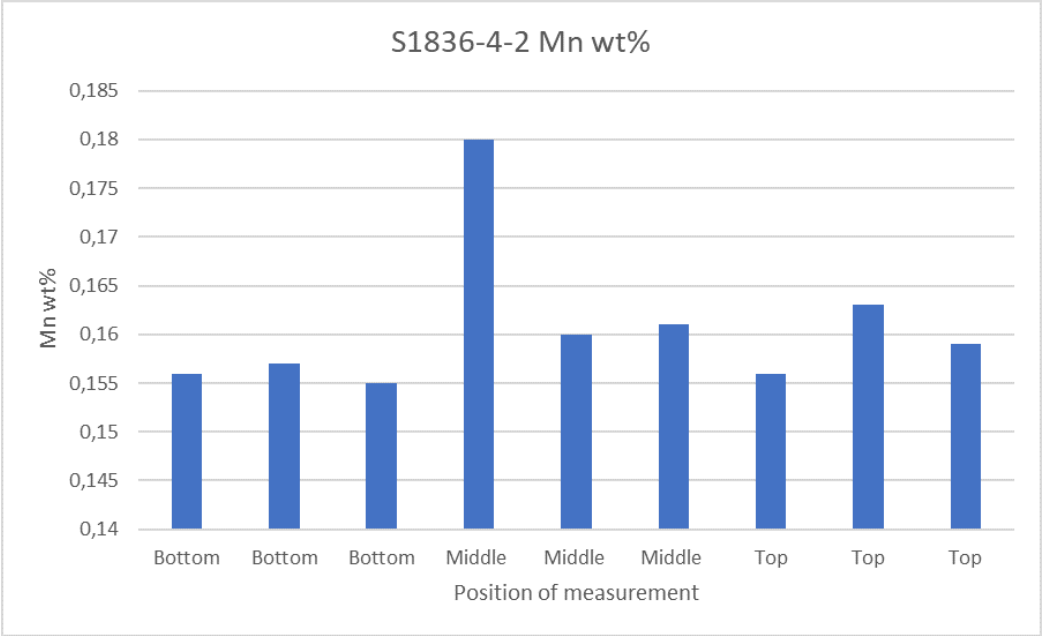

Figure E.4: Weight percentages of manganese throughout sample S1836-4-2, measurements are taken from left to right at the indicated position.

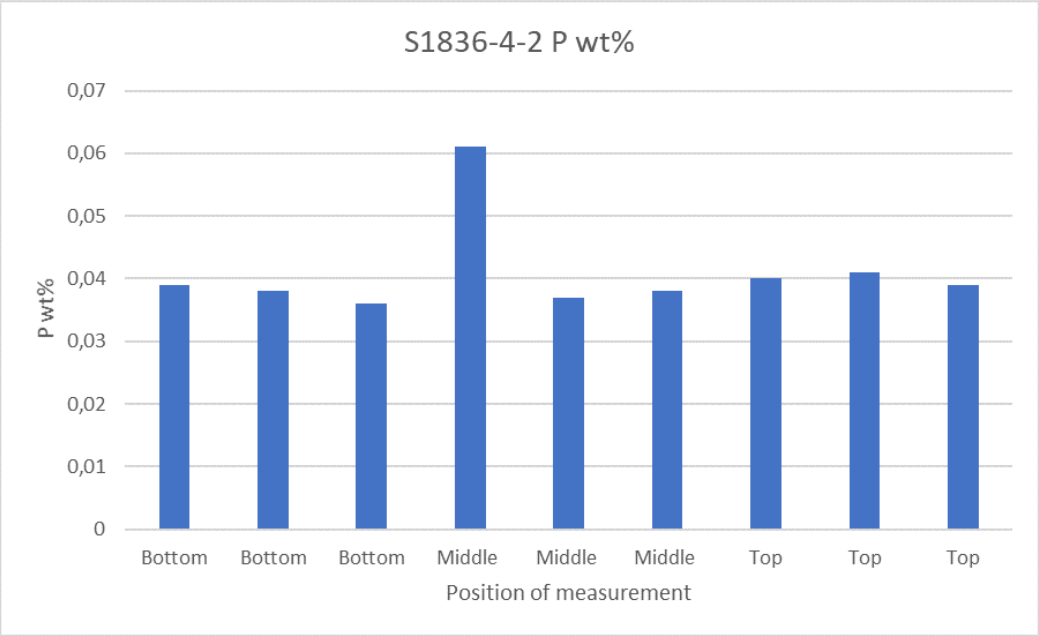

Figure E.5: Weight percentages of phosphorus throughout sample S1836-4-2, measurements are taken from left to right at the indicated position.

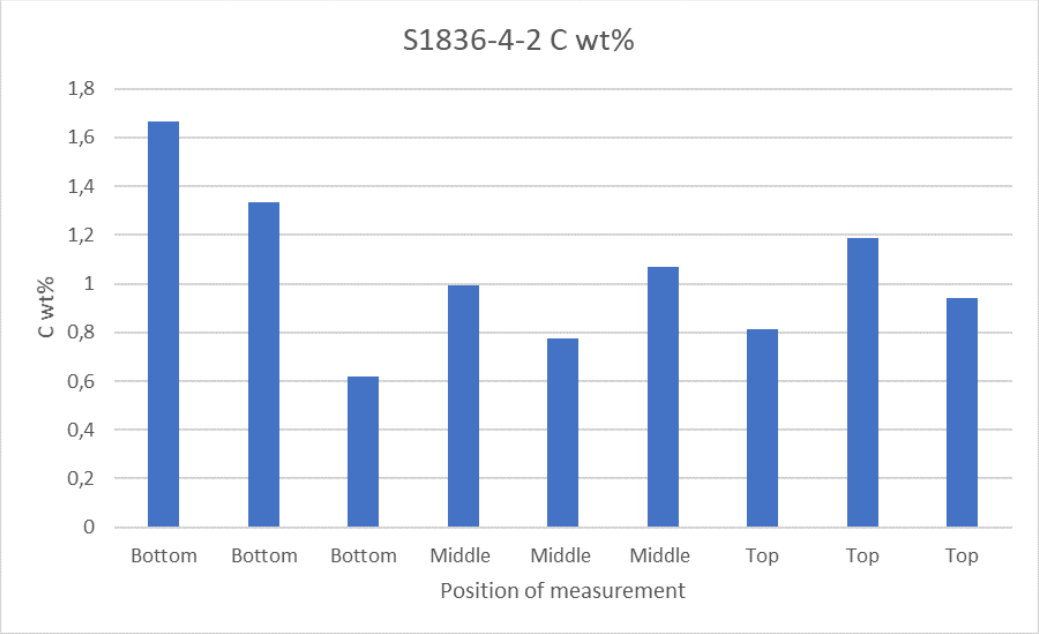

Figure E.6: Weight percentages of carbon throughout sample S1836-4-2, measurements are taken from left to right at the indicated position.